Master Thesis

Acoustic Emission Monitoring of Fatigue Damage in Steel Materials for Marine Applications

Offshore Engineering

A. Gautam

Delft University of Technology

TU Delft

Master Thesis

Acoustic Emission Monitoring of Fatigue Damage in Steel Materials for Marine Applications

by

A. Gautam

to obtain the degree of **Master of Science**
in Offshore Engineering
at the Delft University of Technology,
to be defended publicly on Thursday September 5, 2024 at 15:00.

Student number:	5837642	
Project duration:	November 14, 2023 – September 5, 2024	
Thesis committee:	Dr. ir. L. Pahlavan,	TU Delft, Supervisor
	C. Saccone,	TU Delft, Daily Supervisor
	Dr. ir. J. H. den Besten,	TU Delft

An electronic version of this thesis is available at http://repository.tudelft.nl/.

TU Delft

Preface

This thesis, part of my master's program in Offshore and Dredging Engineering at TU Delft, addresses the critical issue of fatigue damage in materials, which accumulates over time due to repeated loading cycles. This research is focused on enhancing fatigue damage monitoring using the Acoustic Emission (AE) method.

The successful completion of this thesis would not have been possible without the support and guidance of several individuals. First and foremost, I would like to express my deepest gratitude to my supervisor, Pooria Pahlavan, for providing me with this opportunity and ensuring that the research process was smooth and successful. As someone new to conducting research experiments, I greatly benefited from his guidance and invaluable feedback. His advice on maintaining a professional attitude, effective communication, and standing by one's ideas were among the most important lessons I learned throughout this journey. I am sincerely grateful for his constant support and encouragement, which enabled me to complete this thesis on time.

I would also like to extend my heartfelt thanks to Cecilia Saccone for her time, effort, and unwavering support during the research period. Her motivation and encouragement helped me navigate through the challenging phases of this journey. She played a pivotal role in helping me understand the acoustic emission method and provided crucial assistance during the experiments. Moreover, she imparted valuable life lessons, particularly in developing a critical outlook and truly understanding complex concepts.

I am also grateful to Filippo Riccioli for his assistance with coding and the insightful contributions he made to this research. Additionally, I would like to thank Ruben for conducting the fatigue experiments and collaborating with us. My appreciation extends to all the other individuals who contributed to shaping this research, even if they are not mentioned by name.

Furthermore, I would like to express my sincere thanks to Henk den Besten for graciously accepting the invitation to participate in the graduation committee.

Finally, I am deeply thankful to my family and friends for their unwavering support throughout this journey. In particular, I want to acknowledge Michael Katsouros and Eleftheria Papadaki for their emotional support, which helped me persevere during the challenging times.

I hope you find this research study both informative and engaging.

A. Gautam
Delft, September 2024

Abstract

This thesis investigates the feasibility and effectiveness of Acoustic Emission (AE) methods for monitoring fatigue crack growth in metallic materials, with the aim of enhancing predictive capabilities and understanding of crack propagation under cyclic loading. The research specifically examines the correlation between various AE parameters—such as amplitude, count rate, energy rate, and entropy—and fatigue crack growth rates, using a multi-parametric approach.

Experiments were conducted on multiple specimens under different loading conditions, and both time-domain and frequency-domain AE parameters were analyzed. The study found that parameters like energy rate and rise angle were particularly effective in detecting specific stages of fatigue crack growth, while count rate and amplitude provided consistent indicators of crack initiation and progression. However, the study also highlighted limitations in the use of filtering techniques, such as SNR and amplitude filters, which can inadvertently remove crucial AE signals.

The findings suggest that while AE methods have potential for accurately monitoring fatigue crack growth, their effectiveness is influenced by the choice of AE parameters and the management of noise. To improve accuracy, the study recommends further research that includes a broader range of specimens, explores additional AE parameters, integrates complementary techniques such as Digital Image Correlation (DIC), and applies advanced analytical methods like machine learning. Future research should also consider the impact of environmental factors, such as corrosion fatigue, particularly in marine environments where realistic AE data is critical.

Overall, this study contributes to the broader understanding of AE monitoring for fatigue damage, laying a foundation for future research and practical applications, while acknowledging the need for further refinement and validation of AE techniques across diverse materials and conditions.

Contents

List of Figures

List of Tables

Nomenclature

Abbreviations

Abbreviation	Definition
AE	Acoustic Emission
AF	Average Frequency
CF	Centroid Frequency
CMOD	Crack mouth opening displacement
CT	Compact Tension
DIC	Digital Image Correlation
DAQ	Data Acqusition System
FCG	Fatigue Crack Growth
FCGR	Fatigue Crack Growth Rate
LEFM	Linear elastic fracture mechanics
MT	Mid-crack Tension
PF	Peak Frequency
RA	Rise Angle
RMS	Root Mean Square
RT	Rise Time
SEN	Single Edge Notch

Symbols

Symbol	Definition	Unit
ΔK	Applied stress intensity factor range	[MPa$\sqrt{m}$]
η	Number of counts	[–]
a	Crack length	[mm]
da/dN	Crack growth rate per cycle	[mm/cycle]
dU/dN	Absolute energy rate	[attoJoules (aJ)]
K	Stress intensity factor	[MPa$\sqrt{m}$]
K_{max}	Maximum stress intensity factor	[MPa$\sqrt{m}$]
K_{min}	Minimum stress intensity factor	[MPa$\sqrt{m}$]
K_t	Stress concentration factor	[–]
N	Number of cycles	[–]

1 Introduction

1.1. Background and Motivation

Offshore and marine structures, such as oil platforms, wind turbines, and marine vessels, are subjected to harsh environmental conditions, extreme loads, and corrosive agents. These structures, including offshore platforms, pipelines, and sub-sea components, are particularly vulnerable to fatigue cracks caused by cyclic loading and corrosive environments [22]. Fatigue damage accumulates gradually over time due to repeated loading and unloading cycles, weakening materials and potentially leading to catastrophic failures of the structure. Timely detection of cracks through monitoring is essential to prevent compromising structural integrity, (see Figure 1.1 and Figure 1.2). Thus, effective monitoring of fatigue or structural health becomes imperative to ensure longevity and safety of the structure.

Figure 1.1: Crack caused by fatigue in a joint [19].

For example, offshore wind technology, while promising, often requires substantial financial support due to its capital-intensive nature [48]. Implementing cost reduction strategies is essential for its sustainable development [48]. Findings from a case study by Vieira et al. [48] suggest that installing SHM systems on offshore wind support structures can optimize maintenance strategies, shifting from preventive to predictive maintenance. This approach not only reduces operational costs but also extends the operational life of wind farms [48].

In the realm of structural health monitoring (SHM) techniques, acoustic emission (AE) testing stands out as a critical tool for ensuring the integrity and safety of offshore and marine structures. AE testing is a powerful non-destructive technique, which involves detecting, analyzing, and monitoring the transient stress-induced acoustic waves generated by materials under stress or deformation. When a material is subjected to stress, it undergoes deformation, which results in the release of energy in the form of elastic waves. For instance, the amplitude and frequency of emissions can indicate the type and severity of defects, cracks, or other anomalies which occur within the material or structure [16]. By analyzing these emissions, valuable insights can be gain into the structural health and potential risks.

Figure 1.2: An image depicting a longitudinal stiffener within the deck near the transverse bulkhead, situated within the ballast tank, reveals that the crack initiated from the termination point of the bracket's toe [45].

1.2. Impact of fatigue damage in maritime structures

Accidents stemming from fatigue can lead to abrupt and catastrophic failures. For instance, an oil tanker experienced a rupture due to the brittle propagation of a crack encircling its circumference. This crack originated from a small notch or sharp flaw and rapidly elongated due to heightened stresses at its tip caused by the tanker's movement at sea. Consequently, the crack expanded swiftly, resulting in the complete fracture of the tanker [5].

Figure 1.3: An oil tanker experienced brittle fracture due to the propagation of a crack that extended fully around its girth (Image from book: [5]).

On the evening of March 27, 1980, amidst adverse weather conditions off the coast of Dundee, Scotland, the Alexander L. Kielland semi-submersible drilling rig tragically capsized while housing over 200 workers. With wind gusts reaching 40 knots and waves towering up to 12 meters high, the rig suddenly experienced a ”sharp crack” followed by a significant tilt of 30°. Investigation revealed that a fatigue crack in one of the bracings, specifically bracing D-6, led to the collapse. This crack, traced back to a small 6 mm fillet weld connecting a non-load-bearing flange plate holding a sonar device, was exacerbated by cold cracks in the welds and weakened flange plate, ultimately causing the rig to overturn, claiming the lives of 123 individuals [49].

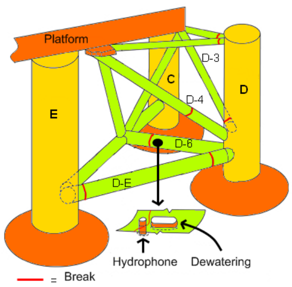

Figure 1.4: Fractures on the Alexander L. Kielland rig [49].

1.3. Scope and objective

In the pursuit of structural integrity and safety assurance, the necessity of regular maintenance is paramount [9]. Nevertheless, conducting routine maintenance operations offshore presents considerable challenges, particularly in detecting and monitoring the development of subsurface cracks that are often not visible. Moreover, the demanding environmental conditions and associated risks significantly escalate maintenance costs.

An effective approach to addressing these challenges is through the Acoustic Emission (AE) technique, which is being widely utilized. Since, it offers real-time damage detection and integrity assessment for materials and structures across diverse operational situations [9]. Its ability to capture stress waves using appropriate sensors enables probing of damage development within materials, providing a more comprehensive understanding of structural integrity and enhancing the effectiveness of fatigue crack monitoring [16, 36]. Given its importance, research on detecting AE and fatigue cracks holds significant engineering relevance.

The principal aim of this literature review is to assess,

> 'What is the current state of knowledge for characterizing damage-induced acoustic emission during fatigue crack growth in metallic materials?'

Additionally, the study seeks to

- Identification of knowledge gaps within the current understanding of the AE monitoring during FCG.
- Proposal of potential research directions to address identified gaps in using different AE parameters.
- Emphasis on enhancing understanding and application of fundamental concepts related to the fatigue crack detection methods. as well as after failure.
- Integration of findings on selected material and load conditions to contribute to the advancement of the AE testing.

1.4. Outline

Chapter 1 of this report provides background information and outlines the motivation behind the chosen research topic. It also delineates the scope and structure of the report.

In Section 2.1, fundamental concepts regarding fatigue failure and relevant theories pertaining to structural health monitoring techniques such as ultrasound waves and acoustic emission are elucidated. This foundational knowledge is essential for comprehending the subsequent sections, namely Sections 2.2 and 2.3.

Section 2.2 delves into the current state-of-the-art concerning the analysis of fatigue crack growth using Acoustic Emission techniques.

Lastly, Section 2.3 deliberates on identified knowledge gaps and proposes potential research directions to address these gaps effectively.

2

Literature Review

2.1. Preliminary knowledge

2.1.1. Fatigue Assessment Concepts

Fundamental Aspects of Fatigue analysis

In material science, fatigue is a failure mechanism that involves the cracking of materials and structural components due to cyclic (or fluctuating) stress. One of the intriguing factors about fatigue development is that fatigue cracks can be initiated and propagated at stresses well below the yield strength of the material of construction [5].

There are three stages in which fatigue failure occurs - crack initiation, crack propagation and failure (see Figure 2.1 for all of the stages of the fatigue lifetime and its factors) [38]. According to Schijve [38], a crucial aspect to consider is that the fatigue life leading to failure comprises two distinct phases: the crack initiation period and the crack growth period. It is essential to distinguish between these phases as certain surface conditions significantly impact the initiation period, whereas they have minimal influence on the subsequent crack growth phase [38]. These two phases are discussed in Section 2.1.1 and Section 2.1.1 respectively.

Fatigue prediction methods differ between two periods, focusing on crack initiation and crack growth [38]. Stress concentration factor (K_t) is crucial for predicting crack initiation, while stress intensity factor (K) is used for predicting crack growth. K_t quantifies stress concentration in a material, while K represents the ratio of maximum stress at the crack tip to the nominal applied tensile stress.

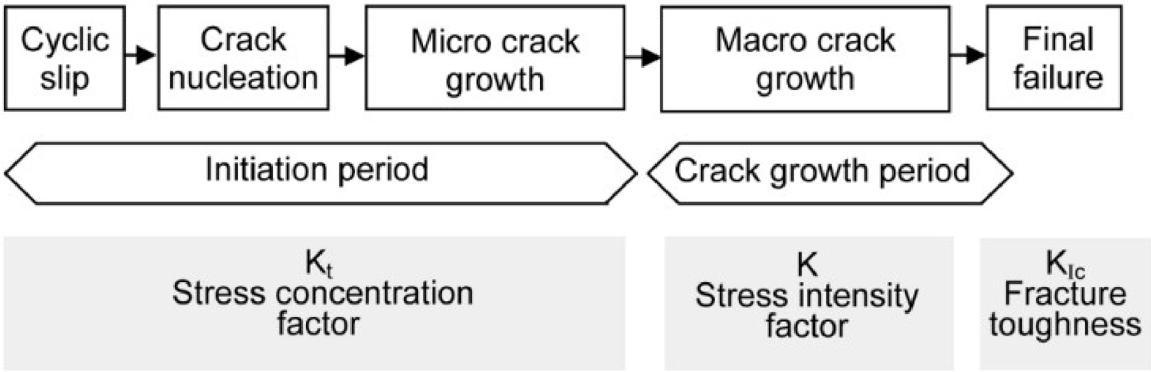

Figure 2.1: Different phases of the fatigue life and relevant factors [38].

Fatigue cracks typically initiate on a component's surface at points of stress concentration. The region of a fracture surface that formed during the crack propagation phase can be distinguished by two types of markings known as beachmarks and striations. Beachmarks form on components experiencing stress interruptions, often visible to the naked eye, while fatigue striations are microscopic features, each believed to represent the crack tip's advance distance over a single load cycle, as shown in Figure 2.2,[5].

Furthermore, fatigue failures can manifest in various forms, with mechanical fatigue and thermal fatigue representing two primary categories, as outlined by Callister Jr and Rethwisch [5]. Corrosion fatigue results from the combined effects of chemical attack and mechanical fatigue [5]. While corrosion fatigue also holds significance in the offshore and marine industry, resource constraints necessitate a focus on mechanical fatigue in this study. Therefore, this study specifically targets mechanical fatigue, given its crucial role in the context of offshore structures subjected to severe marine conditions.

As per Callister Jr and Rethwisch [5], fatigue behaviors can be categorized into two distinct domains. One domain is characterized by relatively high loads that induce both elastic and plastic strain during each cycle. Consequently, fatigue life spans are relatively short within this domain, termed as low-cycle fatigue, typically occurring at less than approximately 10^4 to 10^5 cycles. Conversely, at lower stress levels where deformations remain entirely elastic, longer life spans are observed. This phenomenon is referred to as high-cycle fatigue, as it requires a relatively large number of cycles to induce fatigue failure. High-cycle fatigue is distinguished by fatigue life spans exceeding approximately 10^4 to 10^5 cycles. This study zeroes in on High-Cycle Fatigue, which denotes failure occurring over millions of cycles due to stresses lower than the yield strength of materials. Moreover, cyclic stresses are typically categorized into three general stress-versus-time cycle modes: reversed, repeated, and random. Reversed and repeated modes are defined in terms of mean stress, range of stress, and stress amplitude [5].

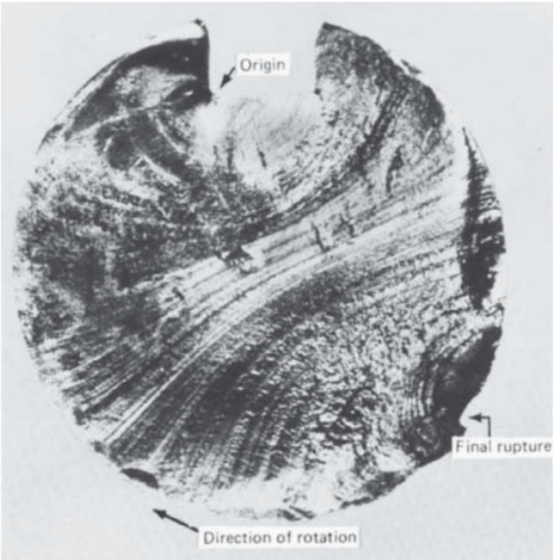

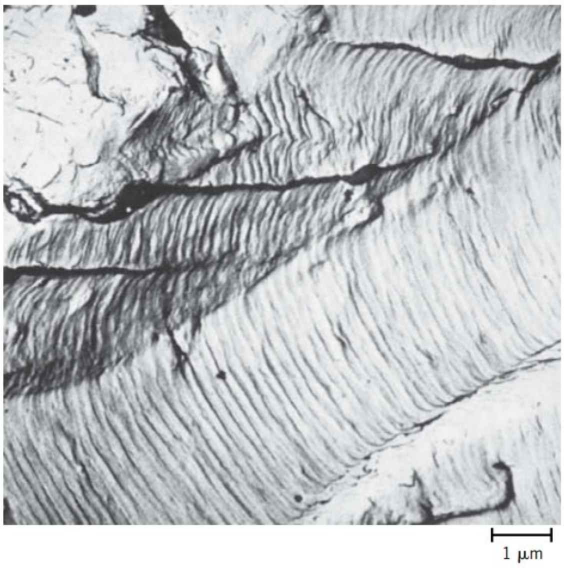

Figure 2.2: Fracture surfaces [5].

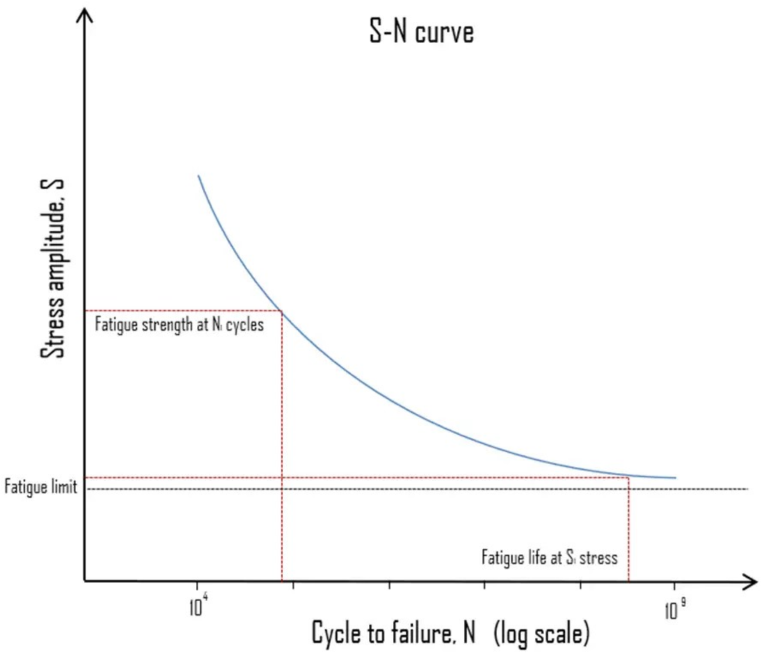

Figure 2.3: S-N curve example [11].

The S-N curve, as shown in Figure 2.3, is a graphical representation of test data plotting stress (usually stress amplitude) against the logarithm of the number of cycles to failure. For many metals and alloys, stress decreases progressively with an increasing number of cycles until failure occurs, with fatigue strength and fatigue life serving as parameters to characterize the fatigue behavior of these materials. However, for certain metals like ferrous and titanium alloys, stress eventually stabilizes and becomes independent of the number of cycles, leading to the concept of fatigue limit to express their fatigue behavior [5, 38].

In terms of definitions:

Table 2.1: Definitions

Fatigue limit	the stress level below which fatigue failure will not occur.
Fatigue strength	the stress level at which failure will occur for a specified number of cycles.
Fatigue life	the number of cycles required to cause failure at a specified stress level.

Fatigue crack initiation in metallic materials

Crack initiation in metallic materials is a phenomenon intricately tied to cyclic slip and surface conditions. Fatigue crack initiation and subsequent crack growth stem from cyclic slip, which involves cyclic plastic deformation or dislocation activities. This process occurs at stress amplitudes below the yield stress, primarily affecting a limited number of grains, particularly those at the material surface where constraints on slip are lower. The cyclic shear stress responsible for slip is not uniformly distributed throughout the material, varying between grains due to factors such as grain size, shape, crystallographic orientation, and elastic anisotropy [38].

For example, Jesus et al. [21] conducted a comparison of fatigue performance between S355 and S690 steel grades. Their findings underscore the superior fatigue resistance of S690 steel, attributed to its finer grain structure. Grain boundaries serve as effective crack arrestors, as they impede slip band development, thereby slowing down the progression of cracks. Consequently, materials with smaller grain sizes exhibit more crack retardation [21].

At the material surface, conditions are conducive to cyclic slip, leading to the creation of slip steps, or slip bands. These features, formed during cyclic loading, expose fresh material to the environment, which often results in the immediate formation of an oxide layer. The cyclic loading and unloading induce strain hardening in the slip band, which, upon unloading, results in a larger shear stress in the reversed direction, promoting further slip in subsequent cycles, as shown in Figure 2.4. This process, while seemingly reversible, is hindered by factors such as the adherence of oxide layers to the material surface and the irreversibility of strain hardening [38].

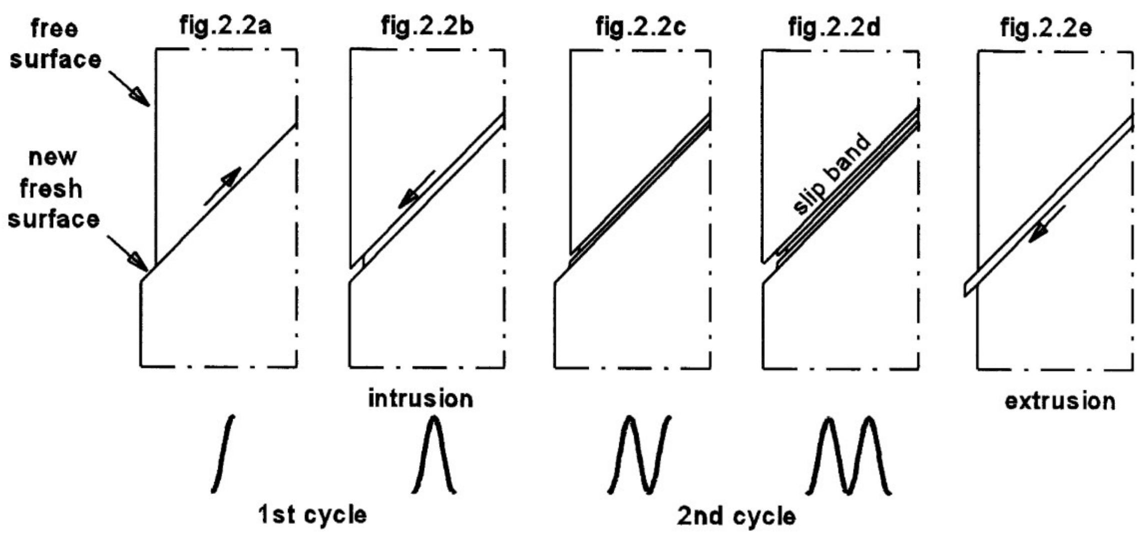

Figure 2.4: Cyclic slip [38].

Surface characteristics play a critical role in facilitating fatigue crack initiation. Inhomogeneous stress distribution due to geometric discontinuities, surface roughness, corrosion pits, and fretting fatigue damage contribute to stress concentration at the material surface. These factors create favorable conditions for crack initiation, particularly along slip bands. Thus, fatigue crack initiation emerges as a material surface phenomenon, influenced by both microstructural factors and surface conditions, ultimately dictating the initiation and propagation of fatigue cracks in metallic materials.

Previous research has not reached a consensus regarding the transition from the initiation phase to the crack growth phase. As noted by Schijve [38], a clear definition of this transition remains elusive. While quantitative characterization poses difficulties, a qualitative description suggests that the initiation period concludes when micro-crack growth becomes independent from surface conditions of the material [38].

Fatigue crack growth

The growth of microcracks within an elastically anisotropic material with a crystalline structure triggers an inhomogeneous stress distribution at the microscale, accentuating stress concentrations at the microcrack tip [38]. Consequently, activation of multiple slip systems may occur due to the complex interplay of constraints on slip displacements within neighboring grains [38]. As microcracks propagate into adjacent grains, the constraint on slip displacements intensifies, necessitating accommodation of slip on multiple slip planes rather than a single plane. This deviation from the initial slip band orientation often results in microcrack growth perpendicular to the loading direction, as depicted in Figure 2.5, [38].

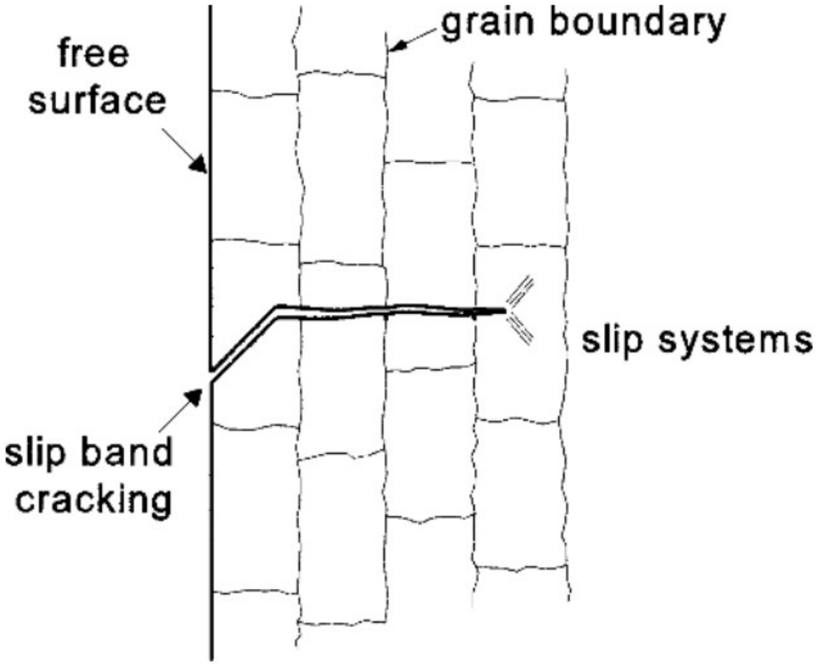

Figure 2.5: Microcrack growth [38].

The dependence of microcrack growth on cyclic plasticity implies the existence of barriers to slip, which can act as thresholds for crack propagation. Observations, as illustrated in Figure 2.6, reveal a fluctuating crack growth rate as the crack tip traverses grain boundaries. Notably, the crack growth rate decreases upon approaching the first grain boundary, increases upon entering the next grain, and then decreases again near the subsequent grain boundary. However, upon surpassing numerous grain boundaries, as depicted in Figure 2.6, the crack front maintains coherence, preventing significant variations in crack growth rate along its trajectory. Consequently, crack growth becomes a continuous process along the entire crack front, resembling a semi-elliptical line. The rate of crack propagation is contingent upon the material's crack growth resistance, rendering surface-related factors irrelevant and emphasizing the transition of crack growth from a surface phenomenon to a bulk property-dependent process.

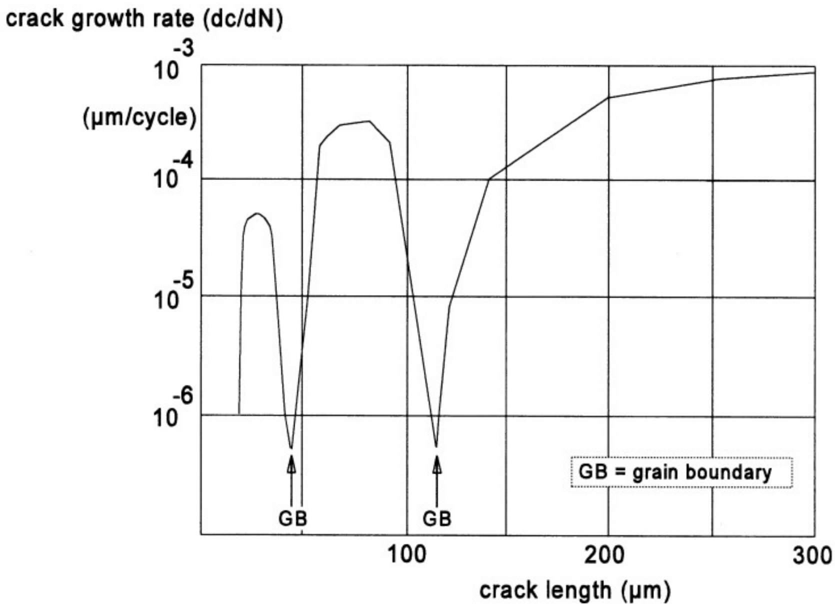

Figure 2.6: Effect of grain boundary on crack growth in an Al-alloy [38, 4].

Several previous studies have established that during fatigue crack growth, the crack growth rate can be described by the Paris-Erdogan equation (see Figure 2.7) [9, 31, 50, 13, 35, 34]:

$$da/dN = C(\Delta K)^m \tag{2.1}$$

where a is the crack length, da/dN is the crack growth rate, N is the number of load cycles, C and m are material constants, and ΔK is the stress intensity factor range that is related to the applied load, crack length and material geometry.

Equation (2.1) can also be expressed as [9, 35, 34]:

$$\log(da/dN) = m \log \Delta K + \log C \tag{2.2}$$

The Equation (2.2) can be used as a means to establish a relationship between the fatigue crack growth rate and acoustic emission count rate (see Equation (2.13)), with a more comprehensive discussion provided in Section 2.2.1.

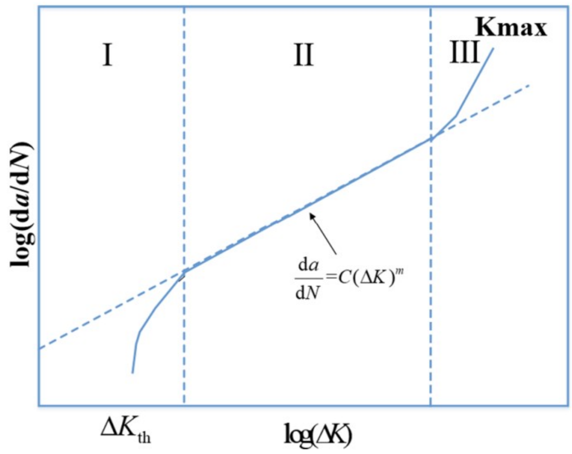

Figure 2.7: Fatigue crack growth stages and typical relationship between log(da/dN) and log(ΔK) [25].

2.1.2. Acoustic Emission

General aspects of AE

Acoustic Emission is an elastic wave generated by the rapid release of energy from sources when a crack or deformation occurs within a material subjected to stress [16]. Consequently, when an irreversible phenomena or process occurs in the material, it triggers the release of these transient elastic waves. These waves are then detected and monitored using the AE technique [16].

In other words as expressed by Carrasco et al. [7], when a solid material is exposed to operational conditions surpassing its mechanical strength, its internal structure experiences dislocations and fractures, releasing a specific amount of energy. This energy propagates through the medium in the form of mechanical waves, recognized as acoustic emissions (AEs).

Given that AE is generated by stress waves within a material under stress, it may originate from various sources which can be classified as either primary or secondary. Primary AE sources are generated in metal can be due to micro and macro cracks initiating and propagating, micro-dynamical events such as twinning, movement of dislocations, fracture of brittle inclusions, chemical reaction like corrosion and phase transformation due to strain effects caused by change in volume [9, 16]. However, it is important to note that there are also secondary AE sources, which are associated with crack closure processes, leading to rubbing and fretting of fracture surfaces [52, 3, 42, 16, 14].

Stress waves propagation

AE monitoring involves the transmission of high-frequency stress waves inducing temporary deformations in the medium, characterized by their rapidly decaying amplitude, reflecting their transient nature. According to Carrasco et al. [7], AE waves within materials manifest in four types. Among them, two arise within the internal structure of the material, namely longitudinal P-waves and shear S-waves, while the other two are surface waves, known as Rayleigh waves and Love waves, shown in Figure 2.8. A single AE source may generate one or multiple of these waves, which can coexist and interact [16, 7].

For instance, when reaching the surface of the material internal P-waves can produce Rayleigh waves [7].

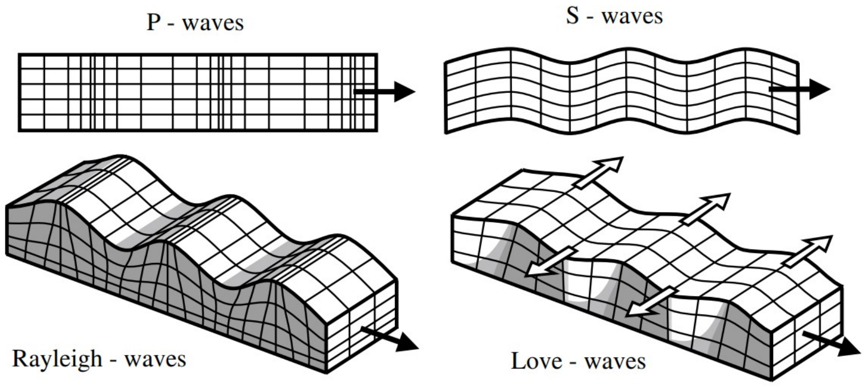

Figure 2.8: AE wave types [7].

The typical procedure for AE monitoring includes positioning a sensing element directly on the surface. Most AE sensors utilize the piezoelectric effect, where certain materials generate a voltage when subjected to mechanical stress [7].

AE senors

Carrasco et al. [7] mentions two groups of piezoelectric AE sensors: BAW sensors (bulk acoustic waves) that detect all AE wave types. For instance, the resonant type relies on the natural frequency of the piezoelectric sensor [7]. Additionally, SAW sensors (surface acoustic waves) are mentioned, primarily used to measure surface Rayleigh waves [7]. Typically, the AE signals obtained are pre-amplified and subsequently sampled using high-speed analog-to-digital converters, ideally operating above 1 MHz [7].

In the present research, resonant type sensors will be employed to detect and monitor AE waves. Therefore, any stress wave emitted within the operating frequency range will be recorded as AE signals.

Characteristics of AE signal

AE signals can be classified into two different types: continuous and burst. These two basic types cover wide range of energy levels and frequencies. Continuous emission is measured by root mean square (RMS) voltage, in other words, it is a sustained signal from rapidly occurring emission events. In burst type, signal burst in a field of continuous emission and come from individual emission events, as shown in Figure 2.9. For characterizing burst type AE signals, several threshold-dependent parameters are used. Threshold is the voltage level set in the instrument to minimize low-amplitude noise from AE signals [27, 7, 16].

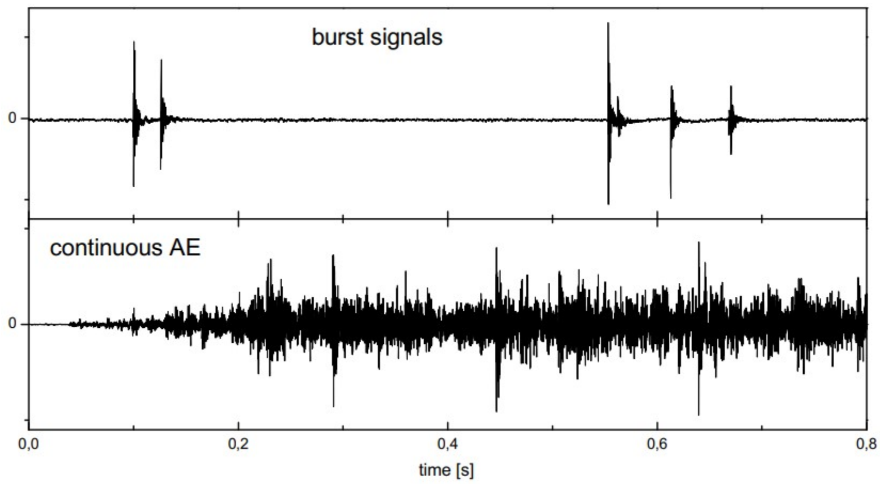

Figure 2.9: An illustration of burst signals contrasted with a continuous emission of acoustic waves [16].

Analysis of AE signals

There are two fundamental types of analysis for AE signals, namely, waveform-based analysis and parameter-based analysis.

Analysis of acoustic emission (AE) signals is crucial for understanding the underlying processes in materials and structures. There are two fundamental approaches to analyzing AE signals: parameter-based analysis and signal-based analysis [41, 16].

Parameter-based analysis involves extracting a set of characteristic parameters or features from the AE signal and storing them, rather than storing the entire waveform [16]. These parameters, such as arrival time, maximum signal amplitude, rise time, and signal duration, provide essential information about the AE events [16]. This approach is cost-effective, can be performed with as few as one sensor, and is suitable for real-time monitoring [16]. However, it offers only a limited view of the physics of AE sources and may be influenced by recording settings, making comparisons between datasets challenging [16].

On the other hand, signal-based analysis involves recording and storing the complete AE waveforms [16]. This approach allows for more comprehensive analysis but is typically performed in a post-processing environment, not in real-time [16]. Signal-based analysis includes waveform analysis, where entire waveforms are analyzed and compared over time, and quantitative AE analysis, which aims to accurately describe the nature of each AE source [16]. While quantitative AE analysis offers high accuracy, it requires sophisticated equipment and computation, limiting its practical application mostly to laboratory settings [16].

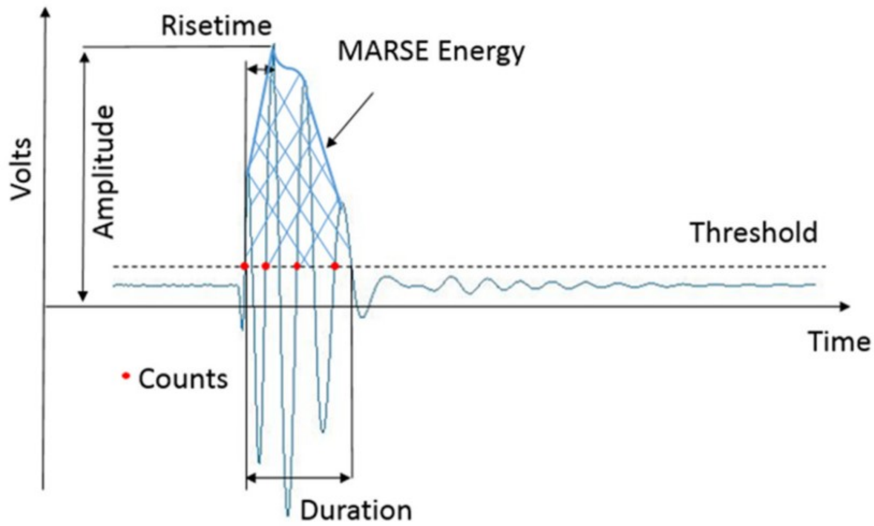

Figure 2.10: Commonly used AE parameter [41].

To delve deeper into parameter-based analysis, some commonly utilized AE parameters and their definitions, as provided by various research sources [16, 7, 9, 41], are illustrated in the table below (see Table 2.2). The choice between parameter-based and signal-based analysis depends on the specific application and requirements. In the context of this research study, parameter-based analysis is suitable for simple monitoring tasks and real-time applications.

Table 2.2: Definitions of some commonly used AE parameters [7, 9, 41]

AE Parameters	Explanation
Counts (η)	Number of excursions above the threshold. It is a function of the threshold and frequency. It is influenced by the magnitude of the AE source, as well as on the acoustic properties of the sample and the sensor.
Peak amplitude	Highest measured voltage or amplitude, expressed in decibels (dB). It is directly related to the energy in the AE signal.
Duration (D)	Time elapsed above the threshold i.e. time difference between first and last threshold crossing. The duration is dependent on the magnitude and frequency of the AE source. It can be utilized to identify different types of emission source, thereby facilitating the filtration of noise.
Rise time	Time interval between first threshold crossing and the signal peak. It is related to the propagation of the wave between the source and the sensor. Rise time is employed to assess and filter out noise.
MARSE	Measured Area under the Rectified Signal Envelope. Tells us about the energy levels. This is a measure of the signal strength. Sensitive to duration and the amplitude. But does not take into account the user defined threshold and operating frequency.

Based on the above mentioned features, some additional useful parameters can be deduced, see Table 2.3.

Table 2.3: Definitions of other useful AE parameters [7, 9, 41, 53]

AE Parameters	Explanation
Average Frequency (AF)	Computed in time domain, and is derived as the ratio of the total number of counts over the duration of the waveform, measured in kHz.
Peak Frequency (PF)	This waveform-based feature is determined in real-time through the fast Fourier transform (FFT) of recorded waveforms. It denotes the frequency exhibiting the highest magnitude in the FFT.
Centroid Frequency (CF)	Also, a waveform-based feature which denotes the centroid of the FFT.
Root mean square (RMS)	The square root of the average of the squared values of the signal.
Rise Angle (RA)	Quotient between rise time and amplitude
True energy	The integral of the squared signal envelope.
Absolute energy (U)	It accurately represents the energy of the AE impact signal, indicating the extent of internal damage. It is measured in attoJoules (aJ), where 1 aJ equals 10^{-18} J.
Information entropy	Also known as Shannon's entropy of AE waveform. It measures the disorder or uncertainty of the probability amplitude distribution.
Kurtosis	It refers to the measure of the "tailedness" of the AE signal.
Crest factor	It refers to the ratio of the peak value to the RMS value.

Calculation

Crack growth rate [9]:

$$\frac{da}{dN} = \frac{(a_{i+1} - a_i)}{(N_{i+1} - N_i)} \tag{2.3}$$

where, a_i represents the ith crack length, and N_i denotes the ith fatigue cycle. The calculated da/dN signifies an average rate, determined by dividing the increment in crack size $(a_{i+1} - a_i)$ by the increment in fatigue cycles $(N_{i+1} - N_i)$.

Average Frequency [7, 16]:

$$AF = \frac{\eta}{D} \tag{2.4}$$

Here, η is counts and D is duration.

Peak Frequency [16]:

$$PF = \max(H(f)) \tag{2.5}$$

PF represents the frequency with the highest magnitude in the FFT, and $H(f)$ the magnitude of the FFT.

Centroid Frequency [16]:

$$CF = \frac{\int_0^f fH(f)df}{\int_0^f H(f)df} \tag{2.6}$$

where f represents the frequency, and $H(f)$ is the magnitude of the FFT.

MARSE energy [7]:

$$MARSE = \int_{0}^{D} e(t)dt \tag{2.7}$$

where $e(t)$ is the envelope of the AE signal and t is time.

True energy [7]:

$$\text{True energy} = \int_{0}^{D} e^2(t)dt \tag{2.8}$$

where $e(t)$ is the envelope of the AE signal and t is time.

Root Mean Square value [7]:

$$RMS = \sqrt{\frac{\sum_{i=1}^{n} y_i^2}{n}} \tag{2.9}$$

here, y_i is the amplitude of the AE in an amplitude vector.

Rise Angle [7, 16]:

$$RA = \frac{RT}{A} \tag{2.10}$$

where RT is rise time and A is the amplitude.

Absolute Energy rate [1]:

$$\frac{dU}{dN} = \frac{B \cdot t \cdot K_{max}^2}{E'} \cdot \frac{da}{dN} \tag{2.11}$$

where B represents a proportional constant specific to the material, N denotes the number of load cycles, and K_{max} is defined as $\Delta K/(1-R)$, where ΔK stands for the stress intensity range and R represents the load ratio [1]. Additionally, E' is equivalent to Young's modulus E under plane stress conditions and to $E/(1-\nu)^2$ under plane strain conditions, where ν stands for Poisson's ratio [1]. Furthermore, dU/dN and da/dN correspond to the rates of AE absolute energy and crack growth, respectively [1].

Shannon's entropy or Information entropy [40, 23]:

$$I = -c \sum_{i=0}^{n} P(X_i) \ln 1/P(X_i) \tag{2.12}$$

where $X_i = x_1, x_2, ..., x_n$ represents a random variable, $P(X_i)$ denotes the probability distribution of the random variable, I stands for information entropy, and c is a constant considered to be unity in the study by Karimian, Modarres, and Bruck [23]. Additionally, the unit of AE information entropy used is 'nats' since in Equation (2.12) the natural logarithm is used.

2.1.3. Section highlights

Based on the preliminary understanding, we have acquired a foundational understanding of fatigue crack initiation and propagation. Furthermore, we have gained proficiency in the fundamental principles of the acoustic emission (AE) technique, notable for its non-contact nature and capability for real-time monitoring. Equipped with this knowledge, we may now explore approaches designed to establish relationships between fatigue crack propagation and AE signals. Additionally, by leveraging different AE parameters, the transition between various stages of fatigue damage can be tracked. Thus, in order to provide more insight, Section 2.2 will provide an in-depth exploration of the state-of-the-art in AE monitoring.

2.2. State-of-the-art

2.2.1. Acoustic Emission monitoring of fatigue

AE-FCG correlation

According to Roberts and Talebzadeh [35], filtering acoustic emission data for a narrow band containing the fatigue crack using source locating software allows just emissions from the crack's vicinity to be recorded. These separated AE events increase consistently with number of cycles, however for small percentages of the fatigue load range which is close to the peak load. The results show that log (dη/dn) and log K have an almost linear connection for all steel specimens and welded steel girders. This relationship can be expressed by an equation resembling the Paris–Erdogan Equation (2.2):

$$\log(d\eta/dN) = p\log\Delta K + \log B \tag{2.13}$$

where η is the number of counts and, B and p are constants for particular material. This is worth noting because this relation, based on the use of AE count rate parameter, has been used by several authors [35, 34, 9, 24].

The study by Chai et al. [9], Roberts and Talebzadeh [35], and Keshtgar, Sauerbrunn, and Modarres [24], has shown that by eliminating $\log\Delta K$ from Equation (2.2) and Equation (2.13), the following relationship can be obtained between $\log(da/dN)$ and $\log(d\eta/dN)$:

$$\log(da/dN) = \frac{m}{p}\log(d\eta/dN) + \log C - \frac{m}{p}\log B \tag{2.14}$$

By substituting equations,

$$\frac{m}{p} = q, \tag{2.15}$$

$$\log C - \frac{m}{p}\log B = \log D, \tag{2.16}$$

Equation (2.14) can be simplified to yield:

$$\log(da/dN) = q\log(d\eta/dN) + \log D \tag{2.17}$$

The results of study [9] found an approximate linear correlation which can be expressed similarly as Equation (2.17),

$$\log(da/dN) = q\log X + \log D \tag{2.18}$$

where q and D are constants which can be determined by experiments, while X indicates the growth rate of AE data within a certain number of fatigue cycles N. According to Chai et al. [9], X represents the rate of various AE parameters such as amplitude rate, count rate, energy rate, rise angle (RA) rate and root mean square (RMS) rate [9]. This approach enables the correlation of crack growth rate with the rates of different AE parameters.

AE generated during crack growth

In 1987, Scruby also showed that the acoustic emission due to the elastic fracture at the crack tip is much more detectable than the other sources Scruby, Baldwin, and Stacey [39] conducted a research aiming to characterise AE generated from crack extension during fatigue crack growth in 7010 aluminium alloy [14]. The research found that crack extension is not the dominant source of AE in fatigue crack formation [14]. This is due to ductile tearing of the material occurs in every loading cycle, resulting in a much lower rate of recorded AE, averaging about 1 AE signal in 20 cycles [39, 14].

However, Morton, Harrington, and Bjeletich [29] found that the correlation between AE count rate and the stress intensity range (ΔK) was better than the correlation between AE count rate ($d\eta/dN$) and crack growth rate (da/dN) or correlation of crack growth rate (da/dN) with the stress intensity range (ΔK). This implies that the observed AE signals were more closely associated with the plastic volume near the crack tip [29].

Several studies have explored the sources of AE during plastic deformation [26, 39, 37, 6, 14]. In Table 2.4, various sources of AE observed in these studies are illustrated. For instance, a study conducted by McBride, MacLachlan, and Paradis [26] aimed to quantitatively explore the connection between acoustic emission (AE) and fatigue crack growth in 7075 aluminum. The study revealed that burst emissions resulted from brittle fracture of inter-metallic inclusions in 7075-T6 aluminum, aligned with prior findings. AE signal amplitude correlated quantitatively with inter-metallic inclusion size distribution, aiding in predicting AE signals from crack growth [26]. Additionally, the study revealed that a reduction in material strength eliminated burst AE activity, emphasizing the role of surrounding material strength in generating localized stresses [26].

Fretting of crack surfaces can occur during fatigue crack propagation and may be influenced by crack closure [14]. According to McBride, MacLachlan, and Paradis [26] and Yu et al. [53], AE signals from this source are often considered to be of the continuous type. Furthermore, Han et al. [17] conducted an investigation into the AE behaviors and source mechanisms during fatigue crack growth in both the base metal and weld of Q345 steel. The study also examined fatigue properties and acoustic emission characteristics based on microstructural and fractographic observations [17]. A comprehensive analysis was provided on the source mechanisms of acoustic emission throughout three distinct stages of fatigue, namely crack initiation, plastic activities ahead of the crack tip, and shearing of ligaments between micro-voids and micro-cracks.

Daniel et al. [12] also conducted a similar investigation to analyze AE generation in aluminum and steel coupons across different phases of the fatigue loading cycle. They identified several distinct categories of AE signals, associating them with plasticity, crack closure, and the transition from plain strain to plain stress during crack propagation [14].

Table 2.4: Summary of frequency content across various AE sources of metallic materials [51].

Authors	Metallic Material	Specimen Type	Sources	Loading Frequency
Han et al. [18]	AZ31 magnesium alloy	6*CT	Twinning Crack extension	2 Hz, 10 Hz, and 20 Hz.
Roberts and Talebzadeh [34] and Roberts and Talebzadeh [35]	S275JR grade steel	CT, T-section girders	Crack extension	1 Hz
Chai et al. [9]	2.25Cr1Mo0.25V steel	CT	Fatigue crack growth	15 Hz
Yu et al. [53]	ASTM A572G50	CT	Crack extension	1 Hz
Yao et al. [51]	Al2024-T3	4*coupon	Crack opening, Crack extension, Crack surface closure	4 Hz
Chai et al. [10]	316LN stainless steel	6* single edge notch (SEN)	Crack growth	–
Keshtgar, Sauerbrunn, and Modarres [24]	Al7075-T6 and Ti-6Al-4V	15 * CT	Crack growth	2 Hz, 5 Hz, 7 Hz and 10 Hz
Gagar, Foote, and Irving [14] and Gagar, Foote, and Irving [15]	2014 T6 aluminium alloy	11*SEN and 1 *Mid-crack Tension (MT)	Crack initiation, Crack growth	2 Hz
McBride, MacLachlan, and Paradis [26]	7075-T6 aluminium	SEN	Crack growth, Brittle fracture of inter-metallic inclusions	1 Hz

AE behaviour in various fatigue stages

The study by Han et al. [17] examined the characteristics of AE during fatigue crack growth revealed three distinct AE stages across all specimens, as depicted in Figure 2.11, [17]. In Stage 1, AE counts showed rapid growth at the onset of tests, followed by a noticeable decline in growth rate during Stage 2, where AE activities were sporadic and weak over an extended period, encompassing 80% of the total fatigue life. Stage 3 saw an increase in AE counts until the completion of tests. Investigations into AE source mechanisms for these stages in micro-alloyed steel and its welds revealed that Stage 1 corresponded to fatigue crack initiation, while Stage 2 primarily involved plastic activities within the plastic zone ahead of the crack tip. Stage 3 was attributed to the shearing of ligaments between micro-voids and micro-cracks, indicative of fatigue crack growth.

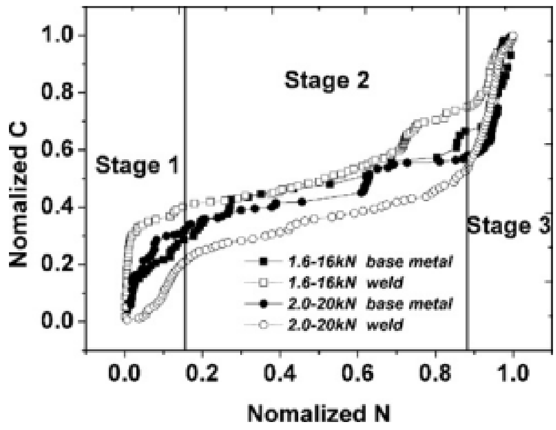

Figure 2.11: Normalized AE counts C versus Normalized fatigue cycles N for the base metal and weld under the peak loads of 16 kN and 20 kN [17].

Han et al. [17] further associated the transition from Stage 2 to Stage 3 with a fracture mode transition, characterized by facets and striations observed on fracture surfaces. This transition suggests a shift in AE source mechanisms from plastic activities to ligaments shearing between micro-voids and micro-cracks. While the transition from stable to unstable crack growth defined by linear elastic fracture mechanics (LEFM) also involves a change in fracture mode, the AE method appears to be more sensitive to this fracture mode transition [17].

2.2.2. Characterization of AE from fatigue

Quantitative correlation

According to Grosse et al. [16], the objective of quantitative AE analysis is to provide an accurate description of each AE source's characteristics, rather than making conclusions based solely on the effects observed at sensor locations distant from the source.

Chai et al. [9] demonstrated that analyzing multiple AE parameters effectively characterized FCG behavior. This study emphasized the importance of calculating various time domain parameters (such as amplitude, count, energy, information entropy, RA, RMS, kurtosis, and crest factor) and frequency domain parameters (such as centroid frequency) for qualitatively assessing crack growth and quantitatively correlating it with AE data.

Furthermore, Shi et al. [41] proposed the use of the fitted power law distribution of AE parameters for monitoring FCG in Hadfield steel, unlike existing AE fatigue monitoring methodology, which relies solely on the analysis of AE parameter trends. However, in this study, AE absolute energy and duration values were not fitted well with the power law.

Keshtgar, Sauerbrunn, and Modarres [24] investigated the effectiveness of acoustic emission (AE) techniques in detecting crack growth during high cycle fatigue tests on aluminum alloy. They introduced an AE intensity index, which showed a linear relationship with crack growth. The study demonstrated a method for detecting crack initiation using AE monitoring, employing filtering techniques to reduce noise. The AE intensity index considered factors like count, amplitude, and rise time, showing promising results for detecting crack initiation and small crack growth. Further research is needed to explore different weighting features for intensity calculation and establish a probabilistic estimate of crack length probability density function at crack initiation.

The diverse AE parameters and loading conditions utilized in several studies are displayed in Table 2.5.

Table 2.5: Summary of various AE parameters and loading conditions used in experiments.

Authors	AE Sensors	AE Parameters	Load range / Peak load	Load ratio
Han et al. [18]	2*R15	Count	3 kN	0.1
Roberts and Talebzadeh [34] and Roberts and Talebzadeh [35]	4 * miniature Nano 30 sensors, with 280 kHz resonant frequency	Count	$1 \leq x_{min} \leq 24$ – $10 \leq x_{max} \leq 80$ kN	0.1, 0.3, 0.5 and 0.7
Chai et al. [9]	1 * R15a	Amplitude, Count, Energy, Information entropy, Rise time, Duration, Rise Angle (RA), Root mean square (RMS), Kurtosis, Crest factor, Centroid frequency	26 kN	0.5
Yu et al. [53]	5 * R151-AST	Absolute energy, Count	-	0.02 and 0.1
Yao et al. [51]	4 * wideband PKWDI	Count	6.7-53.3 MPa, and 26.7-53.3 MPa	0.125 and 0.5
Chai et al. [10]	1* R15a	Count, Energy, Entropy, Amplitude, Peak frequency, Centroid frequency	4 kN	0.1, 0.3, and 0.5
Keshtgar, Sauerbrunn, and Modarres [24]	1* 100–900 kHz wideband	Count	2.22 kN and 4 kN	0.1, 0.3, and 0.5
Gagar, Foote, and Irving [14] and Gagar, Foote, and Irving [15]	2*Guard Sensors	Number of hits, Count, Absolute energy	52.2 MPa and 27 MPa	0.1 and 0.5
McBride, MacLachlan, and Paradis [26]	Dunegan Endevco S9201 transducer	Amplitude	30.18 – 60.36 MPa	1 Hz

Qualitative correlation

When AE events are captured using one or more sensors, and a set of parameters is extracted from the signal and stored without retaining the signal itself, this process is commonly known as qualitative AE analysis or parameter-based AE analysis [16].

Aggelis, Kordatos, and Matikas [1] introduced a method utilizing the rise angle (RA) of AE waveforms to assess damage accumulation and fracture mode changes in metal plates. They observed a significant increase in RA value before final fracture, as shown in Figure 2.12, signaling the transition from tensile to shear fracture modes [9].

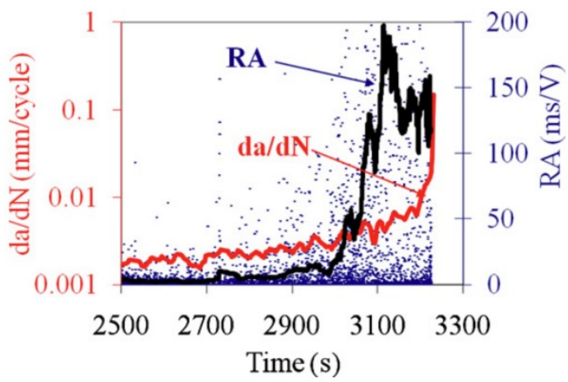

Figure 2.12: Time plot of crack growth and RA [1].

Chai, Zhang, and Duan [8] introduced AE entropy, a new qualitative parameter derived from Shannon's entropy or information entropy, for damage monitoring in AE non-destructive testing. Unlike traditional parameters, AE entropy is independent of threshold settings, providing a more accurate reflection of original AE waveforms. Tests on different materials validated its effectiveness in distinguishing damage stages and identifying critical damage, particularly through sudden increases indicating crack initiation and rapid crack growth. Further research is required to fully understand and integrate AE entropy into AE data acquisition systems.

Tanvir et al. [46] conducted a comparison between AE entropy and count, confirming that the threshold independence of AE entropy is due to its computation method, which considers all possible discrete voltage values in each waveform [46].

Additionally, Karimian, Modarres, and Bruck [23] investigated using information entropy of acoustic emission (AE) signals to detect fatigue crack initiation in AA7075-T6 aluminum alloy. They found that information entropy provided more accurate and earlier identification of fatigue crack initiation compared to traditional AE parameters like count and energy. The study demonstrated that minimum information entropy values preceded macrocrack formation, and a rapid increase in cumulative information entropy reliably indicated fatigue crack initiation. Furthermore, they observed that the amplitude of signals associated with minimum information entropy values fell within a consistent range, independent of loading conditions.

Yu et al. [53] conducted a study for predicting crack growth behavior in steel bridges using acoustic emission (AE) signals, particularly focusing on the correlation between AE absolute energy rate and crack growth rate. Furthermore, the study suggests that AE absolute energy rate may be a more suitable predictor than count rate for estimating fatigue life and predicting crack length in steel bridge structures.

2.2.3. Validation of AE crack detection

According to Zhao et al. [54], a range of advantages and drawbacks exist within the popular fatigue crack length measurement methods found in literature. These methods encompass various approaches, including visual observation, acoustic emission, compliance, potential difference, eddy current, strain-based, and image processing methods. While some methods are restricted to metallic specimens or offer limited accuracy, certain techniques like digital image correlation, potential drop, acoustic emission, and ultrasound methods enable real-time measurements. For example, Vanlanduit et al. [47] employed a hybrid digital image correlation (DIC) technique to detect edge characteristics of metal fatigue cracks.

Considering the DIC technique has advantages over foil crack gauges and traditional crack mouth opening displacement (CMOD) gauges, Pullin et al. [32] tested monitoring of crack growth to allow a comparison with the detected and located AE signals. However, monitoring crack had to be non-contact with the specimen to avoid frictional sources of AE in the crack region, preventing the use of CMOD gauges. Due to the fact that these traditional methods can introduce AE sources into the experiment either through frictional noises from the CMOD contact point with the specimen or glue cracking in foil gauges [32].

DIC represents a non-contact optical method utilized for strain and displacement measurement. Through DIC, high-speed, full-field experimental data regarding structural deformations can be acquired. This technique, which doesn't require physical contact, is particularly advantageous for analyzing flexible materials. Its implementation entails employing digital cameras to capture a sequence of images depicting a surface adorned with a randomized speckle pattern [28].

The potential drop method is an electrical technique that involves passing an electric current through a material or component and then measuring the resulting potentials at designated locations relative to a crack. This method is frequently employed for the continuous or instantaneous monitoring of cracks in conductive materials [3]. Based on the understanding that a crack, which interrupts the continuity of the conductive material, will induce significant alterations in the electrical potential field within the component. Therefore, crack growth can be monitored by establishing calibration curves for different crack scenarios [33].

2.2.4. Section highlights

This section has assessed the current state-of-the-art in detecting cracks within materials using AE method. Efforts have been made to establish a correlation between AE parameters and FCG rates, revealing a better understanding of interpretation of AE data. Similarly, the AE generated from different sources was also observed during FCG, to characterize AE sources related to various mechanisms such as crack growth, crack closure, fretting of the surface, etc. Nonetheless, examining the characteristics of AE during FCG revealed eminent changes in AE activities in across different stages of fatigue life. Quantitative and qualitative correlation of few AE parameters helped in defining a transition in different fatigue stages. Furthermore, some AE parameters were found to be more suitable for estimating fatigue life and predicting crack length. Moreover, the use of monitoring techniques, such as digital image correlation (DIC), and potential drop method, for measuring fatigue crack length and validating results without affecting AE method were discussed. Section 2.3 will delve into the knowledge gaps and outline potential research directions aimed at achieving the objectives of the present study.

2.3. Research Overview

2.3.1. Discussion and knowledge gap

The previous section examined the state-of-the-art of AE monitoring of FCG.

Fatigue monitoring using AE method

In the context of FCG, the AE method emerges as a notably effective non-contact approach offering real-time monitoring capabilities, applicable across various specimen types. Nevertheless, it has limitations, particularly with certain metals which are highly attenuative and may not yield reliable outcomes. Despite this, its sensitivity to minor defects offers qualitative insights into defect presence, yet quantitative data on crack growth mechanisms may not be precise. Moreover, mitigating noise and accurately distinguishing AE signals from crack growth remains an ongoing challenge.

Numerous studies have endeavored to establish a robust correlation between AE and FCG. However, the majority of experimental investigations have been restricted to individual materials or similar specimen types, further constrained by specific loading frequencies, load ratios, peak loads, and environmental conditions. Notably, materials commonly employed in offshore industries, such as S355 and S690, have not yet been comprehensively studied in conjunction with the AE method. Therefore, further investigation is required to explore the applicability of the AE method to these materials.

2.3.2. Research direction

Considering the current state of the art and identified gaps in the literature, the following main research question arises:

> 'Is the Acoustic Emission method capable of accurately measuring fatigue crack growth rates in the material?'

The main research question can be answered with the help of the following sub-questions,

- What are the specific limitations of the AE method that hinder its direct monitoring of crack growth, and how can these limitations be overcome?

- What strategies can be implemented to mitigate noise and accurately distinguish AE signals from crack growth in the monitoring process?
- What AE parameters demonstrate superior efficacy for quantitative characterization of fatigue crack growth in the material?

3

Experimental

This chapter details the materials, equipment, experimental setup, and procedures employed to evaluate the feasibility of Acoustic Emission (AE) monitoring for detecting fatigue crack growth in metallic materials. It includes a description of the materials and equipment, the experimental design, data acquisition, and analysis methods.

3.1. Materials and Experimental Equipment

This section introduces the properties of the specimen used. Additionally, it provides a comprehensive overview of the testing machine used, the servo-hydraulic fatigue testing system (Instron 8801), and the advanced AE Monitoring equipment employed to collect AE signals during testing.

3.1.1. Material

The testing material investigated in the experiment is X65 steel, which is a high yield material used for transportation of liquids over distance like pipe lines [30]. The main chemical composition (in wt.%) of the X65 steel is presented in Table 3.1, [44]. The compact tension (CT) specimen, as shown in Figures 3.1 and 3.7 is used to perform the fatigue crack growth test at room temperature. The dimensions of the CT specimen are in accordance with ASTM [43] standards.

Table 3.1: Chemical composition of the X65 steel (wt.%).

Composition	C	Mn	P	S
X65	0.28	1.40	0.03	0.03

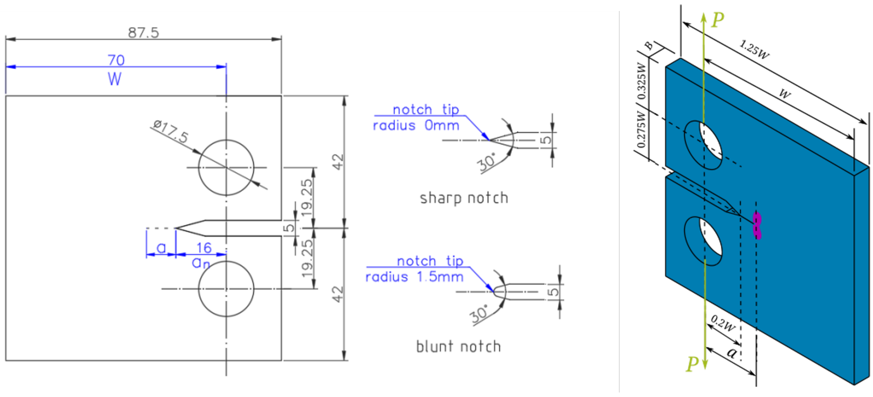

Figure 3.1: Depiction of a CT specimen [2].

3.1.2. The Instron 8801

The Instron 8801 is a compact servo-hydraulic fatigue testing system designed for both static and dynamic testing requirements. It is suitable for advanced materials and component testing, particularly in fatigue testing and fracture mechanics. Its key features include a force capacity of up to ±100 kN (±22 kip), a usable stroke length of 150 mm (6 in), a high-stiffness load frame equipped with twin columns, and the utilization of patented Dynacell load cell technology, ensuring precise load measurements [20].

Moreover, the Instron 8801 system provides a range of accessories, including grips, fixtures, chambers, and customization options for hydraulic configuration, allowing users to adapt the system to diverse testing scenarios. The CT specimen grips used in the experiment are shown in Figures 3.2 and 3.7. Its design also caters to dynamic performance needs tailored to specific applications, ensuring accuracy and reliability in testing processes [20].

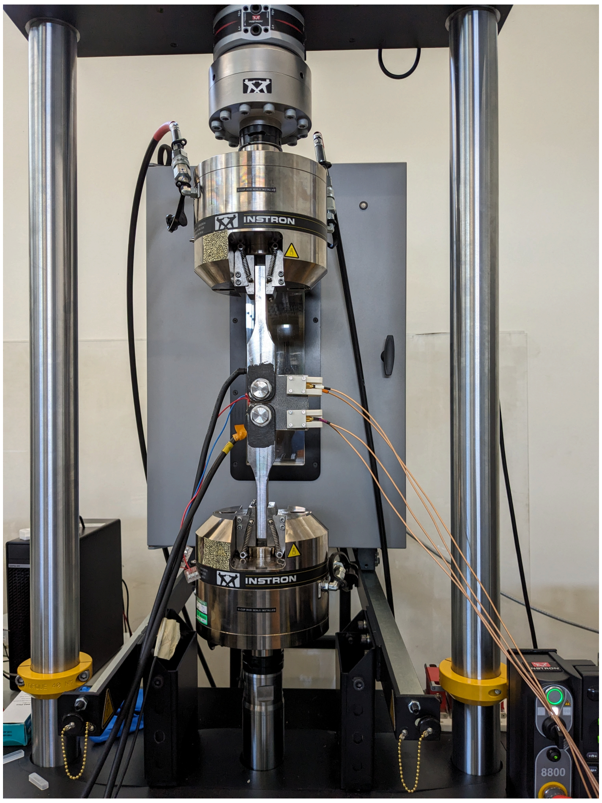

Figure 3.2: Specimen installed in Instron 8801.

3.1.3. AE measurement system

AE sensor

The R15α sensor (see Figure 3.3) offers exceptional performance with its high sensitivity and narrow band resonant capabilities, making it a versatile solution for various operational needs. It operates within a frequency range of 50-400 kHz and is optimized for resonant frequencies.

Figure 3.3: R15α sensor.

Placement of AE Sensors

AE sensors were placed using a 3D-printed sensor holder and a small plate was screwed at the back of each sensor to provide additional support during the experiment test, see Figure 3.4.

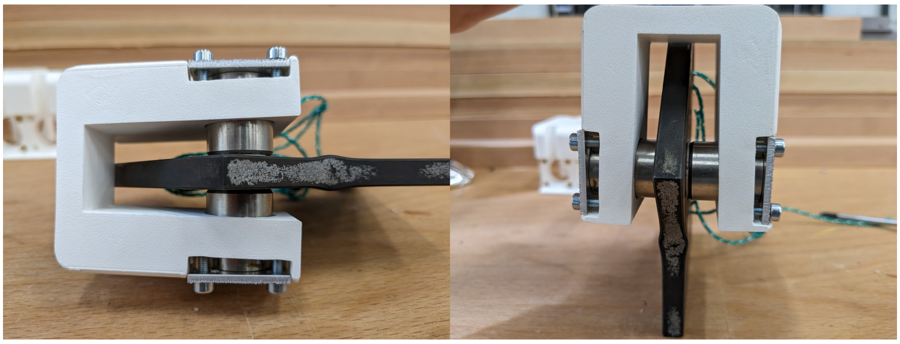

Figure 3.4: An example of AE sensor holder placement.

Pre-amplifier and Data Acquisition (DAQ) system

The AEP5H pre-amplifier (see Figure 3.5), with a gain of 40 dB, was used to amplify the AE waveform. The data acquisition (DAQ) system (see Figure 3.9) then converted these amplified waveforms into digital signals for further storage and analysis.

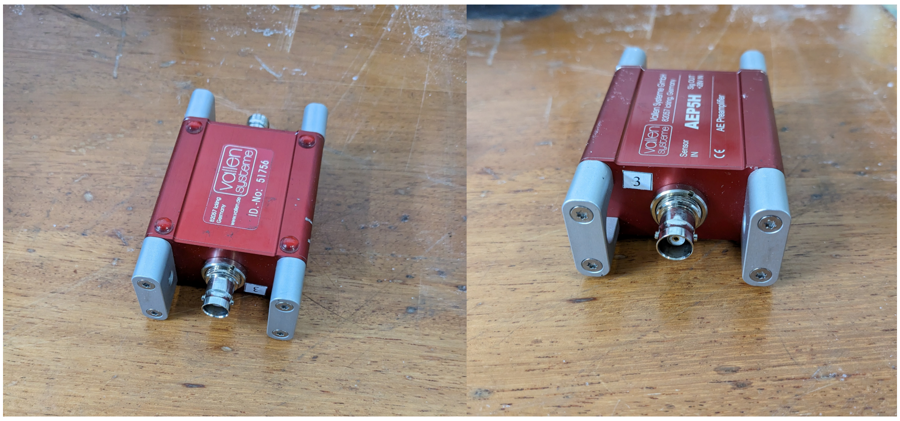

Figure 3.5: Pre-amplifier.

3.2. Methodology

This methodology chapter outlines the experimental procedures and analytical approaches used to investigate the correlation between fatigue damage and AE data in metallic materials under cyclic loading conditions. A parametric analysis of AE data was conducted to identify specific AE parameters that serve as reliable indicators of crack growth stages, thereby enhancing the accuracy of fatigue damage monitoring.

Under cyclic loading, the specimen emits elastic waves due to the sudden release of energy from processes such as crack initiation and propagation. These elastic waves, captured as AE signals, provide real-time data on crack dynamics, allowing for early detection and monitoring of fatigue damage.

Crack growth is categorized into three stages—initiation, propagation, and fracture—based on the methodology of Ma et al. [25]. During the initiation stage, micro-cracks form, resulting in low-amplitude AE signals. The propagation stage is characterized by the growth of these cracks, producing more frequent and higher-amplitude AE signals. Finally, the fracture stage involves rapid crack acceleration, leading to a peak in AE activity. This categorization enables the correlation of various AE parameters, such as energy, amplitude, and hit count, with specific stages of crack growth. For instance, an increased number of AE hits typically signifies heightened crack activity, suggesting that the crack has progressed from the initiation stage to the propagation stage.

To optimize the detection of meaningful AE signals while minimizing background noise, SNR levels of 2, 5, 10, and 20 were selected for observation, and an amplitude filter was also applied.

This approach enables a detailed understanding of AE parameters' behavior across different crack growth stages, providing critical insights for improving fatigue damage detection and monitoring.

3.3. Experimental Setup and Design

The AE sensors were strategically placed at predefined locations on the specimen's surface, as shown in Figure 3.11, to ensure optimal detection of AE signals. The testing was conducted at room temperature, with a sinusoidal cyclic load applied at a frequency of 15 Hz, as specified in Table 3.2. Calibration of the sensors was performed using pencil lead break (PLB) tests to ensure accurate AE data collection.

3.3.1. Introduction

In this experiment, a comprehensive setup (see Figure 3.6) was established to monitor the mechanical behavior and acoustic emissions of the tested specimen under applied loads. The specimen, before installed in the testing machine, was equipped with a potential drop sensor and several acoustic emission (AE) sensors strategically fixed on its surface to capture relevant data during the testing process.

A servo-hydraulic testing machine, integrated with a control system, was utilized to apply and regulate the load on the specimen accurately. This setup ensured precise load application and operational control throughout the experiment.

The AE sensors, crucial for detecting acoustic emissions generated by the specimen, were connected to pre-amplifiers. These pre-amplifiers served to enhance the signals received from the AE sensors, ensuring clarity of the signal waveform. Subsequently, the amplified signals were relayed to a data acquisition (DAQ) system. The DAQ system, in turn, interfaced with an AE monitoring system designed to record and analyze the acoustic emissions in real time.

This arranged experimental setup provided a robust framework for capturing and analyzing the mechanical and acoustic responses of the specimen under load, facilitating a detailed understanding of its behavior and properties.

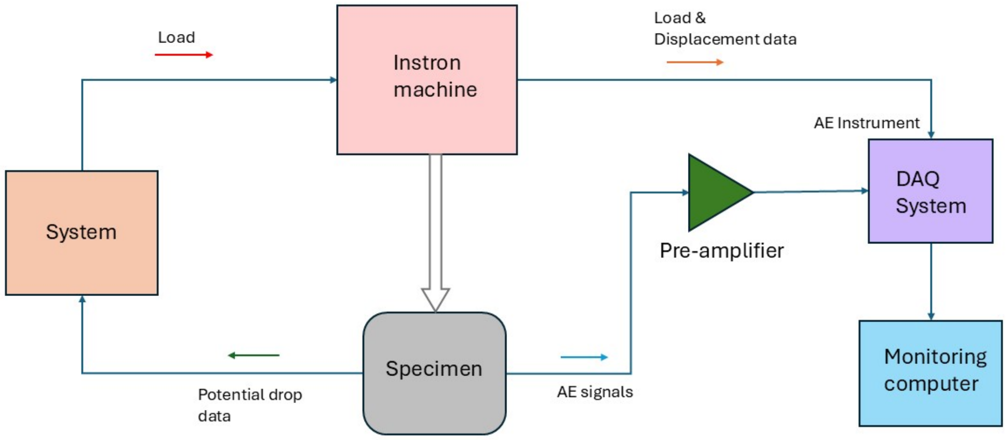

Figure 3.6: Schematic diagram of Experimental Setup.

3.3.2. Small Scale Fatigue test

The CT specimen was fitted in the testing machine using the grips, as shown in Figure 3.7. Additionally, direct current potential drop (DCPD) was installed on the CT specimen to measure crack growth during the test because of its valid measurement stability.

Table 3.2: Loading Condition.

Specimen	Maximum peak load [kN]	Load Ratio	Loading Frequency [Hz]
S1	10 & 21	0.1	15
S2	10	0.1	15

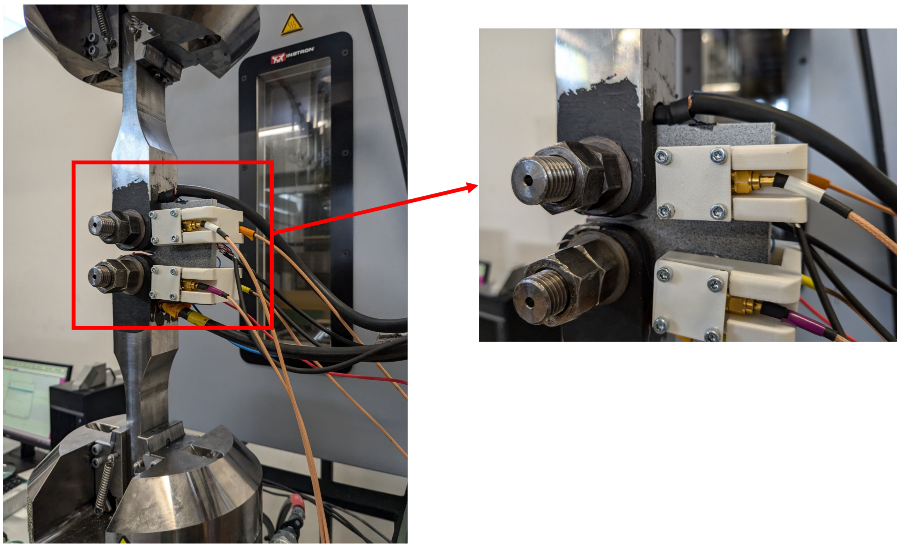

Figure 3.7: Specimen installed in testing machine and placement of AE sensor.

3.3.3. AE Monitoring Setup

Four AE sensors are installed on the specimen using hot glue as a couplant. Additional support for fixing the AE sensors is provided by a 3D-printed sensor holder, as shown in Figure 3.7. Pencil lead break (PLB) tests were performed at different locations on the specimen's surface to confirm the operational integrity of the AE monitoring system.

These four AE sensors were connected to pre-amplifiers using cables (see Figure 3.8), and the pre-amplifiers were then connected to the DAQ system, as shown in Figure 3.9. The converted waveforms to digital signals were further stored and analysed using Data acquisition program (Vallen Systeme), see Figure 3.10).

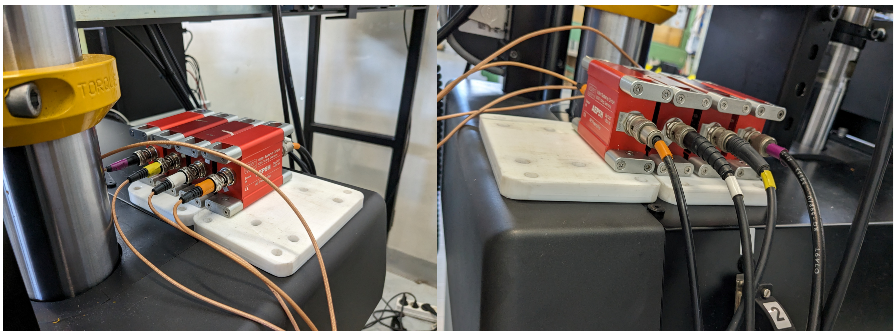

Figure 3.8: Cables connected through Pre-amplifier.

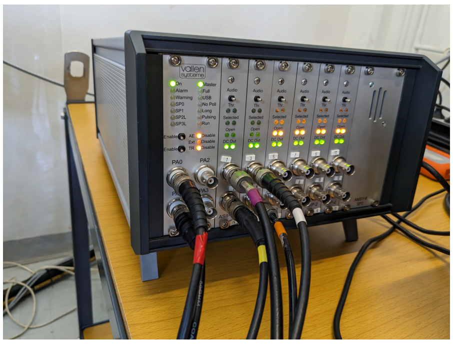

Figure 3.9: Data acquisition (DAQ) system.

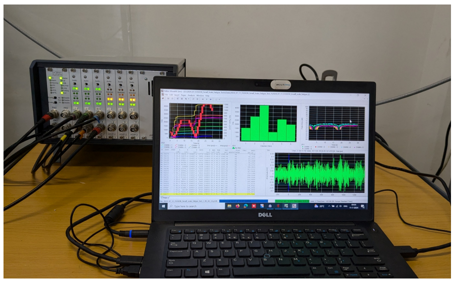

Figure 3.10: Monitoring and storage using DAQ program.

Position of AE sensors

The positions of the AE sensors on the specimens were as follows:

For specimen 1, the distance from the right edge and the top/bottom edge was 2 cm. For specimen 2, the distances varied slightly for all four sensors due to the placement of strain gauges, as mentioned earlier Section 3.3.2. The exact locations for each sensor are shown in the following tables:

Table 3.3: Location of AE sensors in Specimen 1

Channel	Surface of Plate	x [cm]	y [cm]
1	Front	2	2
2	Back	2	2
3	Front	2	2
4	Back	2	2

Table 3.4: Location of AE sensors in Specimen 2

Channel	Surface of Plate	x [cm]	y [cm]
1	Front	2.4	1.9
2	Back	2.3	1.2
3	Front	2.5	2.3
4	Back	2.5	2.3

The x and y are distances from the edges to the center of the sensor, as shown in Figure 3.11.

3.4. Experimental Procedure

This section outlines the procedures for conducting fatigue crack growth tests using AE monitoring. Metallic specimens were subjected to sinusoidal cyclic loading, and crack growth was tracked using both AE data and the direct current potential drop (DCPD) method. Details of the fatigue testing and AE data acquisition setup are provided below.

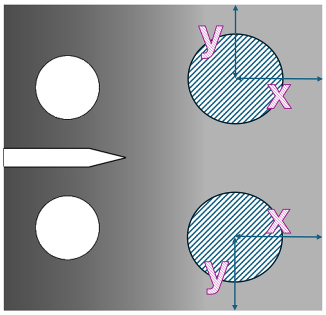

Figure 3.11: Schematic diagram of Sensor Locations

3.4.1. Fatigue Test Procedure

The fatigue crack growth test was conducted on a servo-hydraulic testing machine (see Figure 3.7) and the specimen were subjected to a sinusoidal cyclic load (see Table 3.2) at the room temperature. Direct current potential drop (DCPD) is used to have an additional measurement of crack growth during fatigue loading. Direct Current Potential Drop (DCPD) was used for additional measurement of crack growth monitoring during fatigue loading. After positioning the sensors on the specimen, pencil lead break (PLB) tests were performed to ensure proper sensor operation.

The AE monitoring system was started through auto-manager program before loading the specimen. The test continued until the specimen fractured, providing continuous AE data for the duration of the fatigue process.

3.4.2. Acoustic Emission Data Acquisition

The AE data were collected using the Vallen System AMSY-6 DAQ, configured with a sampling rate of 10 MHz to ensure high-resolution detection of AE signals. The filter frequency ranges were set at 50-500 kHz for the first experiment and 95-400 kHz for the second, based on initial tests indicating optimal signal detection within these ranges. The pre-trigger times were set to 400 μs and 500 μs, respectively, to capture the complete waveform of each AE signal. Additionally, the sample rate of transient data was reduced from 5 MHz to 2.5 MHz. The samples per set were also different: 8192 for the first experiment and 4096 for the second. For specimen 1, the threshold levels were set at 35 dB for two sensors and 45 dB for the other two. For specimen 2, the threshold was uniformly set at 40.1 dB. The system was configured to switch files every 10 minutes, a setting adjusted in the Auto Manager.

3.5. Data analysis method

The collected AE data were decompressed and converted into MATLAB files for further analysis. Key AE parameters such as amplitude, energy, rise time, and counts were extracted for each channel.

Statistical analysis, including linear regression, was conducted to assess the correlation between AE parameters and fatigue crack growth rates. The coefficient of variance (CV) was calculated to evaluate the reliability and consistency of each AE parameter across different datasets.

3.6. Experiment Notes

The fatigue test on Specimen 1 initially began with a peak load of 10 kN and a load ratio of 0.1, and it was conducted over the course of three days. However, the specimen exhibited unusual behavior, as it did not fracture as expected. Consequently, the test was halted and subsequently restarted with an increased peak load of 21 kN, maintaining the same load ratio of 0.1. After this adjustment, Specimen 1 fractured within an hour. The AE data corresponding to the 21 kN peak load includes six datasets, which are analyzed later in Chapters 4 and 5.

For Specimen 2, the experiment proceeded smoothly, resulting in AE data being recorded across 83 database files.

In summary, the methodology outlined in this chapter was designed to rigorously evaluate the feasibility of AE monitoring for detecting fatigue crack growth in metallic materials. By employing a multiparametric approach, strategically positioning AE sensors, and using robust data acquisition and analysis techniques, the study aimed to establish a comprehensive understanding of AE signal behavior and its correlation with crack growth dynamics.

4

Results and Analysis

This chapter presents the results of the Acoustic Emission (AE) monitoring experiments conducted to evaluate fatigue crack growth (FCG) in metallic materials. The findings are analyzed to understand the correlation between various AE parameters and crack growth rates across different stages of crack propagation. Key results are highlighted, followed by a detailed discussion of their implications.

4.1. Introduction

This chapter addresses the research problem centered on assessing the capability of the Acoustic Emission (AE) method in accurately measuring fatigue crack growth rates in materials. The study explores the limitations of the AE method, strategies to mitigate noise, and the efficacy of various AE parameters in characterizing fatigue crack growth. To achieve these objectives, a parametric analysis of AE data was conducted, correlating AE signals with the stages of crack growth under cyclic loading, as described in the methodology, Chapter 3.

The purpose of this chapter is to present the experimental results and observations obtained during the study. The chapter is structured as follows: the behavior of fatigue crack growth is analyzed first, followed by a multi-parameter analysis of AE data. The chapter then discusses fatigue damage identification before concluding with a summary of key findings.

4.2. Fatigue crack growth measurement

Figure 4.1 depicts the variation in fatigue crack length as a function of the number of fatigue cycles N for two specimens. The final crack lengths are approximately 30 mm, with the fatigue lifespans reaching around 663,000 cycles. After determining the crack length, the fatigue crack growth was calculated by using secant method, Equation (2.3):

$$\frac{da}{dN} = \frac{(a_{i+1} - a_i)}{(N_{i+1} - N_i)}$$

The following results are from test on Specimen 2 (S2).

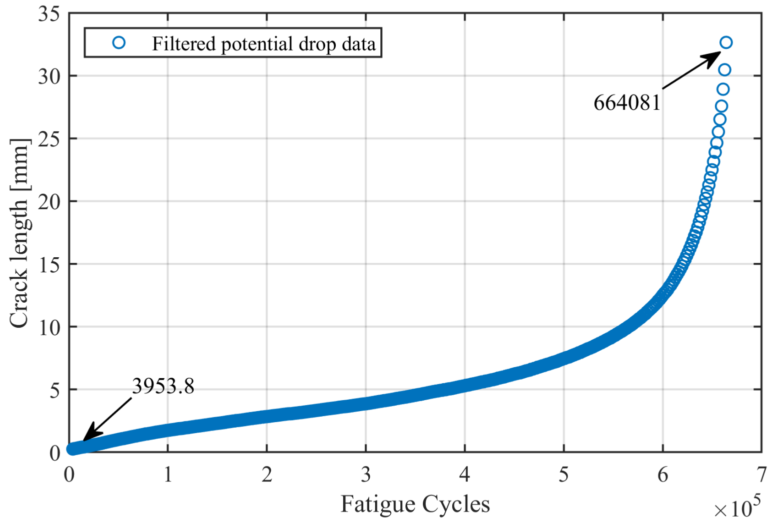

Figure 4.1: Fatigue crack length versus fatigue cycles.

As shown in Figure 4.2, fatigue crack growth rate $(\frac{da}{dN})$ is plotted against stress intensity factor range (ΔK). The behavior of the computed crack growth rate will be further correlated with the analyzed AE parameters to characterize the different stages of fatigue crack growth.

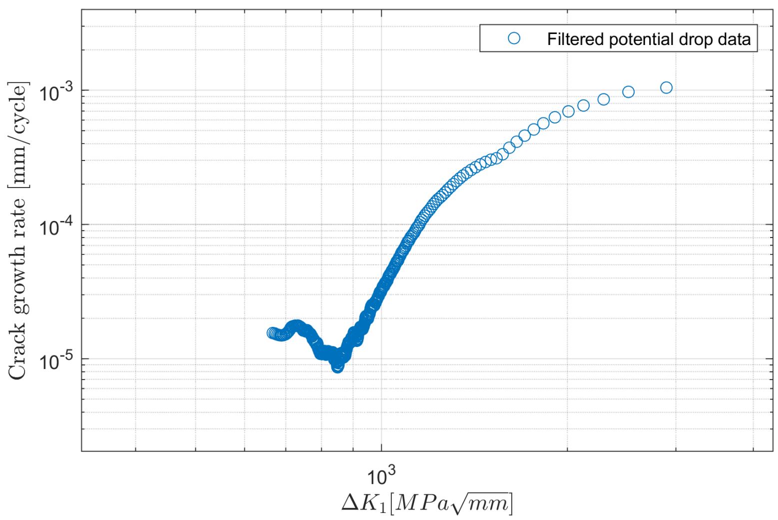

Figure 4.2: Fatigue crack growth rate versus stress intensity factor range.

Figure 4.3 illustrates the linear regression analysis of the fatigue crack growth rate as a function of the stress intensity factor range, from which the material constants m and C were determined. The resulting values for m and $\log C$ were 4.47 and -17.9, respectively.

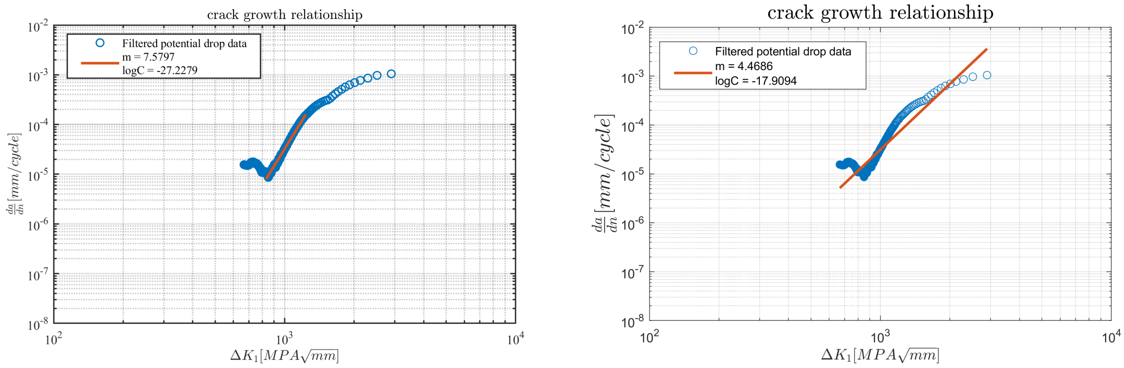

Figure 4.3: Linear fit of fatigue crack growth rate data.

4.3. Multi-Parameter Analysis

4.3.1. Time domain AE parameters

This section examines the AE parameters obtained in the time domain, such as amplitude, counts, energy, rise angle, entropy, RMS, kurtosis, and crest factor, to characterize fatigue crack growth. AE data from Specimen 2 is primarily used for analysis, focusing on how these parameters change over time and fatigue cycles.

Impact of SNR Levels on Signal Clarity

The signal-to-noise ratio (SNR) gauges the clarity of a signal relative to background noise. Consequently, comparing hit rates across various SNRs (see Figures 4.4 and 4.6) for dependable processing of Acoustic Emission (AE) data.

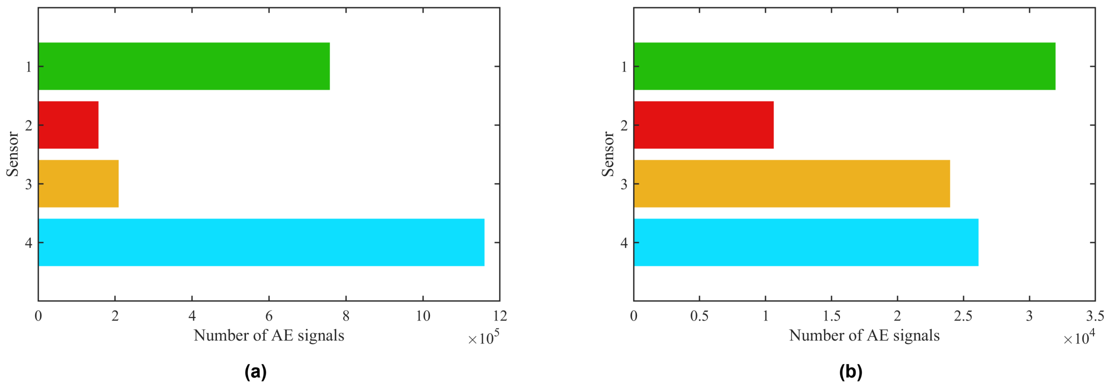

Figure 4.5: (a) Number of AE signals detected for Specimen 1 over time. (b) Number of AE signals detected for Specimen 1 after changing the peak load to 21 kN.

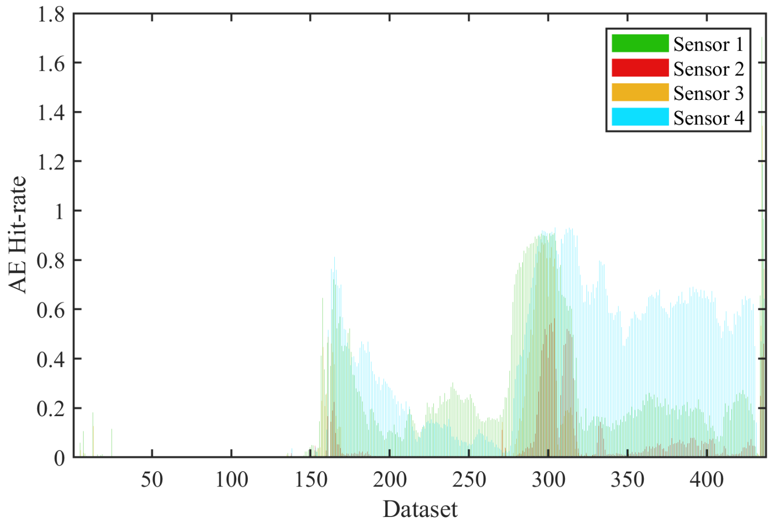

Figure 4.4: AE Hit-rate for Specimen 1 on each datasets at SNR 2

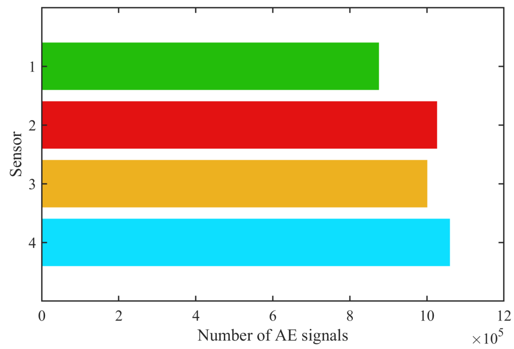

(a)

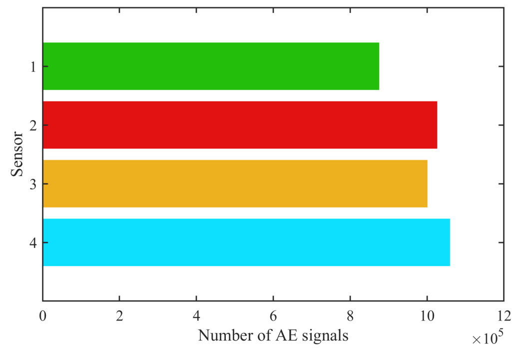

(b)

Figure 4.7: (a) Number of AE signals detected for Specimen 2 over time. (b) Number of AE signals detected for Specimen 2 after applying a filtering process to remove noise and irrelevant data.

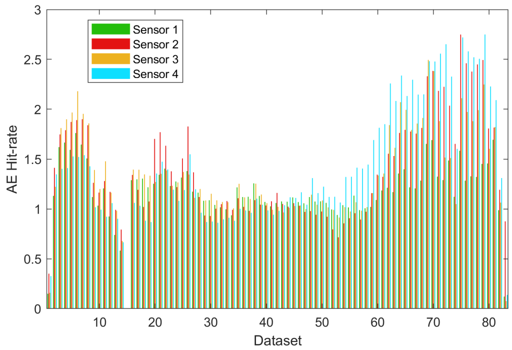

(a) SNR 2

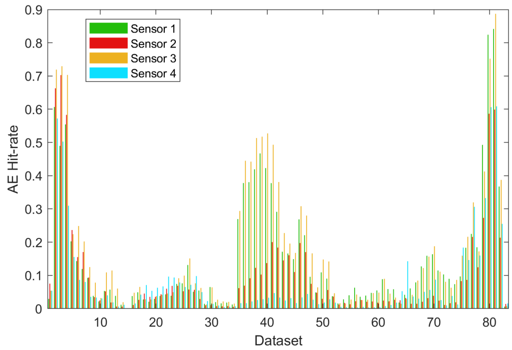

(b) SNR 5

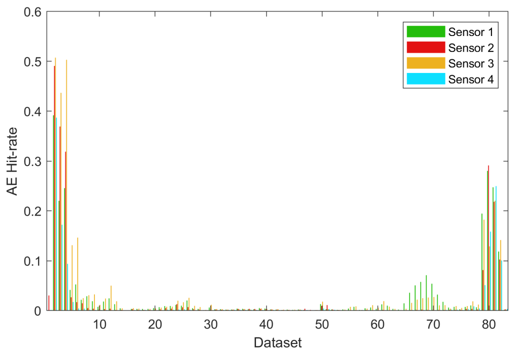

(c) SNR 10

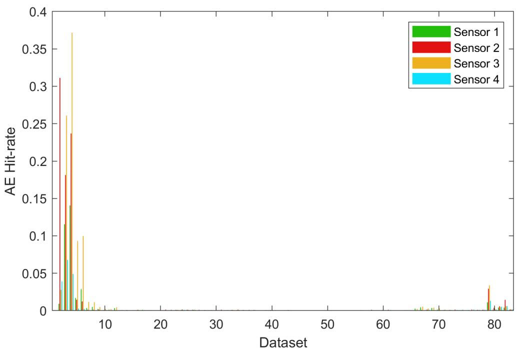

(d) SNR 20

Figure 4.6: AE hit rate for Specimen 2 as a function of each dataset at SNR levels of 2, 5, 10, and 20.

Figure 4.8 represents various AE parameters, filtered using a SNR of 2, to characterize FCG. These figures specifically incorporate data from Specimen 2. To maintain clarity and avoid excessive complexity, only the data from one channel is presented in this chapter. Additional data from other channels are available for review in the Appendix A.

Correlation Between AE Parameters and Crack Growth Stages

To present and analyze the correlation between different AE parameters (like amplitude, energy, counts) and the stages of crack growth (initiation, propagation, fracture).

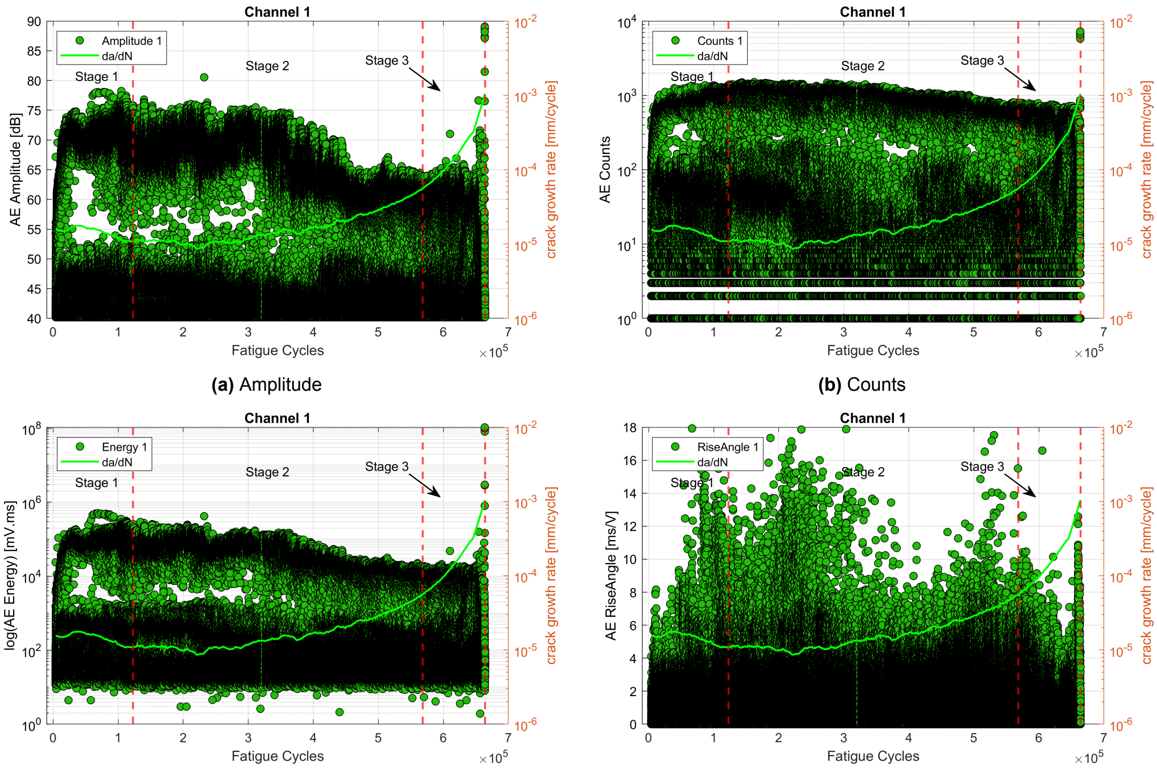

(a) Amplitude **(b)** Counts **(c)** Energy **(d)** Rise Angle

Figure 4.8: Various AE parameters as a function of fatigue cycles, segmented into three stages.

Effectiveness of Amplitude Filtering Techniques

To assess the impact of amplitude filtering on the accuracy and reliability of AE data for monitoring crack growth.

Frequency information is commonly utilized to distinguish effectively between background noise and AE signals resulting from micro- and macro-crack damage. A subset of AE signals was selected at different stages of fatigue life, and their waveform were extracted to obtain frequency data. A Fast Fourier Transform (FFT) was then conducted to analyze these signals and differentiate them from background noise (see Appendix D).

Figure 4.9 shows the stages of waveform extraction from high amplitude signals.

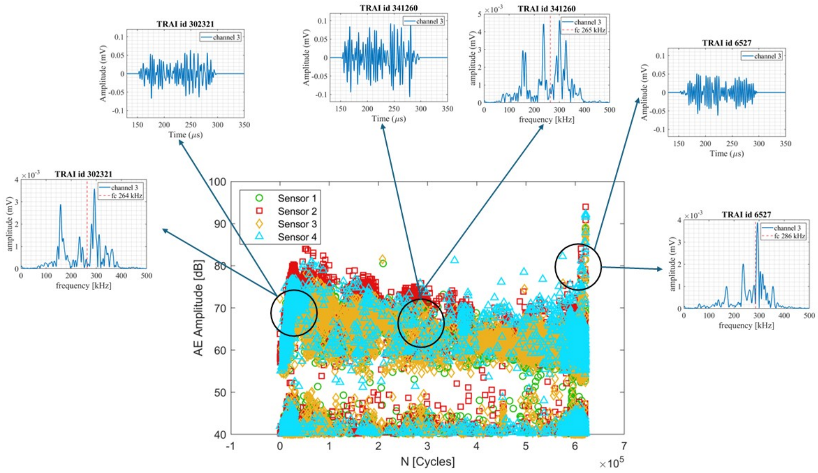

Figure 4.9: Locations of certain AE signals at higher amplitude which have been extracted for waveform visualization.

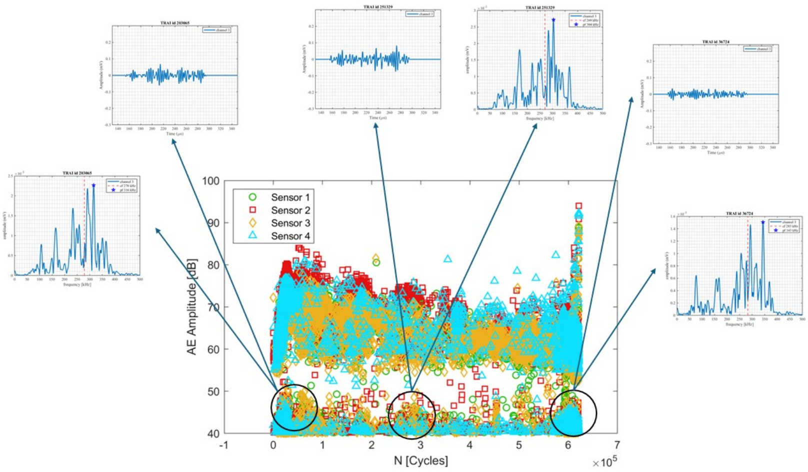

Figure 4.10: Locations of certain AE signals at low amplitude which have been extracted for waveform visualization.

The application of an SNR filter can result in the loss of a significant number of AE signals, which may be crucial for correlation. To mitigate this issue, an amplitude filter of 50 dB was employed to better isolate relevant signals. Figures 4.11 and 4.12 show the employed filter on variations of eight time-domain AE parameters as a function of fatigue cycles for Specimen 2.

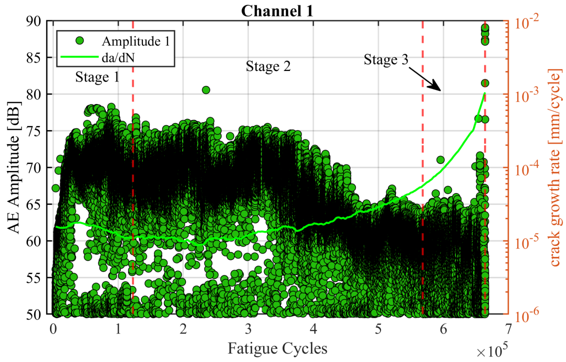

(a) Amplitude

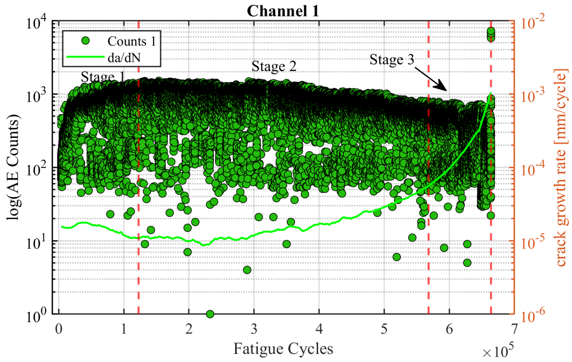

(b) Counts

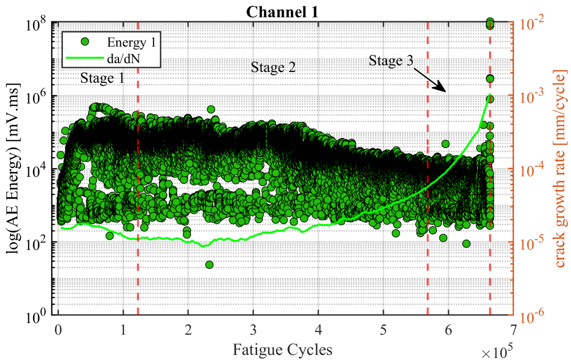

(c) Energy

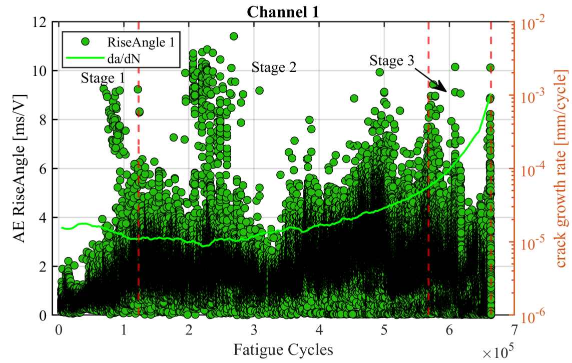

(d) Rise Angle

Figure 4.11: Various AE parameters as a function of fatigue cycles after Amplitude Filter.

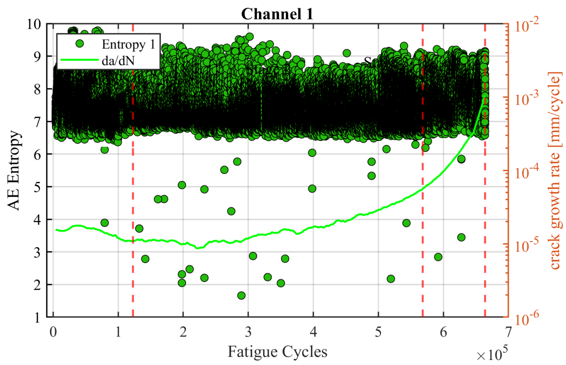

(a) Entropy

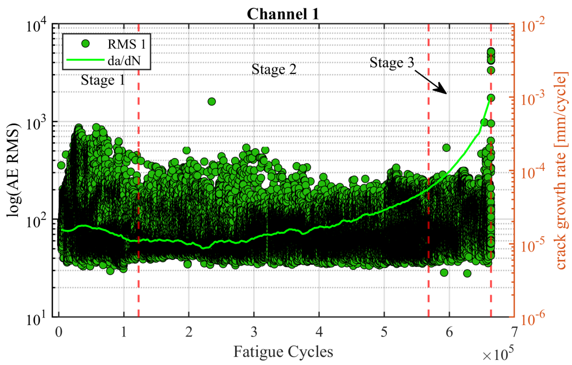

(b) RMS

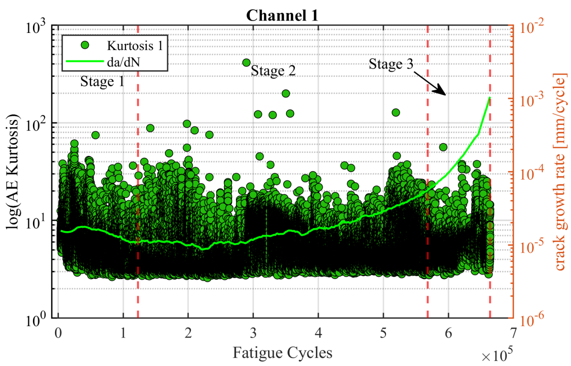

(c) Kurtosis

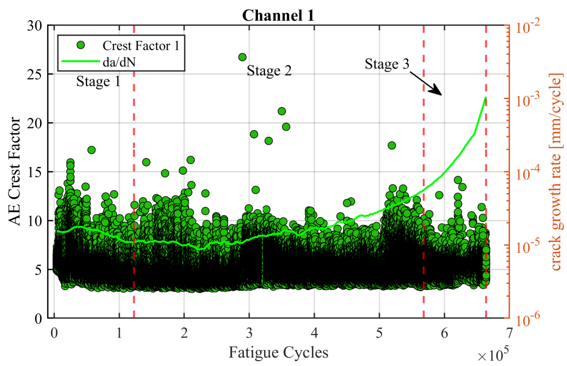

(d) Crest Factor

Figure 4.12: Other AE parameters as a function of fatigue cycles after Amplitude Filter.

4.3.2. Normalized cumulative AE parameters

Figure 4.13 shows the variation of normalized cumulative parameters against fatigue cycles for the data from each channel of Specimen 2. Figure 4.13 show the variation of normalized cumulative parameters versus fatigue cycles for each channel data of Specimen 2.

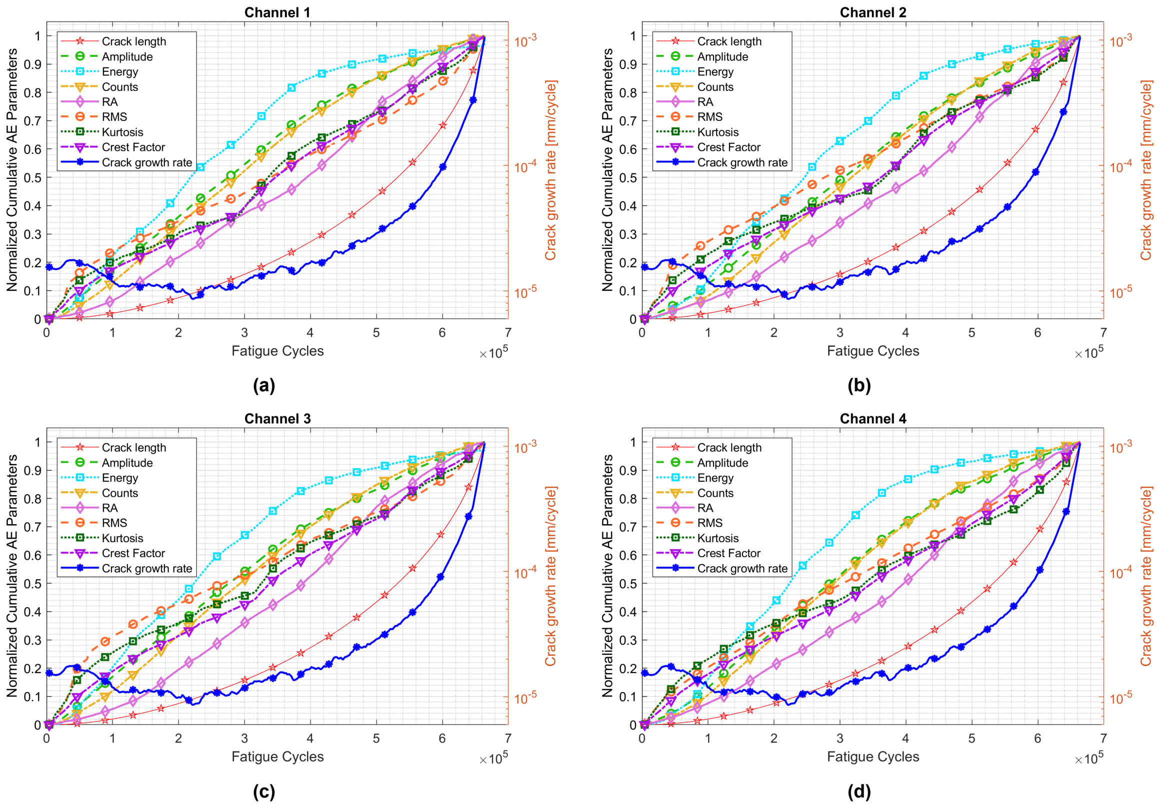

Figure 4.13: Variation of normalized cumulative AE parameters (amplitude, energy, counts, etc.) across different channels as a function of fatigue cycles, showing the correlation with crack growth rate.

4.3.3. Frequency domain AE parameters

This section analyzes AE data in the frequency domain, focusing on parameters like centroid frequency and peak frequency to differentiate between background noise and crack-related signals.

The AE sensor used in this study functions within a frequency range of 50 to 400 kHz, enabling the detection of AE signals over a wide frequency spectrum. The Figures 4.14 and 4.15 demonstrates that the majority of AE signals captured fall within the narrow frequency bands of [200-300 kHz].

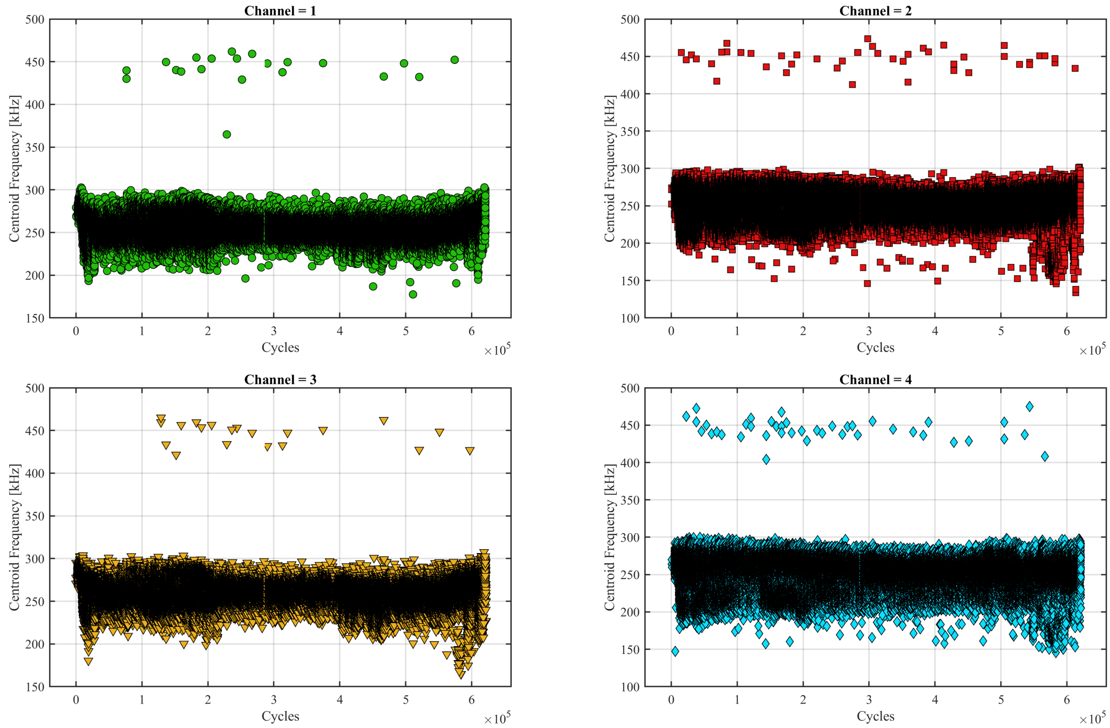

Figure 4.14: Centroid Frequency after Amplitude filter (50 dB).

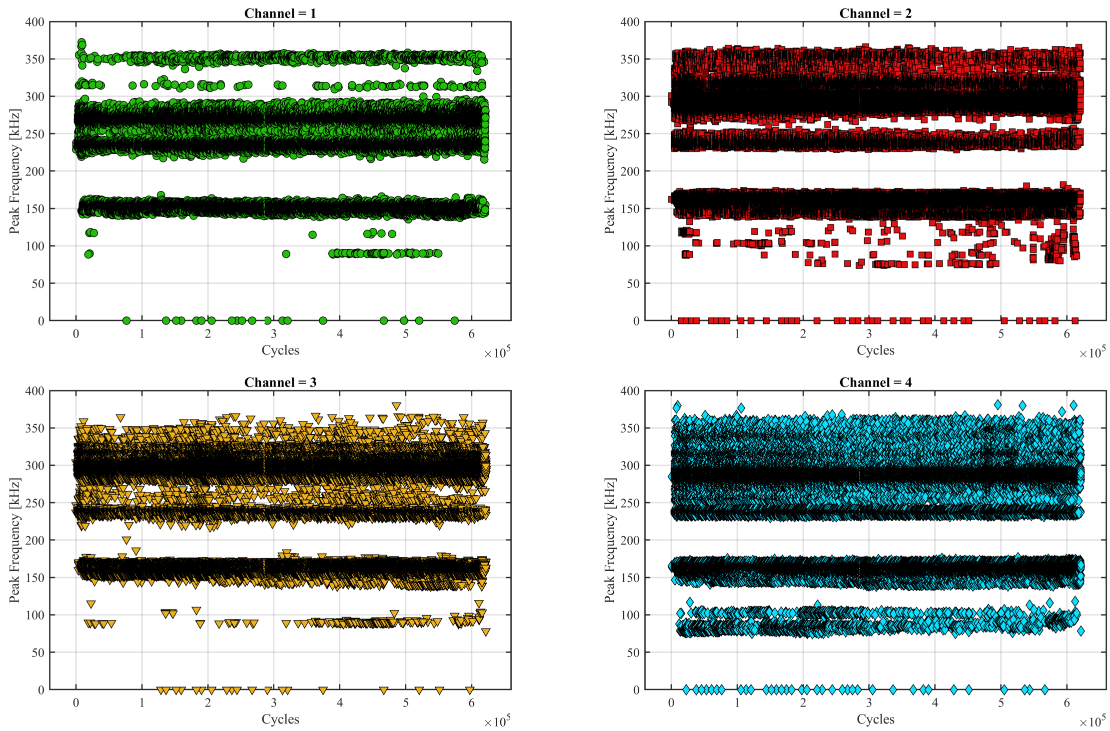

Figure 4.15: Peak Frequency after Amplitude filter (50 dB).

4.3.4. Coefficient of Variance of AE data

The coefficient of variance was calculated of each AE parameter for both specimens (see Appendix C). Table 4.1 presents the six datasets for Specimen 1, as explained in Section 3.6, along with amplitude-filtered data for Specimen 2. The rationale for selecting these specific datasets is discussed in detail in Chapter 5.

Table 4.1: Coefficient of Variance of AE parameters for filtered AE data

Specimen	1				2			
Channel	1	2	3	4	1	2	3	4
Amplitude	0.920	0.686	0.687	0.745	0.539	0.567	0.478	0.598
Count	0.856	1.358	0.753	1.448	0.351	0.389	0.358	0.446
Energy	4.110	2.133	2.812	4.536	8.429	5.501	6.850	6.571
Entropy	0.084	0.092	0.058	0.096	0.060	0.053	0.066	0.048
RA	1.205	1.045	0.579	0.950	0.547	0.551	0.551	0.555
RMS	0.639	0.547	0.502	0.678	0.710	0.926	0.862	0.683
Kurtosis	0.256	0.328	0.245	0.263	0.535	0.631	0.513	0.666
Crest Factor	0.115	0.137	0.134	0.132	0.216	0.227	0.216	0.220

4.4. Quantitative correlations

The counts were used to calculate the count rate, which was then plotted against the stress intensity factor range (ΔK), as shown in Figure 4.16. To facilitate direct comparison, the count rate and fatigue crack growth (FCG) rate data were resampled and plotted together against the stress intensity factor range. Similarly, the energy rate, entropy rate, and kurtosis rate were calculated and plotted against the stress intensity factor range (ΔK). Additionally, the bin width used to calculate the rate was 10.

Table 4.2 presents the calculated values of p and log B for the growth rates of various AE parameters, which were determined through linear regression analysis. Figures 4.16 and 4.17 shows the linear fitting of p and log B values.

Table 4.2: Experimental constants for AE count rate, energy rate, entropy rate and kurtosis rate

	Count rate		Energy rate		Entropy rate		Kurtosis rate	
Channel	p	log B	p	log B	p	log B	p	log B
1	2.319	-5.129	2.941	-5.277	-0.381	4.540	-3.342	13.904
2	2.685	-6.189	3.703	-7.354	1.056	1.841	-3.197	15.190
3	2.422	-5.290	2.903	-5.015	0.070	4.716	-4.831	20.582
4	2.894	-6.784	4.084	-8.591	2.682	-3.602	-0.952	7.287

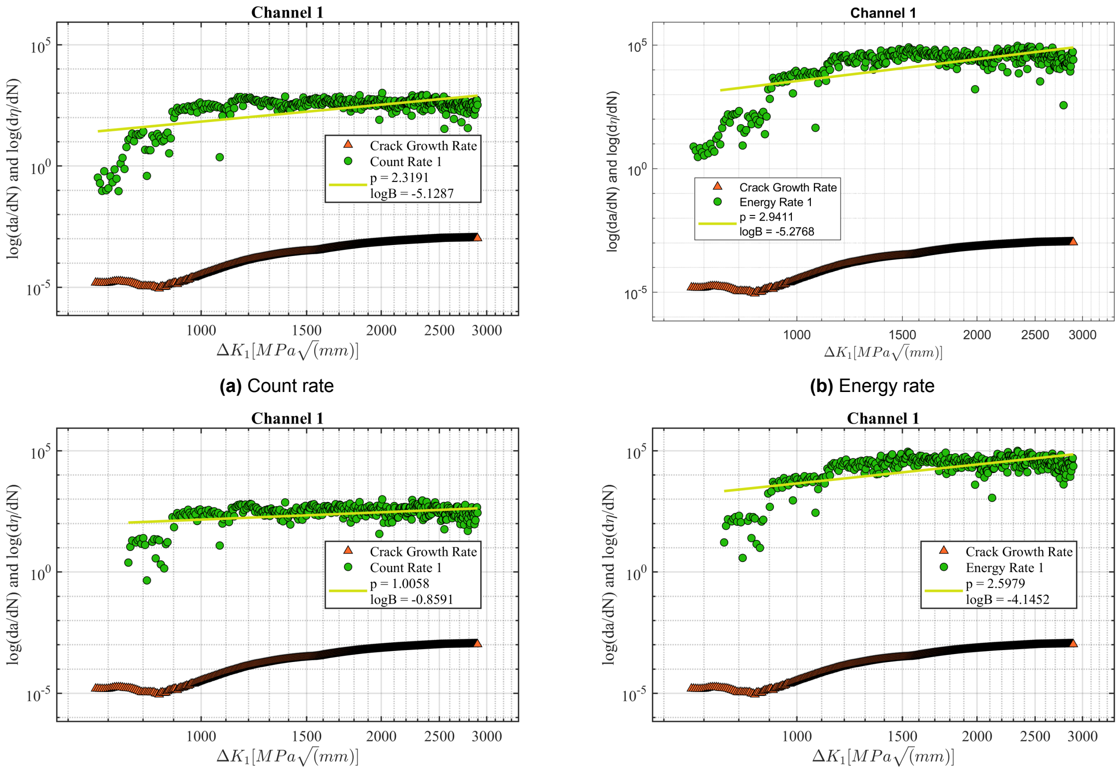

(a) Count rate

(b) Energy rate

(c) Count rate (filtered)

(d) Energy rate (filtered)

Figure 4.16: Fitting of p and log B constants on count rate and energy rate with fatigue crack growth rate versus stress intensity factor range (ΔK), (a,b) before and (c,d) after amplitude filter.

Table 4.3 presents the calculated values of p and log B for filtered AE count rate and AE energy rate.

Table 4.3: Experimental constants for filtered AE count rate and AE energy rate

	Count rate (filtered)		Energy rate (filtered)	
Channel	p	log B	p	log B
1	1.00581	-0.85914	2.597909	-4.14523
2	0.878116	-0.24597	2.417456	-3.08484
3	0.917158	-0.36502	2.345849	-3.17528
4	1.244092	-1.35192	2.80041	-4.34569

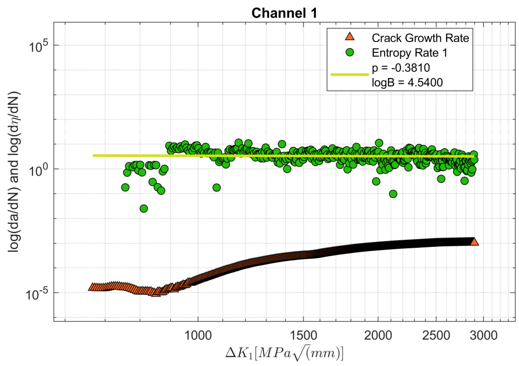

(a) Entropy rate

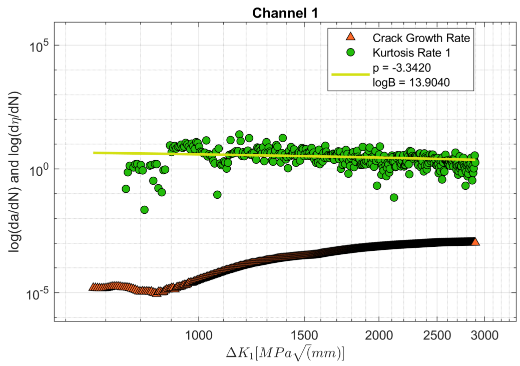

(b) Kurtosis rate

Figure 4.17: Fitting of p and log B constants on (a) Entropy rate and, (b) Kurtosis rate with fatigue crack growth rate versus stress intensity factor range (ΔK)

The prediction of fatigue crack growth was calculated using the Equations (2.17) and (2.18) and the values of the experimental constants m, C, p, and D for fatigue crack growth rate and the acoustic emission, as illustrated in Figure 4.18.

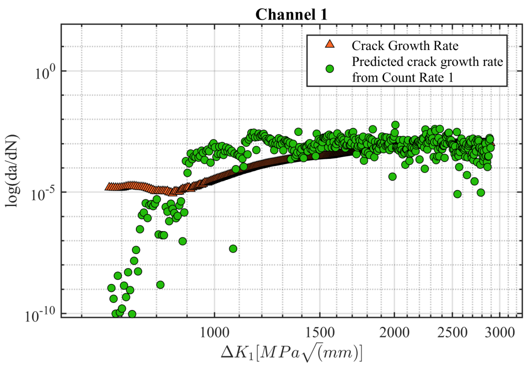

(a) Count rate

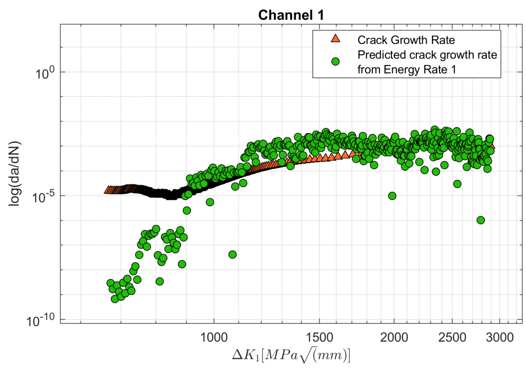

(b) Energy rate

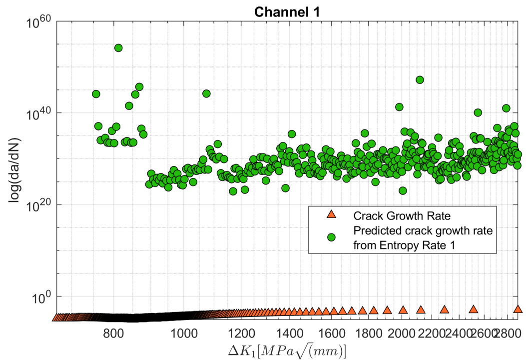

(c) Entropy rate

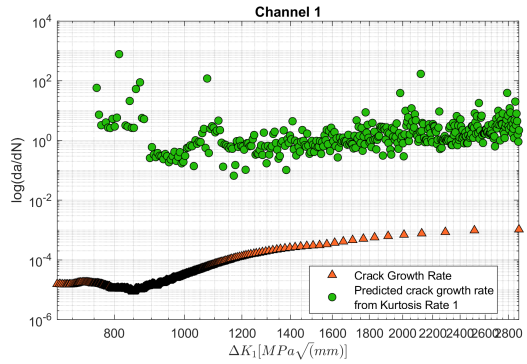

(d) Kurtosis rate

Figure 4.18: Prediction of fatigue crack growth rate using various AE parameter growth rate.

4.5. Summary of Results and Analysis

This chapter has presented the key results from the fatigue crack growth experiments, focusing on the effectiveness of the AE method in monitoring and characterizing fatigue crack growth in materials. The findings reveal that the AE parameters, when analyzed in conjunction with the stages of crack growth, provide valuable insights into the behavior of the material under cyclic loading. Notably, the application of amplitude and SNR filters allowed for the isolation of relevant signals, although the trade-off between signal clarity and data loss was evident. The quantitative correlations between AE parameters and the stress intensity factor range further underscore the potential of AE methods in accurately predicting fatigue crack growth rates.

These results lay a solid foundation for the subsequent discussion Chapter 5, where the implications of these findings will be explored in greater depth. The discussion will delve into the limitations observed, the efficacy of different AE parameters, and the broader impact of these findings on the understanding and application of AE methods in material testing.

5
Discussion

5.1. Introduction

This chapter addresses the central research problem of evaluating the capability of the Acoustic Emission (AE) method in accurately measuring fatigue crack growth rates in materials. The study aimed to identify the limitations of the AE method, develop strategies to mitigate noise, and determine the most effective AE parameters for characterizing fatigue crack growth. To achieve these objectives, a parametric analysis of AE data was conducted, correlating AE signals with the stages of crack growth under cyclic loading.

The purpose of this chapter is to interpret and discuss the findings presented in the previous Chapter 4, examining their implications in the context of the research questions and objectives. The chapter is structured as follows: first, we will analyze the key findings in relation to the research objective, followed by a discussion of the limitations and challenges encountered.

5.2. Interpretation of Fatigue Crack Growth Measurements

5.2.1. Correlation with AE Parameters

Figure 4.11 is divided into three stages based on the results of the crack growth rate to characterize the correlation between AE parameters and fatigue crack growth. The three stages—Stage 1, Stage 2, and Stage 3—are delineated by red dashed lines, as shown in Figure 4.8.

In Stage 1, The initiation of the crack was observed at approximately 3,953 fatigue cycles, according to potential drop data, corresponding to around 420 seconds of testing. Around this point, there was a noticeable increase in the amplitude of AE signals, indicating the onset of crack formation. This early rise in amplitude aligns with Chai et al. [9], as the specimen experiences plastic deformation and the initiation of micro-cracks at the notch, as AE signals become more prominent during the initial stages of crack development.

As the experiment transitioned into Stage 2, the amplitude, counts, and energy of the AE signals initially increased, reflecting the progressive growth of the crack. However, after reaching a peak, these parameters began to decline until around 450,000 cycles. Beyond this point, the peak amplitudes stabilized within the range of 65–70 dB, and the Rise Angle also exhibited an upward trend. Both energy and counts remained stable, suggesting that the crack was undergoing a period of steady propagation. Notably, at the end of Stage 2, the crack growth rate showed a marked increase after 500,000 cycles, indicating a transition to a more accelerated crack propagation phase. This pattern of stable crack growth during Stage 2 is consistent with findings from previous studies [9, 10].

In Stage 3, the crack growth rate escalated exponentially, accompanied by a significant increase in the amplitude of AE signals, reaching up to 90 dB. This sharp rise in amplitude signals corresponds to the onset of unstable crack growth, which typically precedes the ultimate failure of the specimen. The data suggest that during Stage 3, the material enters a critical phase where the crack propagates rapidly, leading to eventual fracture. This correlation between AE parameters and crack growth stages provides valuable insights into the behavior of materials under cyclic loading, particularly in identifying the transitions from stable to unstable crack growth.

5.2.2. Experimental Constants of FCG and AE parameters

The material constants m, C, p, and $\log B$ were determined through regression analysis of the test data. These constants are crucial for predicting the fatigue crack growth rate, as demonstrated in previous studies such as Roberts and Talebzadeh [34]. Using these constants, the predicted crack growth rate was calculated based on the growth rates of various AE parameters, as shown in Figure 4.18. Among the AE parameters analyzed, the predicted crack growth from count rate and energy rate showed the closest alignment with the actual crack growth rate, indicating its superior predictive capability.

As illustrated in Figure 4.16, the count rate and energy rate exhibited a stronger increasing trend with crack growth rate compared to other AE parameters such as entropy rate and kurtosis rate. The corresponding mean values of p and $\log B$ for the count rate and energy rate were found to be 2.580 and -5.848, & 2.94 and -5.28, respectively. These values suggest a more robust quantitative correlation between (count rate & energy rate) and crack growth rate than those observed with other AE parameters, in line with the findings of Roberts and Talebzadeh [35] and Chai et al. [10], reinforcing the (count & energy) rate's reliability as an indicator of fatigue crack propagation. This analysis highlights the importance of selecting appropriate AE parameters for accurate fatigue crack growth prediction.

5.3. Multi-Parameter Analysis

To effectively correlate AE parameters with fatigue crack growth, a multi-parameter analysis was conducted, focusing on the impact of the Signal-to-Noise Ratio (SNR) and the use of amplitude filtering techniques.

5.3.1. Signal-to-Noise Ratio (SNR) Impact

As illustrated in Figure 4.6, increasing the SNR level from 2 to 5 results in the filtering out of a significant number of AE signals. While this filtering reduces background noise, it also risks eliminating AE signals that could be crucial for accurately correlating AE parameters with fatigue crack growth. To address this challenge and minimize the loss of potentially significant data, an amplitude filter was employed. The method aims to balance noise reduction with the retention of key AE signals, which might enhance the data's reliability in detecting crack growth, as observed with specimen 1, where several AE signals around 50 dB were detected prior to crack initiation.

5.3.2. Amplitude Filtering

As discussed in Chapter 4, frequency information is a key tool for distinguishing between background noise and AE signals associated with micro- and macro-crack damage. During the analysis, it was observed that low-amplitude AE signals exhibited a continuous waveform, while high-amplitude AE signals, despite having similar frequencies, displayed burst-type characteristics likely related to fatigue crack damage.

To enhance the clarity and reliability of the AE data, an amplitude filter with a threshold of 50 dB was applied. This filtering process resulted in a 68.64% reduction in the total AE data, effectively removing noise while retaining significant signals associated with crack growth.

Furthermore, the reduction in the AE data helped in calculating other AE parameters which are based on transient data (such as Entropy, RMS, Kurtosis, crest factor) and have large data size.

5.3.3. Time Domain Parameters

Time domain parameters provide crucial insights into the nature and progression of fatigue crack growth by capturing various aspects of AE signals. The eight time-domain parameters analyzed in this study include amplitude, counts, energy, rise angle, entropy, RMS (root mean square), kurtosis, and crest factor.

Amplitude

Amplitude reflects the intensity of AE events, with higher values typically corresponding to significant crack growth, such as sudden fractures or rapid propagation. During the initial crack initiation phase (Stage 1), amplitude values increased and remained elevated throughout periods of active crack growth. As the crack approached a critical state, amplitude spikes frequently occurred, signaling imminent failure, consistent with previous studies [9, 26, 10].

Counts

Counts, which represent the total number of AE events, steadily increased during the crack initiation phase (Stage 1), indicating ongoing damage accumulation. This trend reversed during the crack propagation stage (Stage 2), where counts gradually declined until just before fracture. At the final stage of failure, a sudden increase in counts was observed, coinciding with specimen failure.

Energy

Energy levels, which reflect the total energy released during AE events, correlated with different stages of crack growth. Similar to counts, energy increased during the rapid crack initiation phase (Stage 1) and gradually decreased during the crack propagation stage (Stage 2). This steady decline continued until just before the fracture, at which point there was a sudden surge in energy levels as the specimen failed. These findings highlight energy as an effective parameter for identifying stages of crack growth and detecting critical events.

Rise Angle

Rise angle, which measures the slope of the initial AE waveform, increased during the crack initiation phase (Stage 1) and then dropped sharply following the transition to the crack propagation stage (Stage 2). After a brief period of fluctuation, it remained stable during the latter periods of stable crack growth but increased sharply during the transition to unstable growth (Stage 3). This behavior suggests that the rise angle is useful for detecting critical changes in crack dynamics.

Entropy

Entropy, which measures the complexity or disorder of AE signals, provides additional context for understanding crack growth. During the crack initiation phase, entropy increased, while during stable crack growth, entropy values remained relatively constant, indicating predictable AE events.

Root Mean Square

The RMS (Root Mean Square) value quantifies the overall power of AE signals. It increased during the initial crack initiation phase and decreased after transitioning to stable crack growth, with a sudden rise during the final stage of failure. This pattern points to heightened AE activity and energy release, suggesting that RMS serves as a complementary measure to amplitude and energy, offering a broader perspective on the material's response to cyclic loading.

Kurtosis

Kurtosis, a measure of the peakedness of AE signal distributions, identified periods dominated by high-intensity events, particularly during the crack initiation and the transition from stable to unstable crack growth. High kurtosis values aligned with significant crack propagation, making kurtosis a valuable parameter for detecting critical crack activity.

Crest Factor

The crest factor, which indicates the ratio of peak amplitude to the RMS value, was observed to increase during the crack initiation phase and periods of unstable crack growth. This parameter is particularly useful for detecting sudden changes in crack growth behavior, especially in noisy environments where transient high-amplitude events are significant.

In summary, each time-domain parameter offers unique insights into the crack growth process, and their combined analysis provides a comprehensive understanding of fatigue behavior. Utilizing multiple parameters enhances the accuracy of crack growth monitoring and supports more reliable predictions of material failure, highlighting the value of a multi-parametric approach in Acoustic Emission analysis.

5.3.4. Normalized cumulative AE parameters

In this section, the variation of normalized cumulative AE parameters as a function of fatigue cycles is analyzed across four different channels (Channel 1, Channel 2, Channel 3, and Channel 4), as shown in Figure 4.13. The AE parameters examined include crack length, amplitude, energy, counts, RA (rise time/amplitude ratio), RMS (root mean square), kurtosis, and crest factor. This analysis aims to understand the behavior of these parameters in relation to FCG rate and to evaluate their effectiveness in detecting and monitoring crack propagation.

General Observations

The analysis reveals a consistent upward trend in normalized cumulative AE parameters across all channels with increasing fatigue cycles, indicating the cumulative accumulation of AE activity as fatigue loading progresses. A correlation between the rise in AE parameters (such as energy, counts, and amplitude) and the crack growth rate is evident, suggesting that as the crack propagates, AE activity intensifies and is captured by these parameters.

Detailed Analysis of Each Channel

Across all four channels, the crack growth rate shows a consistent pattern: it starts relatively low and gradually increases, becoming more pronounced around 4×10^5 fatigue cycles. This consistent trend indicates a phase of accelerated crack propagation that occurs across all monitored areas, providing a reference point against which the variation in AE parameters can be analyzed.

In Figure 4.13a, several AE parameters, such as amplitude, energy, counts, RMS, and kurtosis, exhibit a steep upward trend as fatigue cycles increase, reflecting a strong AE response that correlates with the observed crack growth. The cumulative crack length also shows a similar increase, highlighting a clear relationship between AE signals and physical crack propagation in this channel. The consistent increase in these parameters suggests that AE monitoring is effectively capturing crack-related activity.

In Figure 4.13b, the AE parameters—particularly amplitude, energy, and counts—demonstrate a closely clustered and rising trend with the number of fatigue cycles. This indicates a strong correlation between these parameters and crack growth activity. While RA and crest factor also show upward trends, their slopes are less steep, suggesting they might be less sensitive to certain aspects of crack growth or respond differently to the AE signals compared to the more prominent parameters.

In Figure 4.13c, the cumulative AE parameters such as energy, counts, and amplitude continue to rise steadily with increasing fatigue cycles, reinforcing their role as effective indicators of crack propagation. Additionally, RMS and kurtosis display notable increases in alignment with crack growth, while parameters like RA show relatively moderate changes. This suggests variability in how different AE parameters respond to crack progression, with some being more reliable indicators than others.

Figure 4.13d shows the most pronounced increases in amplitude, energy, and counts as the fatigue cycles progress, indicating a strong AE response. Despite the consistent crack growth rate, this channel's data reveal a more intense AE activity, particularly for kurtosis and RMS, which show sharp upward trends. This could point to higher noise levels or more burst-type AE events, potentially associated with a specific local response to crack growth dynamics.

Interpretation of Observed Trends

- The consistent increase in AE parameters with fatigue cycles across all channels indicates that AE monitoring is effective in detecting the initiation and propagation of cracks. Parameters such as amplitude, energy, and counts are particularly responsive, demonstrating significant increases that correlate well with the crack growth rate.
- The variations in trends across the four channels may reflect differences in sensor placement, material properties, or local stress fields. For instance, the delayed but abrupt increase in crack growth rate and AE parameters in Channel 4 suggests that the sensor is in a region experiencing different crack growth dynamics.
- The clustering of parameters such as amplitude, energy, and counts suggests that these are robust indicators of crack growth, showing clear correlations with the observed growth rate. Other parameters like RA, RMS, kurtosis, and crest factor provide supplementary information but exhibit varying levels of sensitivity.
- The variability in trends across different parameters underscores the need for a multi-parameter approach to AE monitoring. Relying on a single parameter may not provide a comprehensive understanding of crack growth behavior, while combining multiple parameters can enhance the reliability and accuracy of detection.
- The consistent increase in AE parameters preceding a marked rise in crack growth rate suggests the potential for using AE data for predictive maintenance. Monitoring these parameters could enable the anticipation of critical stages of crack growth, allowing for timely preventive actions.

Conclusion

The trends observed across the four channels indicate that AE monitoring, utilizing a range of parameters, effectively tracks crack initiation and growth under fatigue loading. The correlation between AE parameters and crack growth rate is evident, although channel-specific variations highlight the complexity of crack growth dynamics and the importance of a comprehensive monitoring approach. The findings suggest that while AE parameters such as amplitude, energy, and counts are reliable indicators, incorporating a broader set of parameters is crucial for achieving more accurate and robust monitoring outcomes. Furthermore, the potential for predictive analysis based on AE data points to the value of ongoing research and development in this area.

5.3.5. Frequency Domain Parameters

Centroid and Peak Frequencies

Frequency domain analysis is a crucial component of Acoustic Emission (AE) studies, offering valuable insights into the energy distribution of AE signals. In this study, centroid and peak frequencies were examined to better understand the characteristics of AE events associated with fatigue crack growth.

The centroid frequency, which represents the weighted average frequency of an AE signal, provides a central measure of where most of the signal's energy is concentrated. The AE sensor used in this study, operating within a 50 to 400 kHz range, primarily captured signals with centroid frequencies within the narrow bands of [200-300 kHz] and [400-500 kHz], as shown in Figure 4.14. These frequency bands suggest a concentration of AE events that are likely linked to specific stages of crack growth, aligning with findings in the literature that associate similar frequency ranges with crack-related activity. Notably, the study by Chai et al. [9] identifies frequencies between [170-220 kHz] as predominantly associated with crack growth, a finding that partially aligns with our observations.

Peak frequency, on the other hand, refers to the frequency at which the maximum amplitude of an AE signal occurs. In this study, peak frequencies showed some variation compared to centroid frequencies, with AE signals concentrated within the frequency ranges of [50-170 kHz] and [220-350 kHz]. This discrepancy between centroid and peak frequencies suggests that peak frequency alone may not be a reliable indicator for identifying crack growth events due to the subtle changes in frequency.

5.4. Quantitative Correlations

5.4.1. Count Rate and FCG Rate

In this study, a linear correlation was observed between the count rate and the FCG rate, particularly during the phase of stable crack propagation. As the crack entered the second stage of growth, an increase in count rate was evident, coinciding with a corresponding rise in FCG rate.

However, the application of SNR and amplitude filters, which aimed to refine the count rate data, did not enhance this correlation. While the filtering process effectively reduced the overall count rate by removing background noise, it also inadvertently eliminated signals essential for accurately representing crack activity. Consequently, the quality of the data did not improve as anticipated, revealing the limitations of filtering in AE analysis for predicting fatigue crack growth.

A linear fit of the count rate data showed mean values of $p = 2.580$ and $\log B = -5.848$ for all four sensors before filtering, which degraded to $p = 1.011$ and $\log B = -0.706$ after filtering. In comparison, for the energy rate, values of $p = 2.94$ and log $B = -5.28$ before filtering were reduced to $p = 2.60$ and log $B = -4.14$ after filtering. The deterioration in the correlation between count rate and FCG rate suggests that the use of the amplitude filter may not be warranted, as the correlation between energy rate and FCG rate was stronger before filtering, indicating that critical AE signal data might have been lost due to the filtering process.

Moreover, when compared to other AE parameters, such as entropy rate and kurtosis rate, the count rate proved to be a reliable indicator of FCG rate as demonstrated in Figures 4.16 and 4.17. The observed patterns in count rate align with existing literature findings Roberts and Talebzadeh [35]. Nevertheless, the current AE data remains insufficient, underscoring the need for more comprehensive testing on specimens equipped with AE sensors.

5.4.2. Other AE Parameters

In addition to the count rate, several other AE parameters—such as energy rate, entropy, and kurtosis—offer valuable insights into the fatigue crack growth process. When analyzed together, these parameters provide a more comprehensive understanding of the material's response to cyclic loading.

Among these, the energy rate, which represents the energy released during AE events, showed a particularly strong correlation with the FCG rate, especially during stages of rapid crack propagation. The energy rate increased as the crack progressed, underscoring its effectiveness as an indicator of significant crack growth. Compared to other AE parameters, the energy rate consistently aligned with observed changes in crack growth rate, reinforcing its reliability as a metric for predicting fatigue damage.

Entropy and kurtosis also contribute meaningful information, but their roles are more complementary. While entropy helps to capture the complexity of the AE signal, kurtosis highlights the frequency and intensity of high-amplitude events. Together with count and energy rates, these parameters provide a multi-faceted approach to characterizing fatigue damage, offering robust potential for more accurate crack growth prediction.

5.5. Coefficient of Variance Analysis

The Coefficient of Variance (CV) is a crucial statistical measure can be used to assess the relative variability of Acoustic Emission (AE) parameters, providing insights into the consistency and reliability of these signals across different datasets or stages of fatigue crack growth. In this study, CV was calculated for key AE parameters, including amplitude, energy, count, and entropy, to evaluate their stability and predictability as indicators of crack growth. A higher CV is typically advantageous as it indicates greater data dispersion, which can facilitate more precise damage identification.

The data presented in Table 4.1 reveal several important trends in the CV of AE parameters for filtered AE data from Specimens 1 and 2.

For both specimens, entropy and crest factor exhibit relatively low CV values, indicating that these parameters are may not be reliable indicators of fatigue crack growth.

In Specimen 2, the CV values for amplitude and count are notably lower compared to those in Specimen 1. This reduced variability indicates that, in Specimen 2, these parameters are not consistent after applying an amplitude filter. As in Table C.2, CV values before filter are around 1.5 for both amplitude and count, which high compared to the results after filter. This shows the demerits of using an threshold to filter data and this may lead to large error in analyzing crack growth.

The CV values for Specimen 2 across all channels are generally similar, with the exception of energy and RMS. Energy and rise angle exhibit significantly higher CV values compared to other AE parameters, indicating greater variability in these measures. This finding aligns with the results of the study by Chai et al. [9], which also reported higher variability in energy-related AE parameters. The high CV for energy suggests that it is sensitive to changes in crack growth dynamics, making it less stable but potentially more informative in detecting specific crack events. The CV of entropy is the lowest among all AE parameters for both specimens, suggesting that it may be less reliable for AE analysis.

In summary, the CV analysis highlights entropy and crest factor as the most stable AE parameters, while energy and rise angle show greater variability, which reflect their sensitivity to different stages of crack growth. The consistency of amplitude and count in Specimen 2 further suggests that these parameters are more reliable in certain experimental conditions. These findings provide valuable insights into the selection of AE parameters for accurate and reliable fatigue crack growth monitoring.

5.6. Implications

The findings of this study have several important implications for the use of Acoustic Emission (AE) methods in monitoring fatigue crack growth in metallic materials.

This research enhances the understanding of how different AE parameters correlate with fatigue crack growth across various stages of crack propagation. The study confirms that energy and rise angle are particularly effective in detecting specific stages of fatigue damage due to their sensitivity to changes in crack growth dynamics. These parameters, along with amplitude and count, have shown to provide reliable indications of crack initiation and progression. However, the variability observed in some parameters, such as peak frequency, emphasizes the need for careful selection and combination of AE parameters to improve accuracy in crack growth monitoring.

The study's findings suggest that a multi-parametric approach, using a combination of time-domain and frequency-domain parameters, can enhance the reliability of fatigue crack growth predictions. For instance, the use of entropy, kurtosis, and crest factor alongside traditional parameters like amplitude and count provides a more comprehensive view of crack growth behavior, particularly under cyclic loading conditions. This approach can improve the identification of transitions from stable to unstable crack growth, supporting more effective predictive maintenance strategies in critical structures, such as offshore platforms and marine vessels.

The results highlight the importance of carefully managing data filtering processes. While applying amplitude and SNR filters can help reduce background noise, the study also demonstrates that these methods can inadvertently remove important AE signals crucial for correlating AE parameters with fatigue crack growth. The findings suggest that a balanced approach to filtering is necessary—one that reduces noise while preserving key data to maintain the reliability of AE monitoring.

This study reinforces the need for selecting appropriate AE parameters that correspond to specific crack growth stages. For example, the robust quantitative correlation observed between energy rate and crack growth rate suggests that energy rate is a particularly reliable indicator of fatigue crack propagation, especially in the later stages of damage. Similarly, entropy and crest factor have been identified as stable parameters, while others like energy and rise angle, though more variable, offer significant insights into the dynamic aspects of crack growth. These findings are crucial for developing more accurate and tailored AE monitoring protocols.

The research identifies gaps in the current understanding of AE's applicability across diverse materials and structural configurations. Existing studies are largely limited to specific materials and controlled testing environments. This study suggests that further research is needed to validate the findings across a wider range of materials, loading conditions, and real-world environments. Expanding the dataset will help generalize the use of AE methods for fatigue monitoring in different contexts, such as marine applications where harsh conditions prevail.

Given the variability observed in certain AE parameters and the limitations related to data filtering, the study recommends further research to refine AE monitoring techniques. Future studies should focus on expanding the scope of testing by including more specimens, applying advanced noise mitigation techniques, and integrating complementary methods such as digital image correlation (DIC) and the potential drop method. Additionally, validating the AE parameters across different materials and conditions will help to establish standardized protocols for using AE in structural health monitoring.

The findings have broader implications for the field of Structural Health Monitoring (SHM). By identifying effective AE parameters and refining monitoring techniques, this research contributes to the development of more reliable and cost-effective SHM systems. This is particularly important for critical infrastructure where early detection of fatigue damage is essential to prevent catastrophic failures, reduce maintenance costs, and enhance overall safety and operational efficiency.

In conclusion, this study provides valuable insights into the effective use of AE methods for fatigue crack growth monitoring, while also highlighting the need for further research to address current limitations and expand the applicability of these techniques across different environments and material types.

5.7. Limitations and Assumptions

While this study provides some insights into the multi-parametric analysis of Acoustic Emission (AE) for fatigue damage monitoring, several limitations must be acknowledged. The complexity of interpreting mixed and attenuated AE signals presents a significant challenge. Overlapping signals from multiple sources can obscure the identification of specific damage events, complicating the accurate correlation of AE parameters with crack growth stages. Additionally, signal attenuation, particularly in thicker or heterogeneous materials, may reduce the effectiveness of AE monitoring by weakening the signals as they propagate, potentially leading to underestimation of damage severity.

Environmental noise also poses a limitation, as external sources of interference can generate AE-like signals, resulting in false positives. Despite the application of filtering techniques to mitigate this noise, complete elimination is difficult, and there remains a risk of inadvertently filtering out genuine AE signals, affecting the accuracy of the analysis.

The sensitivity of AE monitoring to varying loading conditions and material properties further complicates the generalization of the results. Each material and loading scenario requires specific calibration to ensure accurate AE signal interpretation, limiting the applicability of the findings to other contexts. The study assumes that the relationships between AE parameters and fatigue damage are linear, though in reality, these relationships may be more complex.

Moreover, the study's assumptions, such as idealized experimental conditions and uniform material properties, may not fully represent the complexities of real-world scenarios. While necessary for the scope of this research, these simplifications suggest that caution should be exercised when extending the findings beyond the specific conditions tested.

These limitations highlight the need for future research to develop more sophisticated signal processing techniques, explore the non-linear relationships between AE parameters and fatigue damage, and validate the methodology across a broader range of materials and environments.

5.8. Conclusion

In this discussion chapter, we have explored the key findings of our study, focusing on the capability of AE parameters to monitor and predict fatigue crack growth.

The analysis revealed that energy and rise are particularly useful AE parameters, providing consistent and reliable indicators of crack growth across different specimens. Because of more variability energy and rise angle were found to be sensitive to changes in crack growth dynamics, making them valuable for detecting specific stages of fatigue damage. The study also highlighted the limitations of peak frequency as a predictor due to its variability and the challenges posed by filtering techniques that could inadvertently eliminate significant AE signals.

In summary, while AE monitoring shows significant promise for fatigue crack detection, its effectiveness depends on selecting the most stable and relevant parameters, as well as accounting for the limitations identified in this study. Future research should aim to refine these methods and explore their application across a broader range of materials and conditions to enhance the reliability and applicability of AE-based monitoring systems.

6

Conclusion

This study aimed to evaluate the effectiveness of the Acoustic Emission (AE) method in accurately measuring fatigue crack growth rates in materials. The primary research question, ”Is the Acoustic Emission method capable of accurately measuring fatigue crack growth rates in the material?” was addressed through an investigation of AE parameters, noise mitigation strategies, and the inherent limitations of AE methods.

Answering the Research Questions:

1. **What are the specific limitations of the AE method that hinder its direct monitoring of crack growth, and how can these limitations be overcome?**

   The study identified several limitations that hinder the direct monitoring of crack growth using AE methods. These include challenges in obtaining high-quality AE signal data, coupling issues between the AE sensors and the material, and concerns about the reliability of both the sensors and the overall AE monitoring system. These limitations highlight the need for careful calibration, maintenance, and selection of sensors, as well as the importance of understanding the material properties and the testing environment.

2. **What strategies can be implemented to mitigate noise and accurately distinguish AE signals from crack growth in the monitoring process?**

   The study explored various strategies for noise mitigation, such as analyzing AE signal waveforms and identifying burst-type signals, which were found to be effective in detecting fatigue crack damage. A low Signal-to-Noise Ratio (SNR) and amplitude filter were also applied, demonstrating effectiveness in noise reduction but with a risk of losing significant AE signals. The use of

SNR and amplitude filters, including a 50 dB threshold, was intended to refine the count rate data by reducing background noise. However, these filters did not improve the correlation between the count rate and the fatigue crack growth (FCG) rate as expected. Although filtering reduced noise, it also removed signals that were critical for accurately correlating crack activity, highlighting the limitations of using such filters in AE analysis for correlation of fatigue crack growth.

3. **What AE parameters demonstrate superior efficacy for quantitative characterization of fatigue crack growth in the material?**

   Among the AE parameters studied, energy and rise angle were found to be particularly sensitive to changes in crack growth dynamics, making them valuable indicators of crack growth across different specimens. The quantitative analysis further revealed that count rate and energy rate correlated well with fatigue crack growth, showing better trends compared to other AE parameters and offering reliable metrics for predicting fatigue damage.

Main Research Question:

> **'Is the Acoustic Emission method capable of accurately measuring fatigue crack growth rates in the material?'**

The findings of this study suggest that the Acoustic Emission method has the potential to measure fatigue crack growth rates in metallic materials, particularly when certain AE parameters, such as count rate and energy rate, are carefully selected. These parameters demonstrated a reasonable correlation with crack growth in this study, consistent with findings from previous research. However, the accuracy of AE methods can be influenced by several factors, including signal noise and the variability of different parameters. Therefore, while AE methods show promise for fatigue monitoring, their effectiveness depends on managing these limitations and applying appropriate noise mitigation strategies.

Key Contributions and Insights – This research has enhanced the understanding of how different AE parameters correlate with various stages of fatigue crack growth. It shows that specific parameters like energy and rise angle are particularly effective for detecting critical stages of fatigue damage. Additionally, it highlights the necessity of using a multi-parametric approach that incorporates both time-domain and frequency-domain parameters for a more reliable characterization of fatigue crack growth.

In conclusion, the AE method has been demonstrated as a viable tool for monitoring fatigue crack growth, with the potential for further refinement and application across various materials and conditions. The insights gained from this study contribute to the broader understanding of AE in fatigue monitoring and offer a foundation for future research and practical applications.

7 Recommendations

Building on the findings of this study, several areas are recommended for future research to enhance the effectiveness of Acoustic Emission (AE) methods for monitoring fatigue crack growth and to address the limitations identified. The following recommendations aim to improve data accuracy, broaden the applicability of AE techniques, and refine monitoring protocols for a wider range of materials and conditions.

Expand the Scope of Testing – Future research should expand the scope of testing by incorporating a larger and more diverse set of specimens equipped with AE sensors. A broader dataset would allow for more comprehensive comparisons and validation of the findings presented in this thesis. Additionally, tests using a negative load ratio should be considered to detect new AE sources beyond fatigue damage signals. This would enrich the AE data and provide a deeper understanding of various damage mechanisms.

Integrate AE method with Complementary Techniques – Combining AE methods with complementary techniques such as Digital Image Correlation (DIC) and the potential drop method could offer a more holistic approach to fatigue monitoring. These integrated methods would provide cross-validation of AE data, enhancing the reliability and accuracy of crack growth monitoring. Furthermore, validating AE parameters across different materials and environmental conditions would help establish standardized protocols for AE-based monitoring.

Explore Corrosion Fatigue and Stress Corrosion Cracking – Research should be extended to investigate corrosion fatigue and stress corrosion cracking, especially in marine environments where accurate AE data is essential. Understanding these phenomena would improve the applicability of AE methods in environments that expose materials to corrosive conditions, ultimately enhancing the predictive capabilities of AE monitoring techniques.

Apply Advanced Analytical Techniques – Advanced analytical techniques, such as machine learning and neural networks, should be explored to improve the accuracy of fatigue crack growth monitoring. These techniques can analyze large datasets and recognize complex patterns in AE signals, thereby enhancing the correlation between AE parameters and crack propagation. Implementing such approaches could lead to more robust predictive models and monitoring strategies.

Refine Material Constants – The study highlighted the need for more extensive testing to improve the calculation of material constants p and $logB$. Additional research should focus on gathering more AE data and comparing these findings with existing literature to validate and refine these constants. This effort will help ensure that AE monitoring techniques remain effective in predicting material failure across a wide range of applications.

Investigate Additional AE Parameters – Future research should consider incorporating additional AE parameters, such as absolute energy, to enhance both qualitative and quantitative correlation with fatigue crack growth. To reduce dependency on user-defined thresholds and parameters, further studies should explore the processing of AE waveform signals using alternative entropy measures.

Examine AE Signal Clustering – Cluster analysis of AE signal data should be pursued to identify different regimes of acoustic activity, which may correspond to various fracture mechanisms during fatigue crack propagation. This analysis could improve the understanding of distinct crack growth stages and enhance the predictive power of AE monitoring.

References

[1] DG Aggelis, EZ Kordatos, and TE Matikas. “Acoustic emission for fatigue damage characterization in metal plates”. In: *Mechanics Research Communications* 38.2 (2011), pp. 106–110.

[2] Bbanerje. *Schematic and dimensions of a compact tension specimen*. [Online; accessed 14-Feb-2024]. 2011. URL: https://commons.wikimedia.org/w/index.php?curid=15932992.

[3] Fredrik Bjørheim, Sudath C Siriwardane, and Dimitrios Pavlou. “A review of fatigue damage detection and measurement techniques”. In: *International Journal of Fatigue* 154 (2022), p. 106556.

[4] AF Blom, A Hedlund, and W Zhao. “Short fatigue crack growth behaviour in Al 2024 and Al 7475”. In: *Mechanical Engineering Publications, The Behaviour of Short Fatigue Cracks,* (1986), pp. 37–66.

[5] William D Callister Jr and David G Rethwisch. *Callister’s materials science and engineering*. John Wiley & Sons, 2020.

[6] SH Carpenter and FP Higgins. “Sources of acoustic emission generated during the plastic deformation of 7075 aluminum alloy”. In: *Metallurgical Transactions A* 8 (1977), pp. 1629–1632.

[7] Álvaro Carrasco et al. “Short review of the use of acoustic emissions for detection and monitoring of cracks”. In: *Acoustics Australia* 49 (2021), pp. 273–280.

[8] Mengyu Chai, Zaoxiao Zhang, and Quan Duan. “A new qualitative acoustic emission parameter based on Shannon’s entropy for damage monitoring”. In: *Mechanical Systems and Signal Processing* 100 (2018), pp. 617–629.

[9] Mengyu Chai et al. “Characterization of fatigue crack growth based on acoustic emission multi-parameter analysis”. In: *Materials* 15.19 (2022), p. 6665.

[10] Mengyu Chai et al. “Identification and prediction of fatigue crack growth under different stress ratios using acoustic emission data”. In: *International Journal of Fatigue* 160 (2022), p. 106860.

[11] Nick Connor. *What is Fatigue Life – S-N Curve - Woehler Curve - Definition | Material Properties — material-properties.org*. [Accessed 14-02-2024]. 2020. URL: https://material-properties.org/what-is-fatigue-life-s-n-curve-woehler-curve-definition/.

[12] IM Daniel et al. “Acoustic emission monitoring of fatigue damage in metals”. In: *Nondestructive Testing and Evaluation* 14.1-2 (1998), pp. 71–87.

[13] Yan Dong, Yordan Garbatov, and C Guedes Soares. “Review on uncertainties in fatigue loads and fatigue life of ships and offshore structures”. In: *Ocean Engineering* 264 (2022), p. 112514.

[14] D Gagar, P Foote, and PE Irving. “Effects of loading and sample geometry on acoustic emission generation during fatigue crack growth: Implications for structural health monitoring”. In: *International Journal of Fatigue* 81 (2015), pp. 117–127.

[15] Daniel Gagar, Peter Foote, and Philip Irving. “A novel closure based approach for fatigue crack length estimation using the acoustic emission technique in structural health monitoring applications”. In: *Smart materials and structures* 23.10 (2014), p. 105033.

[16] Christian U Grosse et al. *Acoustic emission testing: Basics for research–applications in engineering*. Springer Nature, 2021.

[17] Zhiyuan Han et al. “Acoustic emission during fatigue crack propagation in a micro-alloyed steel and welds”. In: *Materials Science and Engineering: A* 528.25-26 (2011), pp. 7751–7756.

[18] Zhiyuan Han et al. “Acoustic emission study of fatigue crack propagation in extruded AZ31 magnesium alloy”. In: *Materials Science and Engineering: A* 597 (2014), pp. 270–278.

[19] Sajed Nemati Havigh and Mehdi Behdarvandi Askar. “The process of fatigue analysis on fixed metal offshore platforms”. In: *Mar. Sci* 7 (2017), pp. 10–16.

[20] Illinois Tool Works Inc. (ITW). *8801 Servohydraulic Fatigue Testing System*. Accessed: 2024-07-30. 2024. URL: https://www.instron.com/-/media/literature-library/products/2013/10/8801-fatigue-testing-system.pdf.

[21] Abílio MP de Jesus et al. “A comparison of the fatigue behavior between S355 and S690 steel grades”. In: *Journal of constructional steel research* 79 (2012), pp. 140–150.

[22] Moises Jimenez-Martinez. “Fatigue of offshore structures: A review of statistical fatigue damage assessment for stochastic loadings”. In: *International Journal of Fatigue* 132 (2020), p. 105327.

[23] Seyed Fouad Karimian, Mohammad Modarres, and Hugh A Bruck. “A new method for detecting fatigue crack initiation in aluminum alloy using acoustic emission waveform information entropy”. In: *Engineering fracture mechanics* 223 (2020), p. 106771.

[24] Azadeh Keshtgar, Christine M Sauerbrunn, and Mohammad Modarres. “Structural reliability prediction using acoustic emission-based modeling of fatigue crack growth”. In: *Applied Sciences* 8.8 (2018), p. 1225.

[25] Yuefei Ma et al. “Evaluation of prediction models for crack length of duplex 2205 stainless steel based on acoustic emission technology”. In: *Engineering Failure Analysis* 139 (2022), p. 106486.

[26] SL McBride, JW MacLachlan, and BP Paradis. “Acoustic emission and inclusion fracture in 7075 aluminum alloys”. In: *Journal of Nondestructive Evaluation* 2 (1981), pp. 35–41.

[27] Ronnie K Miller and Paul McIntire. “Nondestructive testing handbook. vol. 5: Acoustic emission testing”. In: *American Society for Nondestructive Testing, 1987,* (1987), p. 603.

[28] Anthony F Molland and Stephen R Turnock. *Marine rudders, hydrofoils and control surfaces: Principles, data, design and applications*. Butterworth-Heinemann, 2021.

[29] TM Morton, RM Harrington, and JG Bjeletich. “Acoustic emissions of fatigue crack growth”. In: *Engineering fracture mechanics* 5.3 (1973), pp. 691–697.

[30] Oil and Gas Piping Materials. *Supplier Of Piping Materials, Oil And Gas Tubing In Carbon Steel*. https://www.oilandgaspipingmaterials.com/. Accessed: 2024-07-30.

[31] Paul Paris and Fazil Erdogan. “A critical analysis of crack propagation laws”. In: *Journal of Basic Engineering* 85 (4 1963), pp. 528–533. DOI: 10.1115/1.3656900.

[32] Rhys Pullin et al. “Validation of acoustic emission (AE) crack detection in aerospace grade steel using digital image correlation”. In: *Applied Mechanics and Materials* 24 (2010), pp. 221–226.

[33] RO Ritchie, GG Garrett, and JP Knott. “Crack-growth monitoring: optimisation of the electrical potential technique using an analogue method”. In: *International Journal of Fracture Mechanics* 7.4 (1971), p. 462.

[34] Terence Martin Roberts and M Talebzadeh. “Fatigue life prediction based on crack propagation and acoustic emission count rates”. In: *Journal of constructional steel research* 59.6 (2003), pp. 679–694.

[35] TMand Roberts and M Talebzadeh. “Acoustic emission monitoring of fatigue crack propagation”. In: *Journal of constructional steel research* 59.6 (2003), pp. 695–712.

[36] LM Rogers. “Structural and engineering monitoring by acoustic emission methods–fundamentals and applications”. In: *Lloyd’s Register Technical Investigation Department* (2001).

[37] CM Scala and S McK Cousland. “Acoustic emission during fatigue crack propagation in the aluminium alloys 2024 and 2124”. In: *Materials Science and Engineering* 61.3 (1983), pp. 211–218.

[38] Jaap Schijve. *Fatigue of structures and materials*. Springer, 2009.

[39] CB Scruby, GR Baldwin, and KA Stacey. “Characterisation of fatigue crack extension by quantitative acoustic emission”. In: *International Journal of Fracture* 28 (1985), pp. 201–222.

[40] Claude Elwood Shannon. “A mathematical theory of communication”. In: *The Bell system technical journal* 27.3 (1948), pp. 379–423.

[41] Shengrun Shi et al. “Acoustic Emission Monitoring of Fatigue Crack Growth in Hadfield Steel”. In: *Sensors* 23.14 (2023), p. 6561.

[42] ACE Sinclair, CL Formby, and DC Connors. “Acoustic emission from a defective C/Mn steel pressure vessel”. In: *International Journal of Pressure Vessels and Piping* 3.3 (1975), pp. 153–174.

[43] ASTM Standard. “E647-00”. In: *Standard test method for measurement of fatigue crack growth rates. Annual book of ASTM Standards* 3 (2000).

[44] Octal Steel. *API 5L Grade X65 Pipe: Chemical Composition and Mechanical Properties*. https://www.octalsteel.com/resources/api-5l-x65-pipe. Accessed: 2024-07-30.

[45] G Storhaug. “Experimental Investigation of Wave Induced Vibrations and Their Effect on the Fatigue Loading of Ships (PhD thesis)”. In: *Norwegian University of Science and Technology* (2007).

[46] Farhan Tanvir et al. “Identification of fatigue damage evaluation using entropy of acoustic emission waveform”. In: *SN Applied Sciences* 2 (2020), pp. 1–15.

[47] Steve Vanlanduit et al. “A digital image correlation method for fatigue test experiments”. In: *Optics and Lasers in Engineering* 47.3-4 (2009), pp. 371–378.

[48] Mario Vieira et al. “Economic Viability of Implementing Structural Health Monitoring Systems on the Support Structures of Bottom-Fixed Offshore Wind”. In: *Energies* 16.13 (2023), p. 4885.

[49] Wikipedia contributors. *Alexander L. Kielland (platform) — Wikipedia, The Free Encyclopedia*. [Online; accessed 18-February-2024]. 2024. URL: https://en.wikipedia.org/w/index.php?title=Alexander_L._Kielland_(platform)&oldid=1199429073.

[50] WF Wu and CC Ni. “Probabilistic models of fatigue crack propagation and their experimental verification”. In: *Probabilistic Engineering Mechanics* 19.3 (2004), pp. 247–257.

[51] Xinyue Yao et al. “Acoustic Emission Source Characterisation during Fatigue Crack Growth in Al 2024-T3 Specimens”. In: *Sensors* 22.22 (2022), p. 8796.

[52] Jianguo Yu et al. “Acoustic emission detection of fatigue damage in cruciform welded joints”. In: *Journal of Constructional Steel Research* 86 (2013), pp. 85–91.

[53] Jianguo Yu et al. “Prediction of fatigue crack growth in steel bridge components using acoustic emission”. In: *Journal of Constructional Steel Research* 67.8 (2011), pp. 1254–1260.

[54] Yan Zhao et al. “High resolution and real-time measurement of 2D fatigue crack propagation using an advanced digital image correlation”. In: *Engineering Fracture Mechanics* 268 (2022), p. 108457.

A

Parametric analysis results

A.1. Specimen No. 1

A.1.1. SNR 2: All datasets

Counts

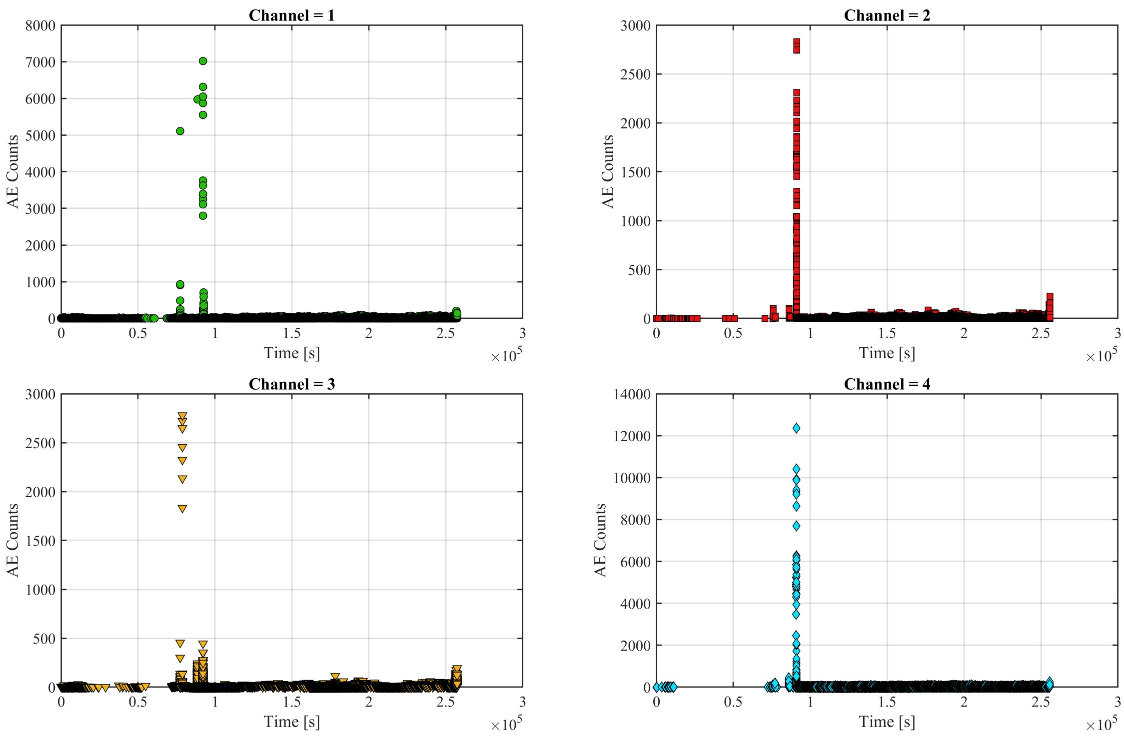

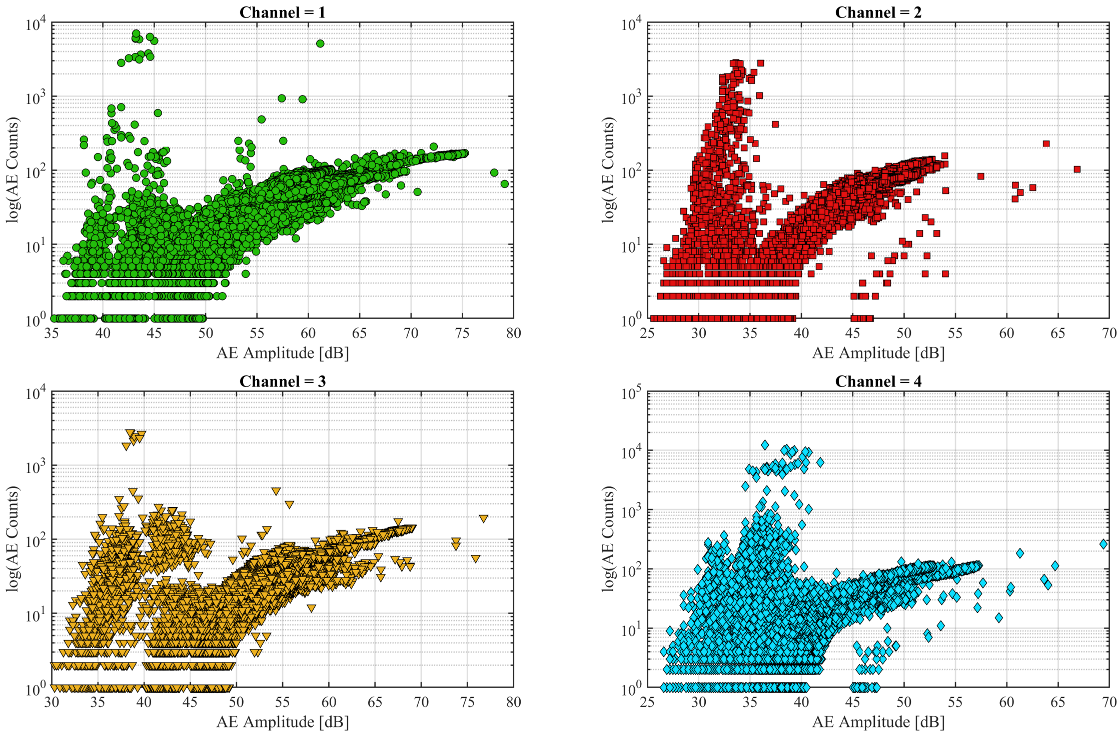

Peak Amplitude

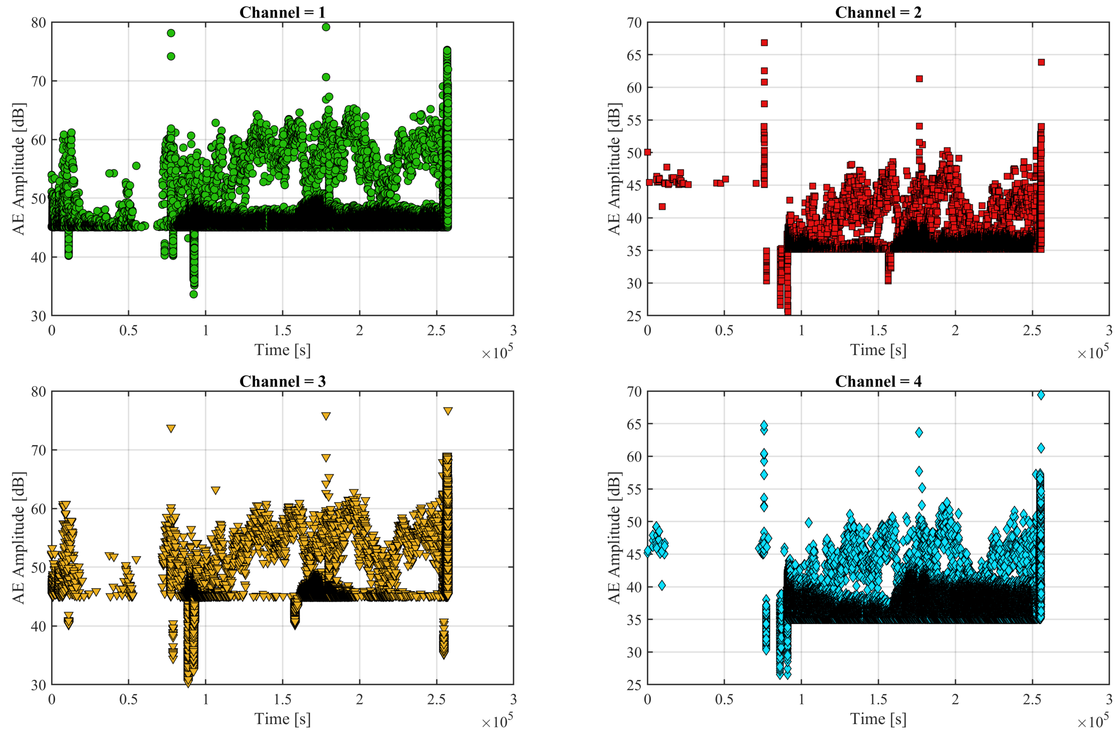

Energy

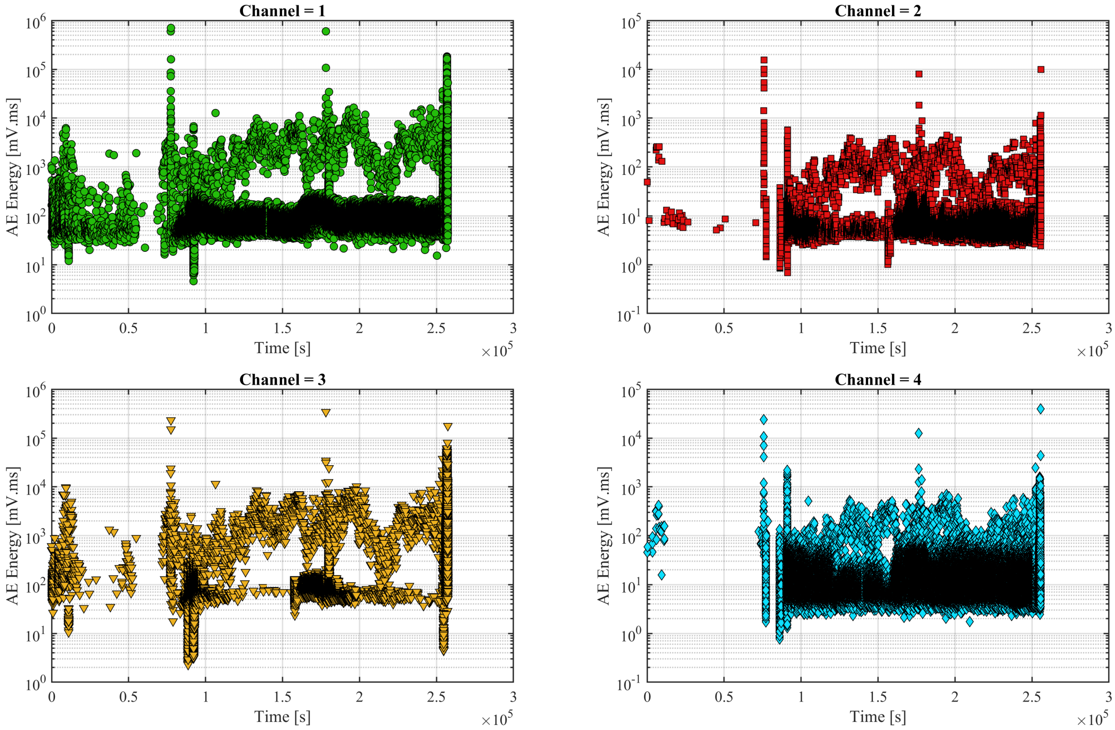

Duration

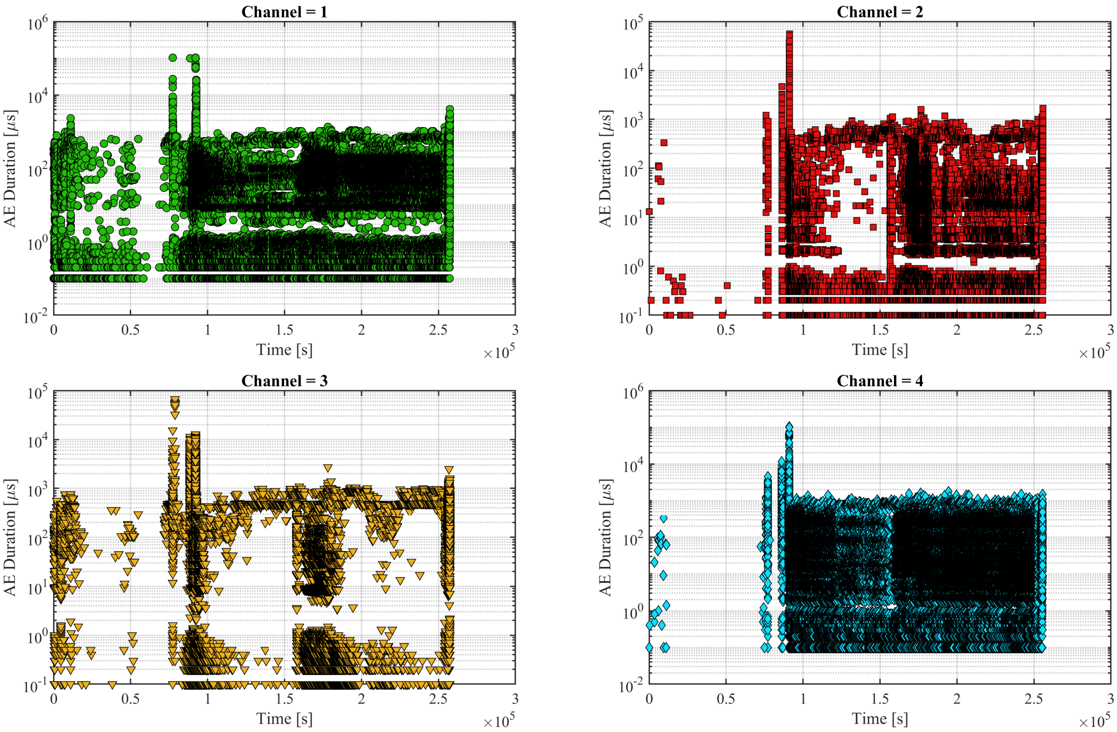

Rise Angle

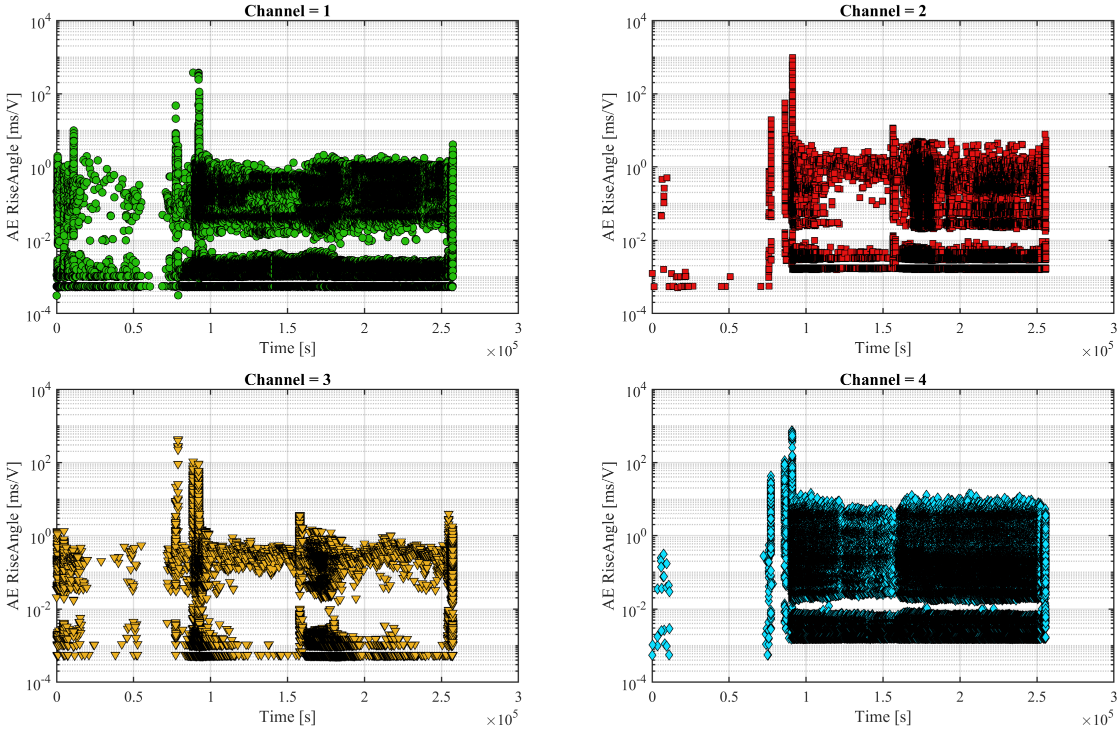

Average Frequency and Rise Angle

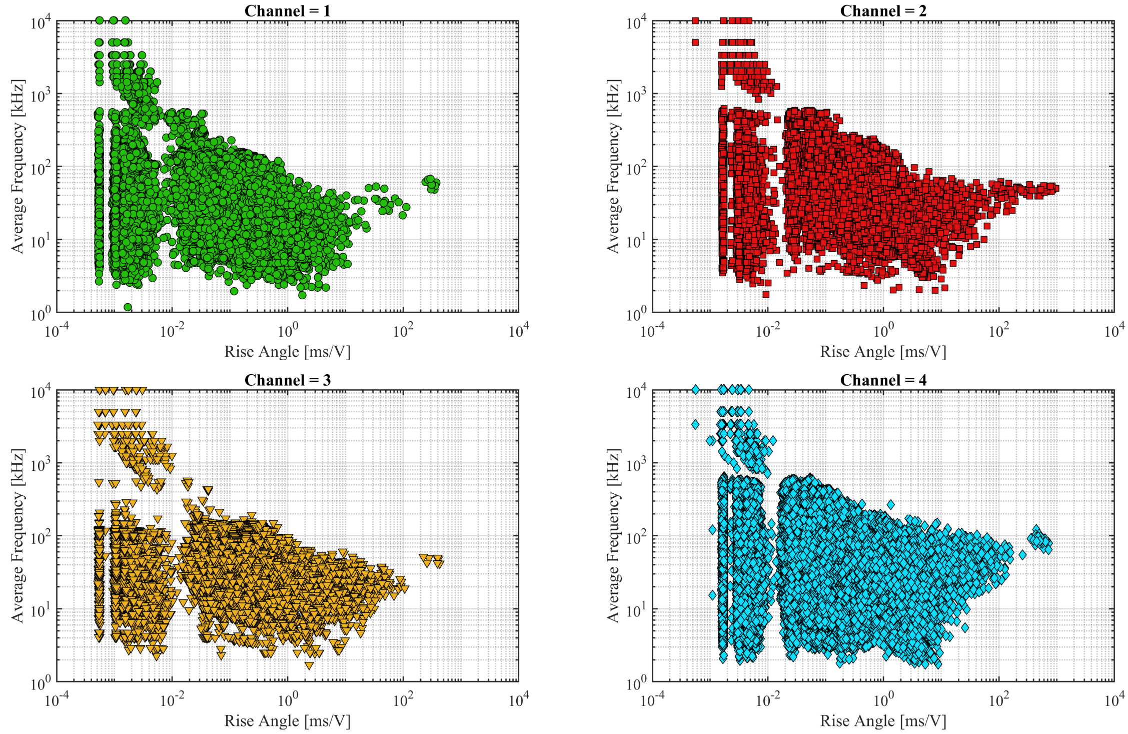

A.1.2. SNR 2: Last 6 datasets

Counts

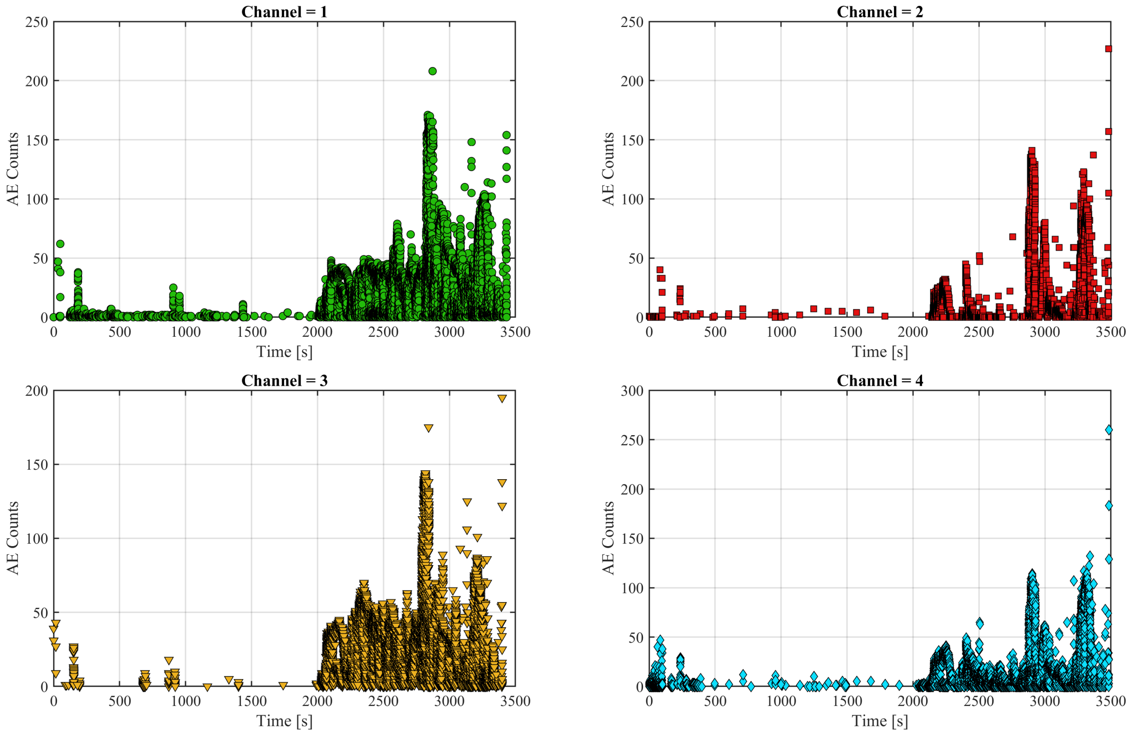

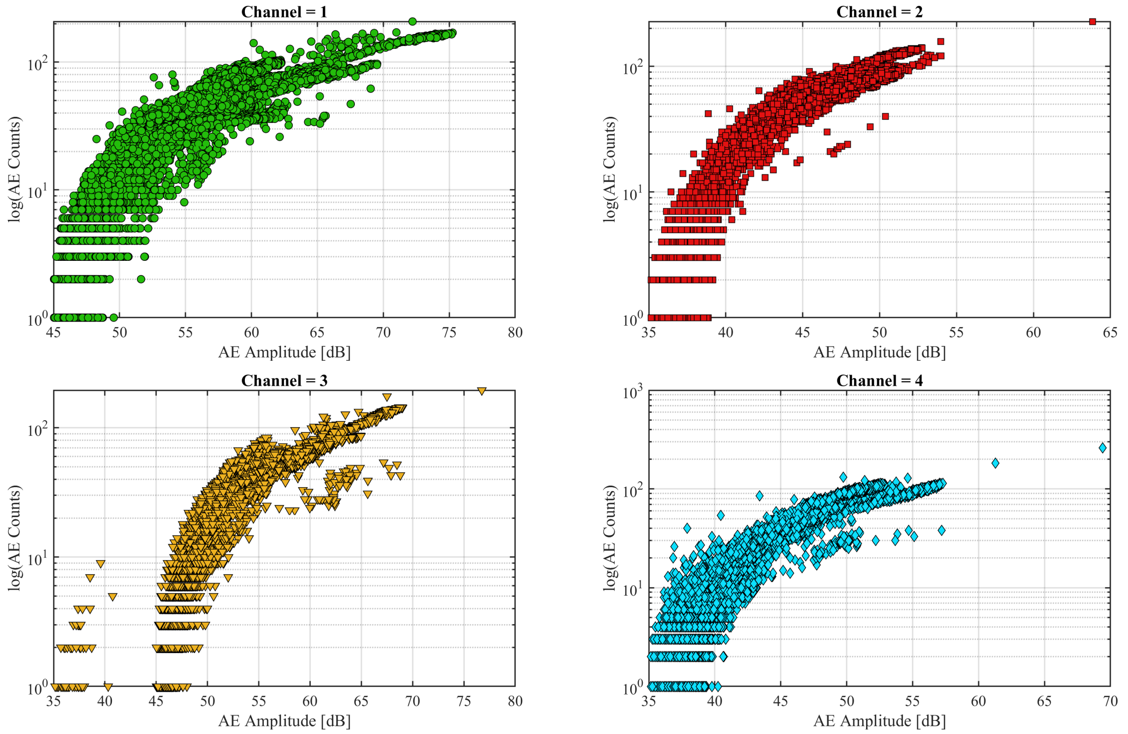

Peak Amplitude

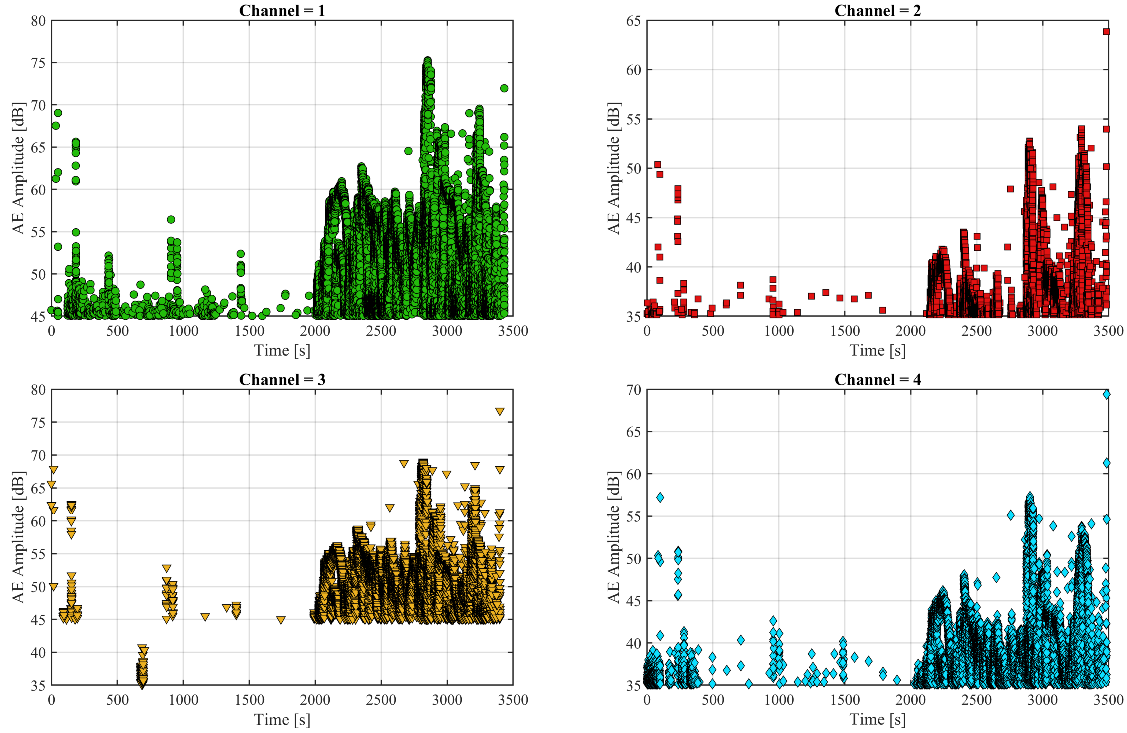

Energy

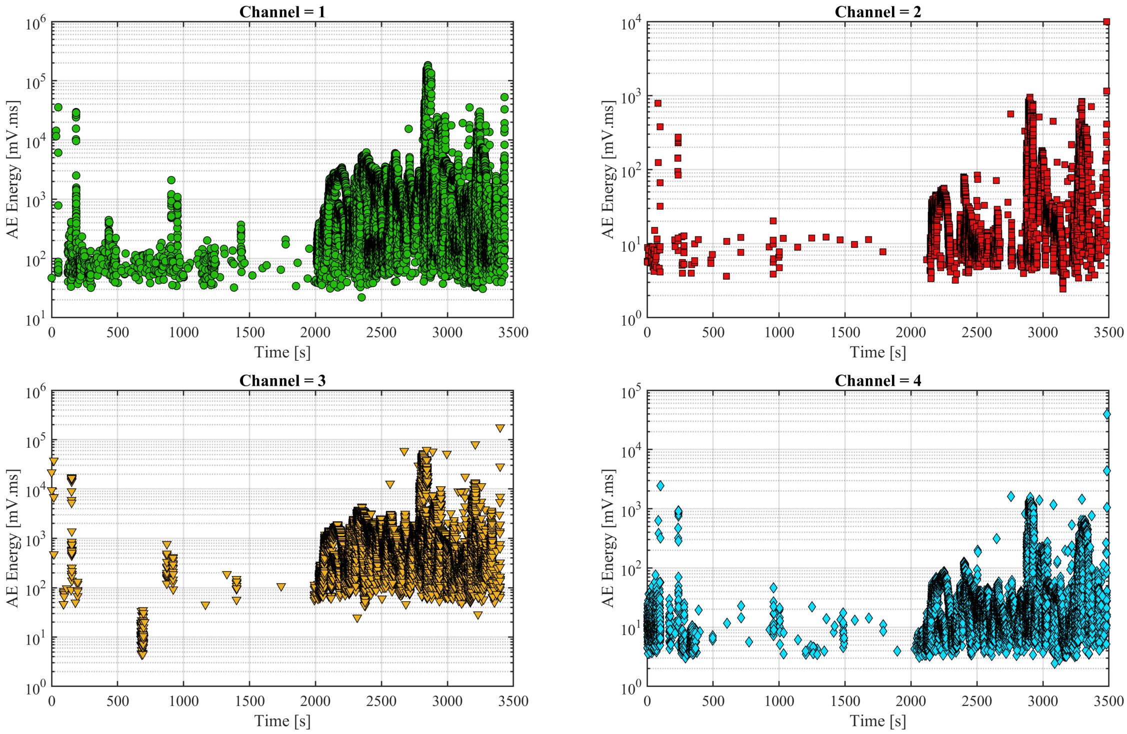

Duration

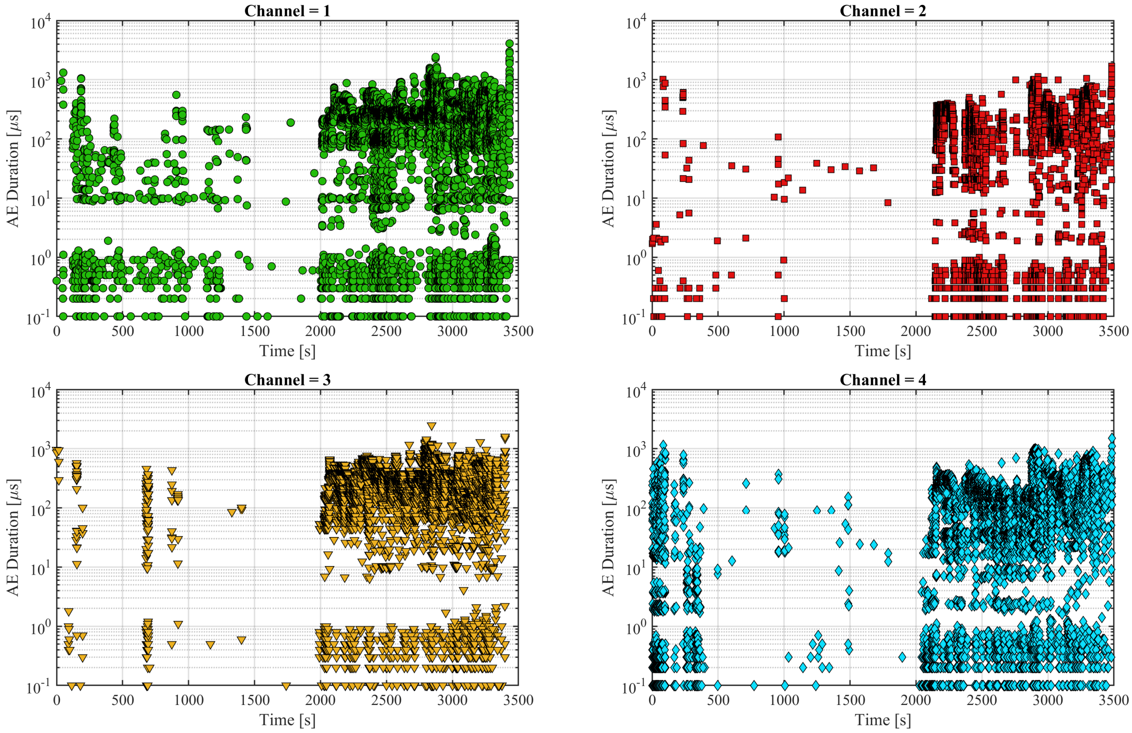

Rise Angle

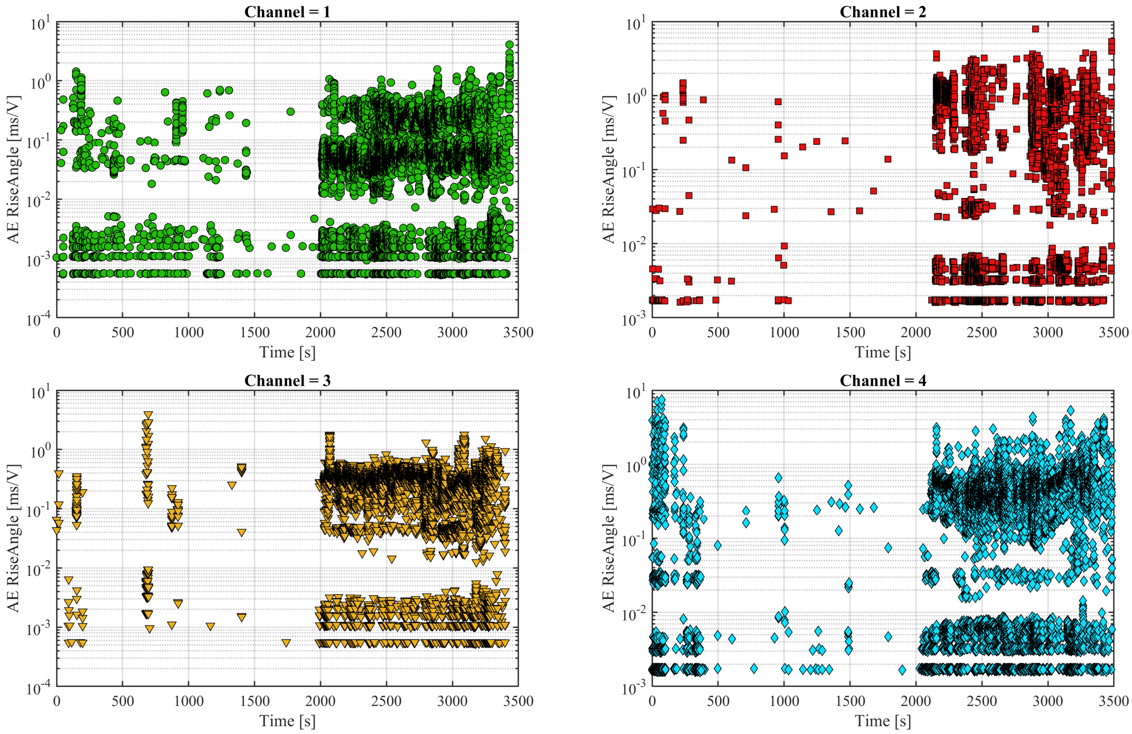

Average Frequency and Rise Angle

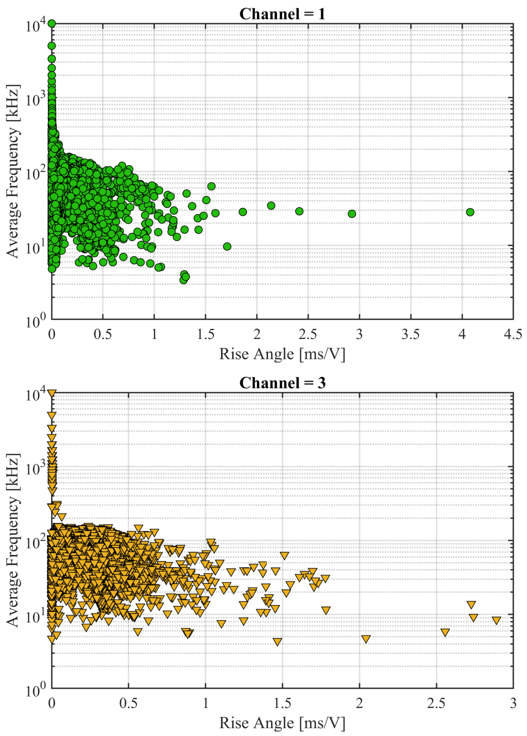

Entropy

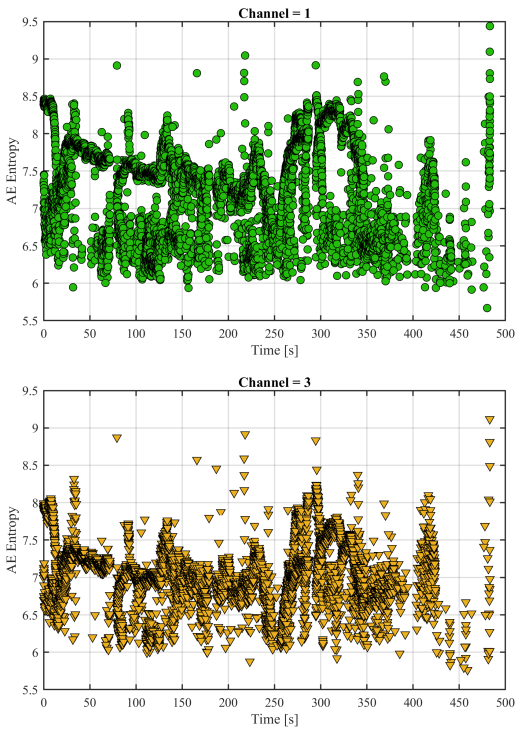

Root mean square (RMS)

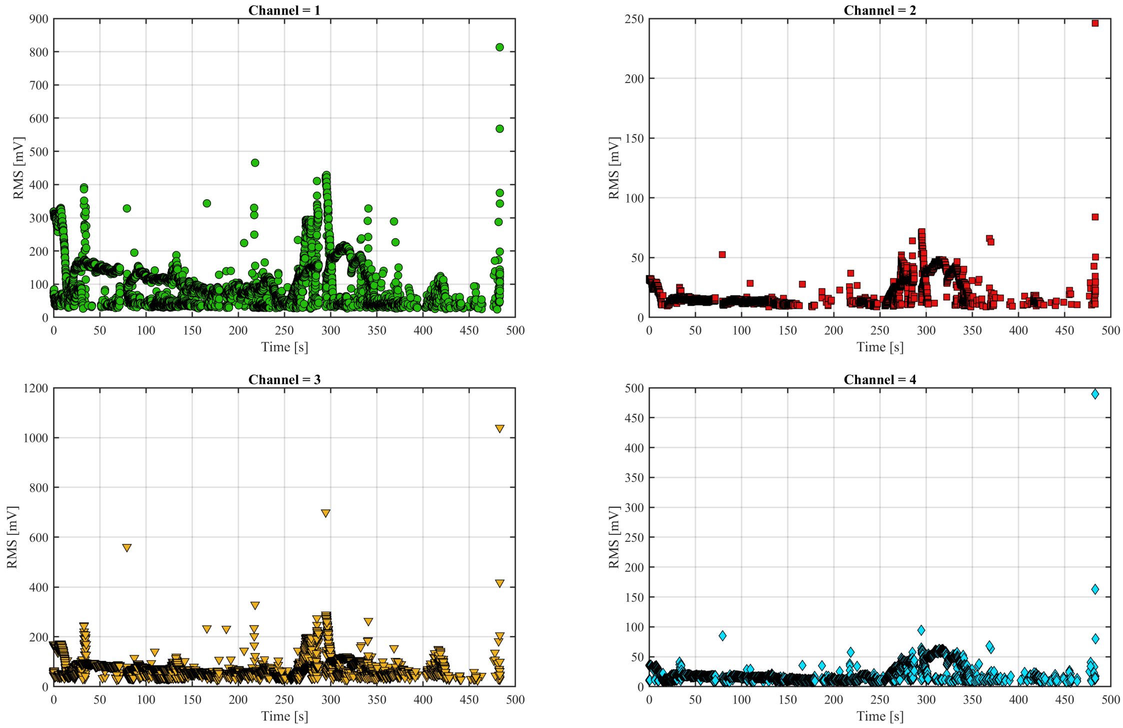

Crest Factor

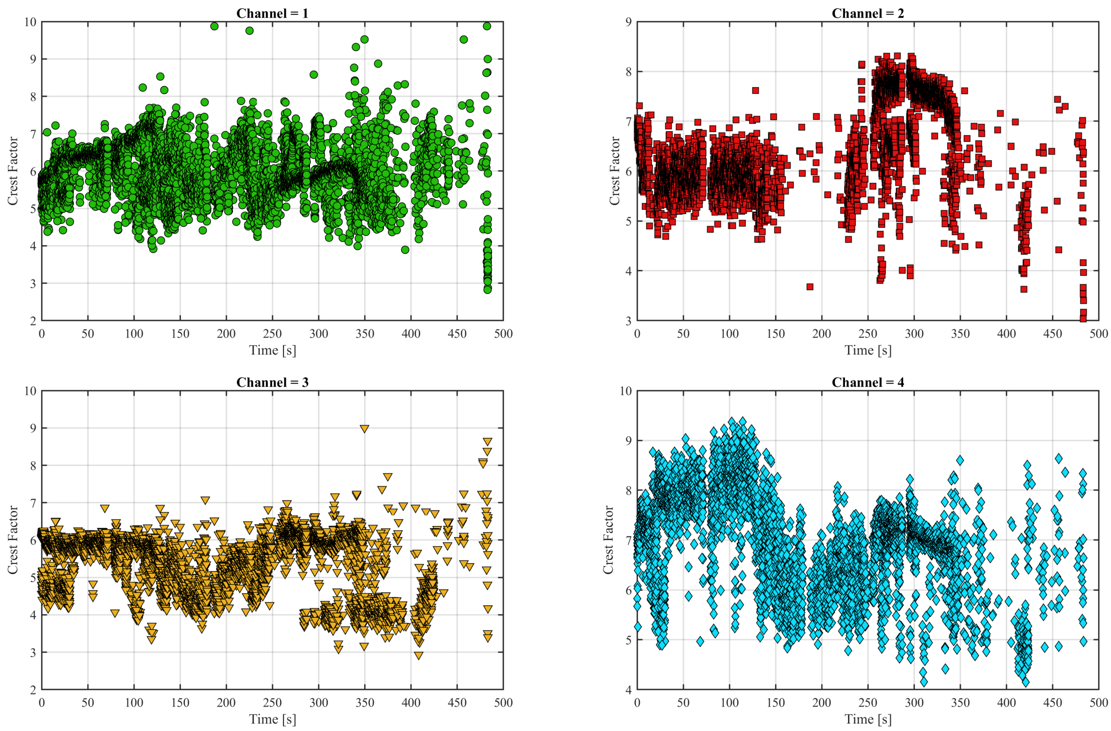

Kurtosis

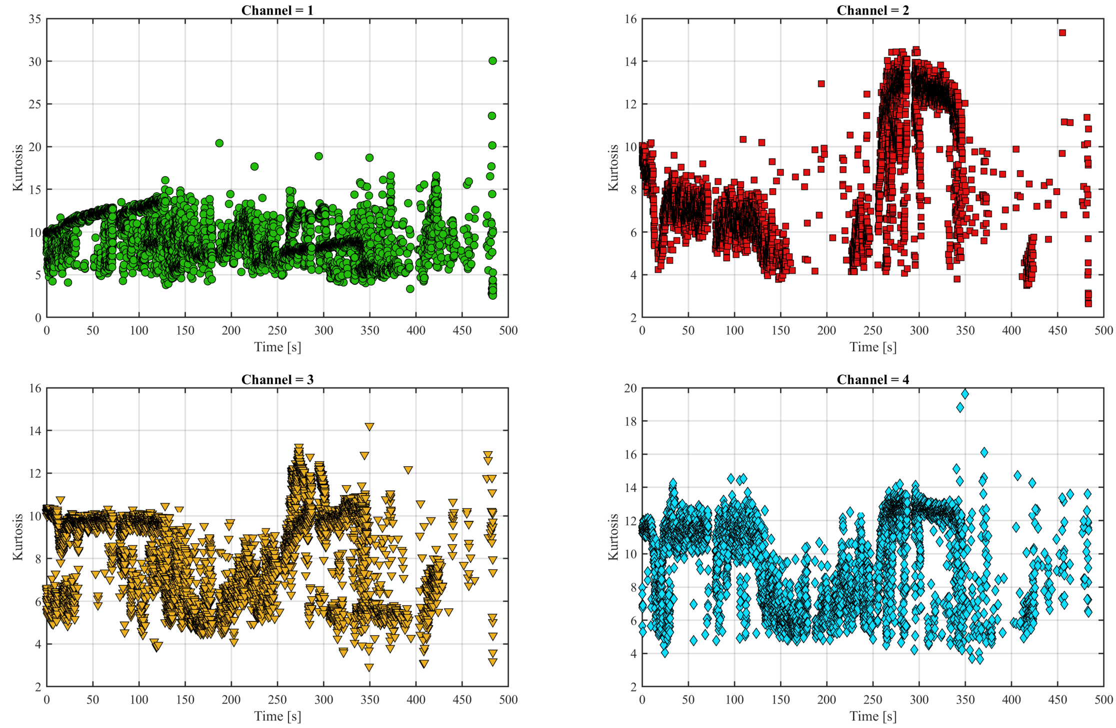

Centroid Frequency

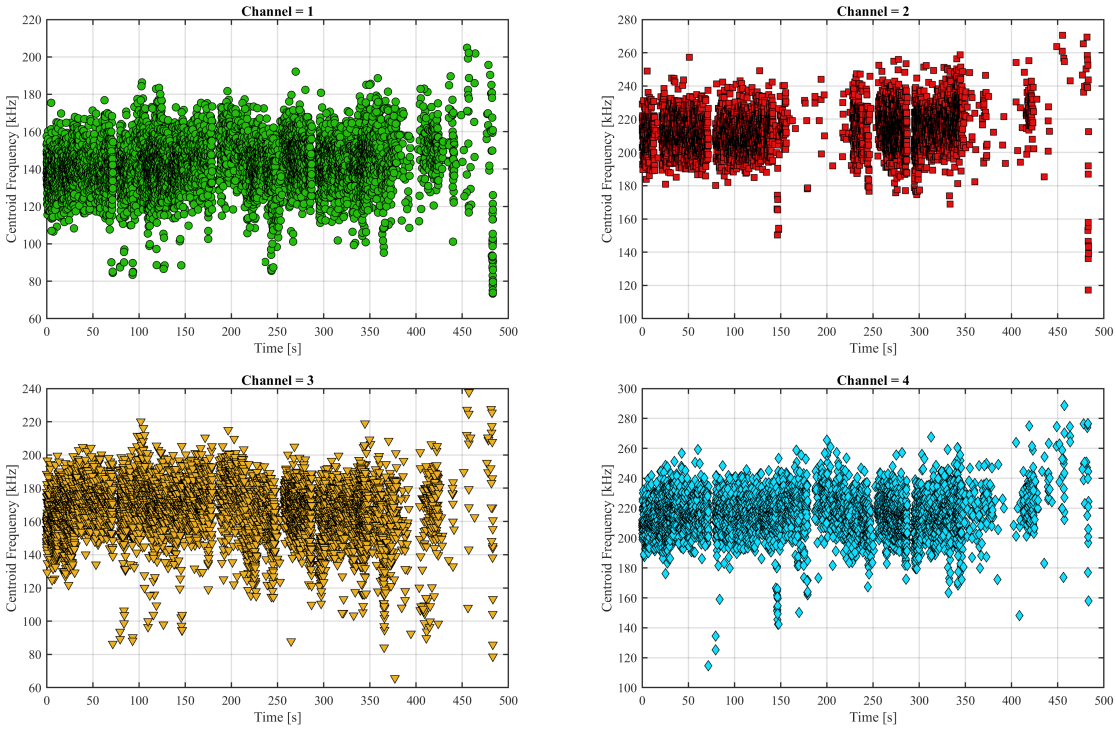

Peak Frequency

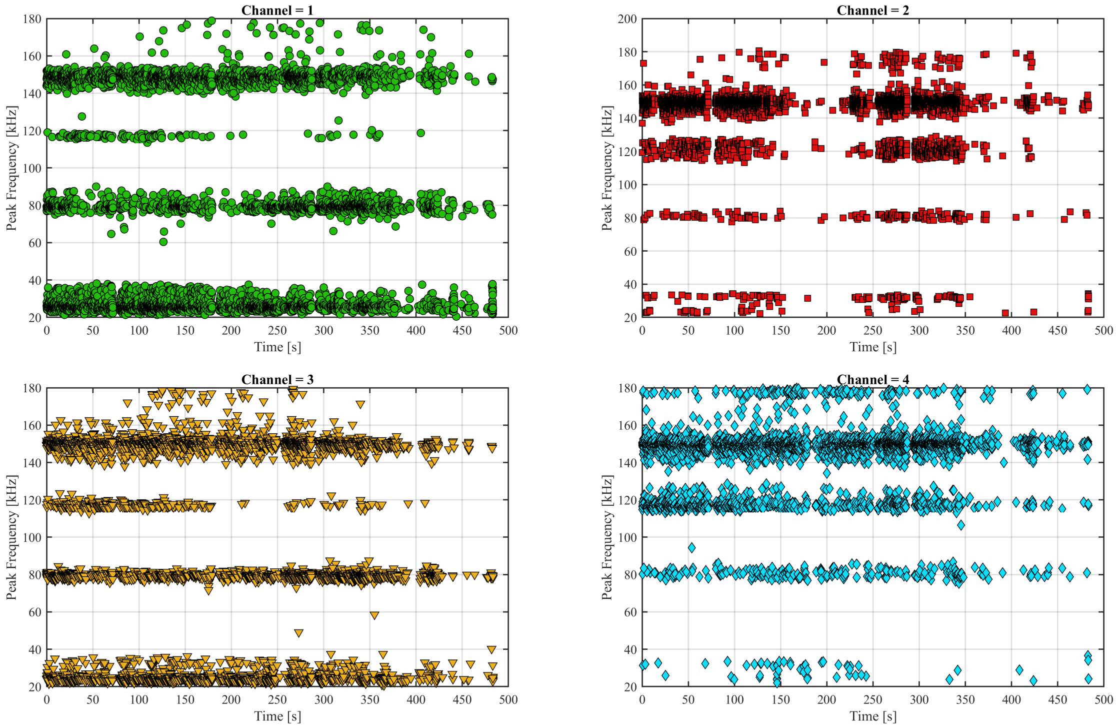

A.2. Specimen No. 2

A.2.1. SNR 2

Counts

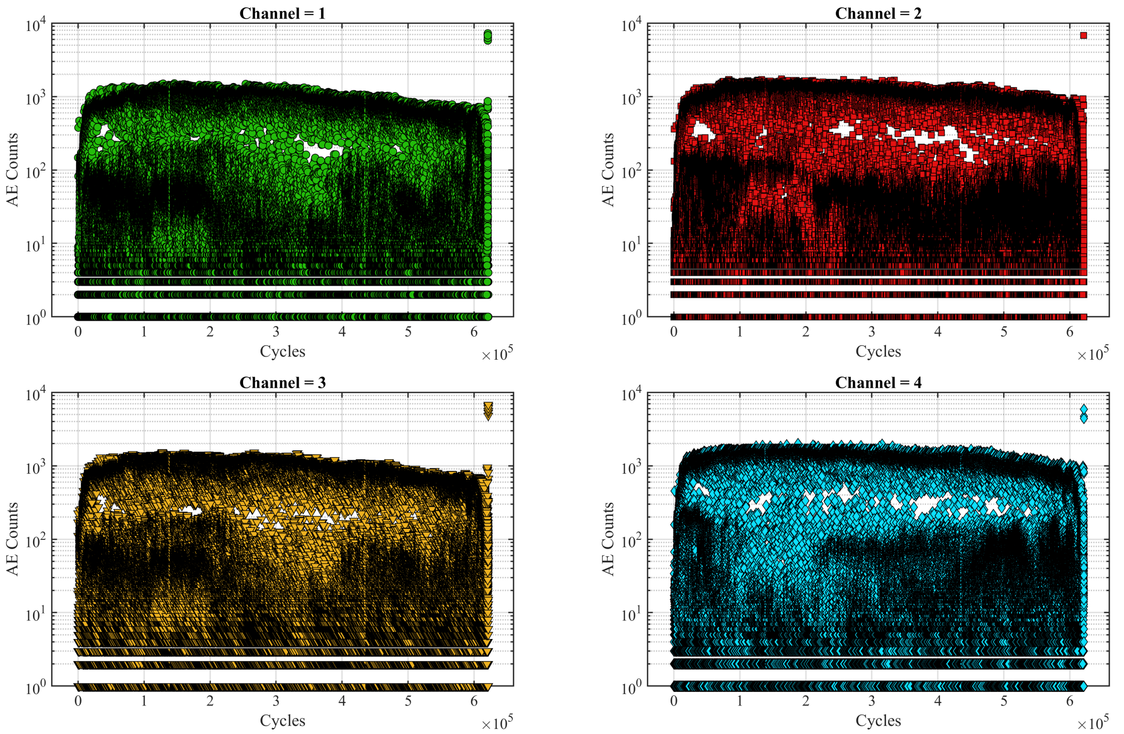

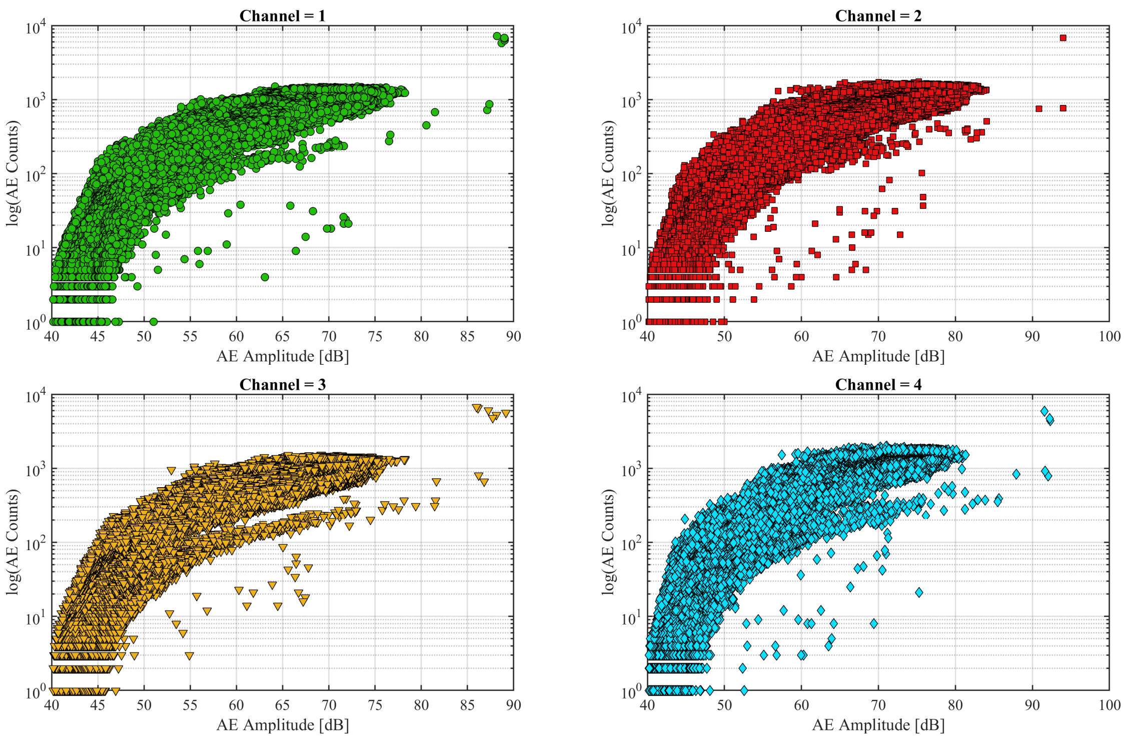

Peak Amplitude

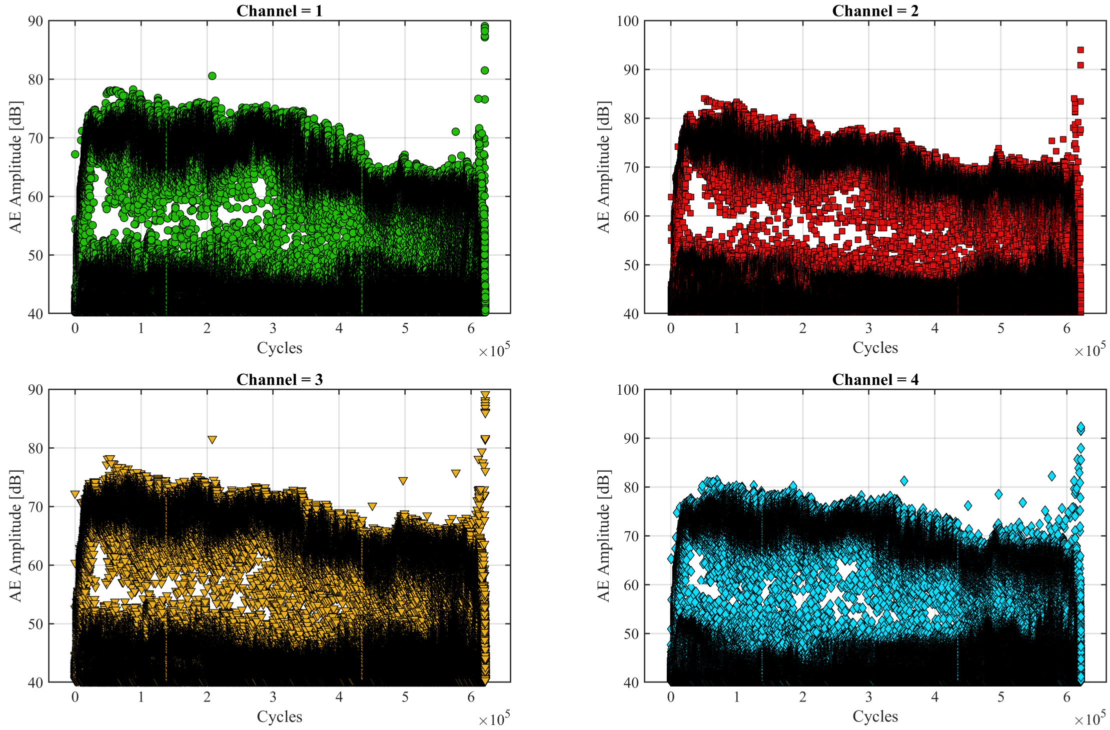

Energy

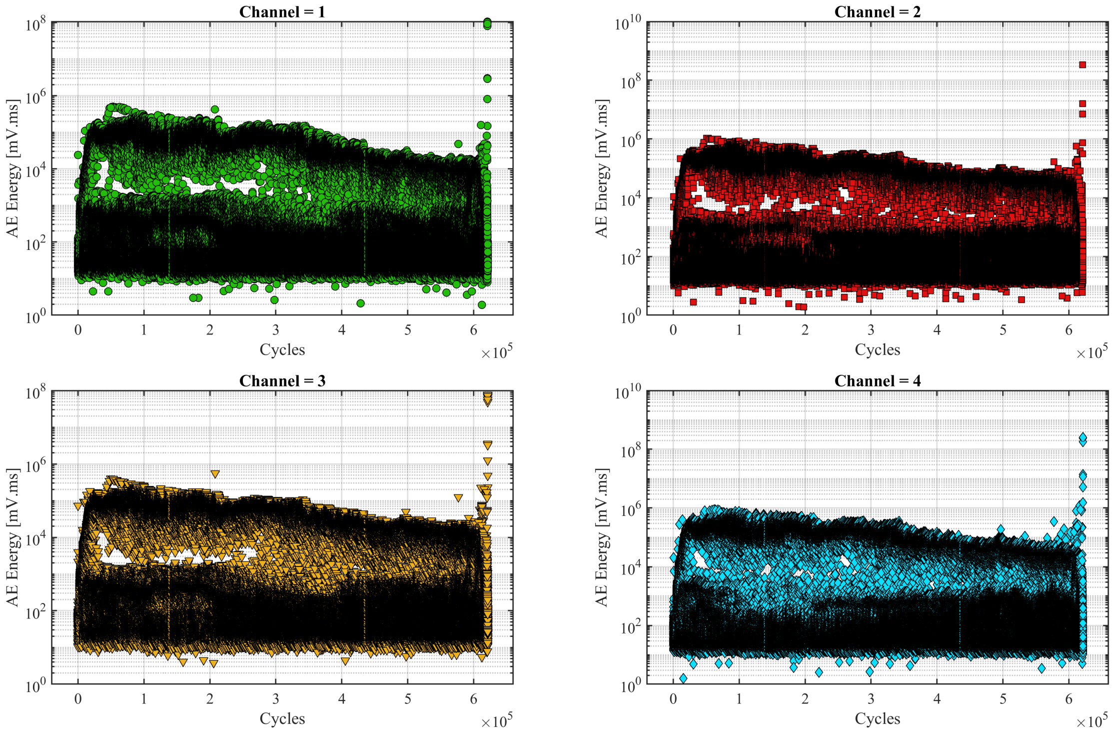

Duration

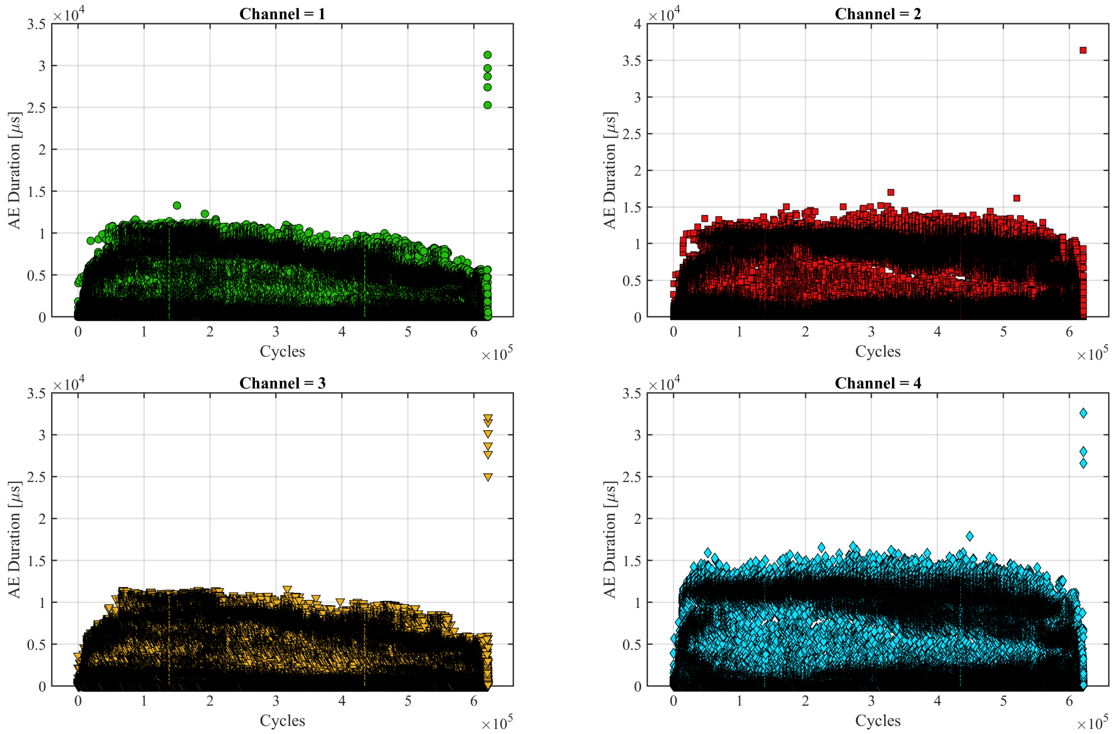

Rise Angle

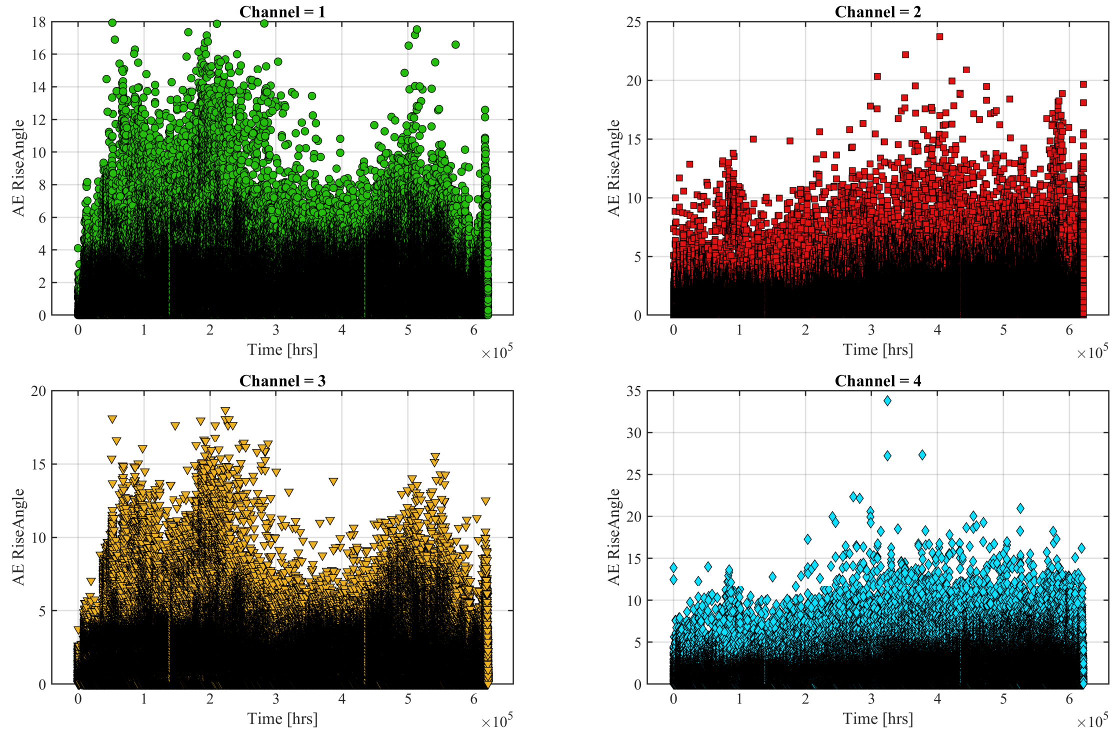

Average Frequency and Rise Angle

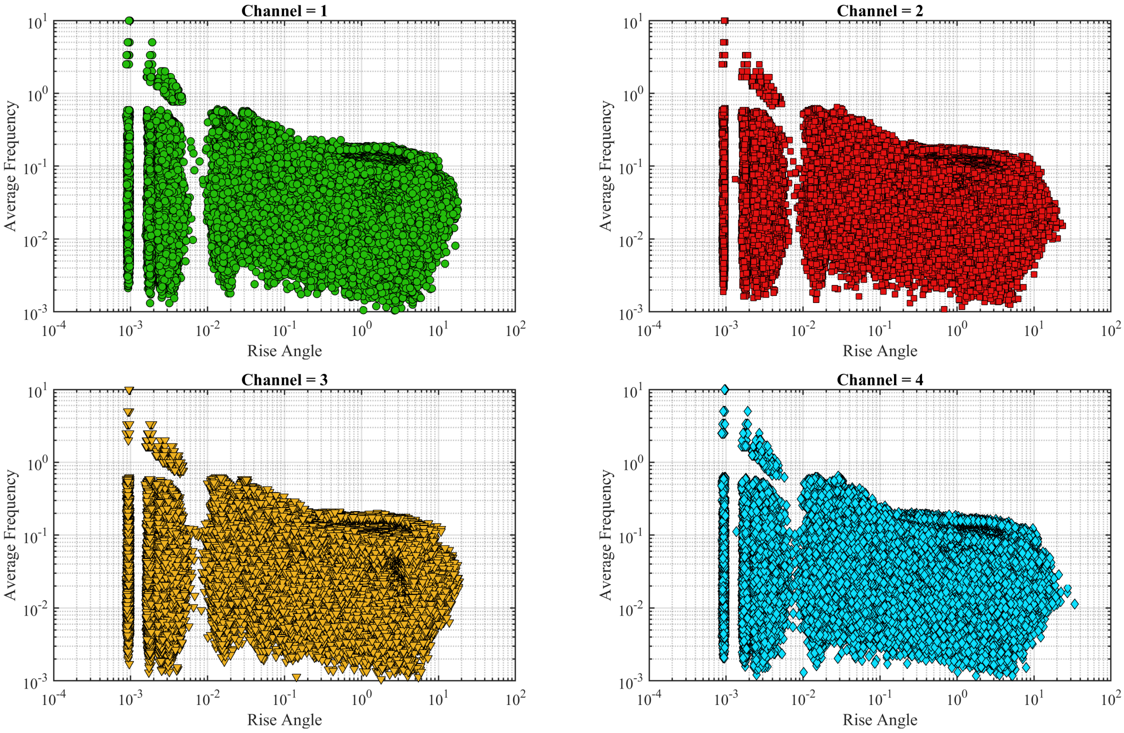

A.2.2. After Amplitude Filter (50 dB)

Counts

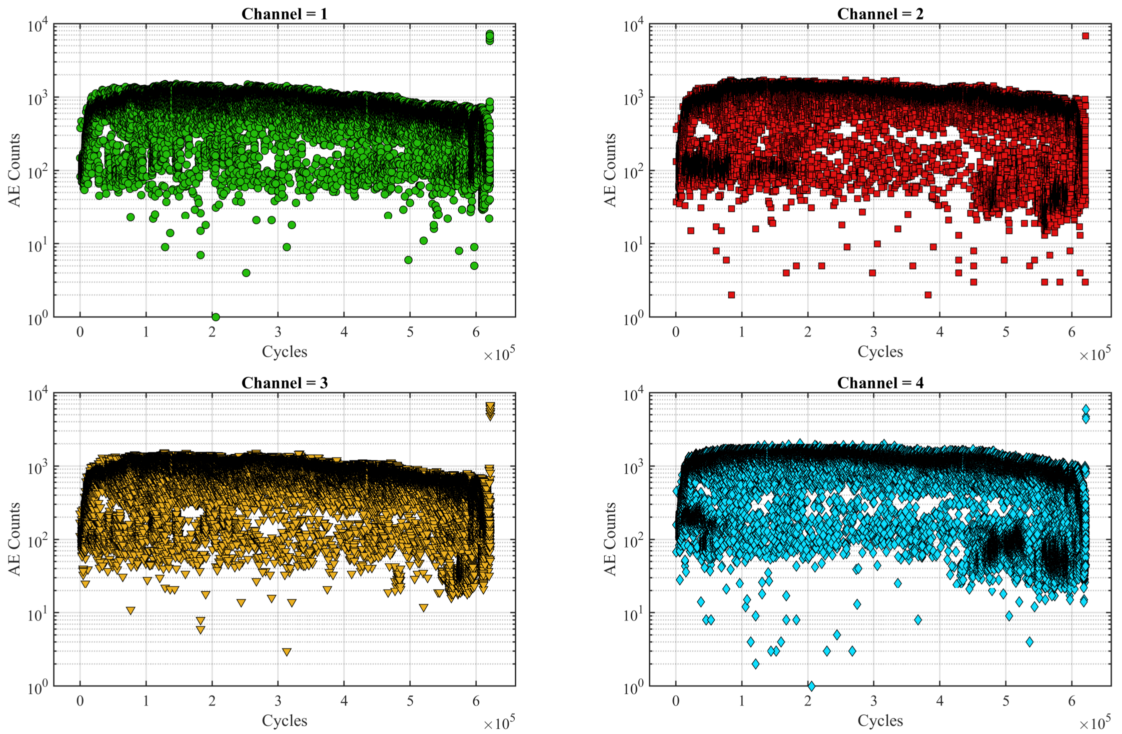

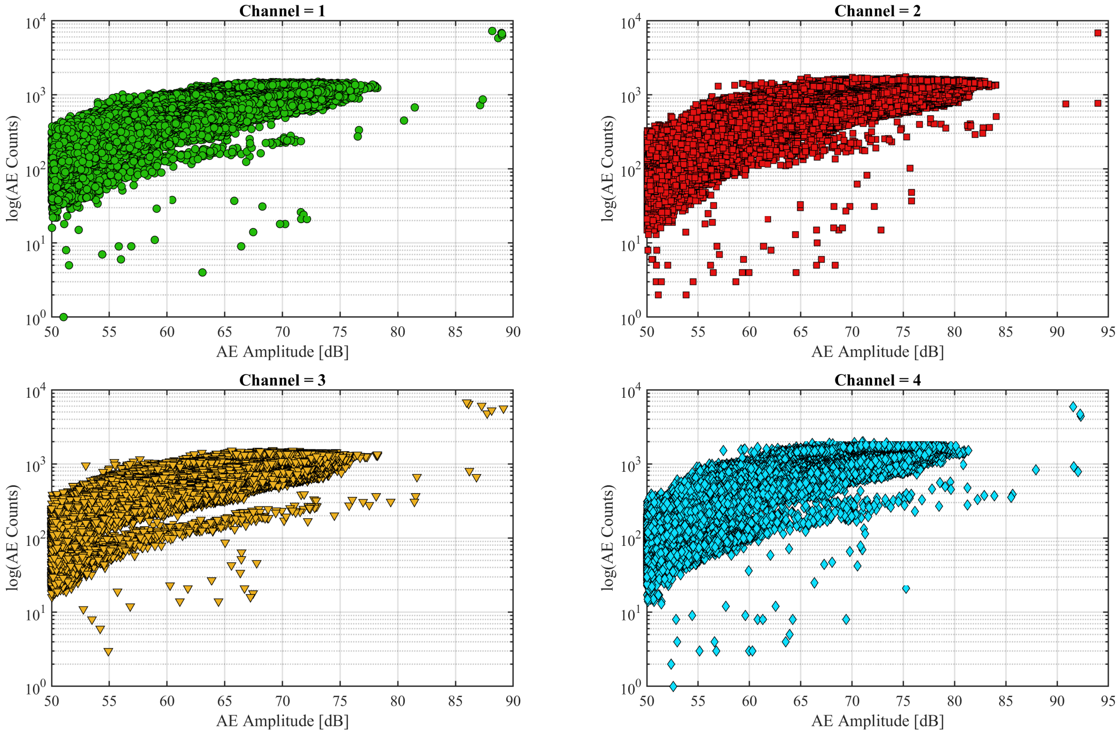

Peak Amplitude

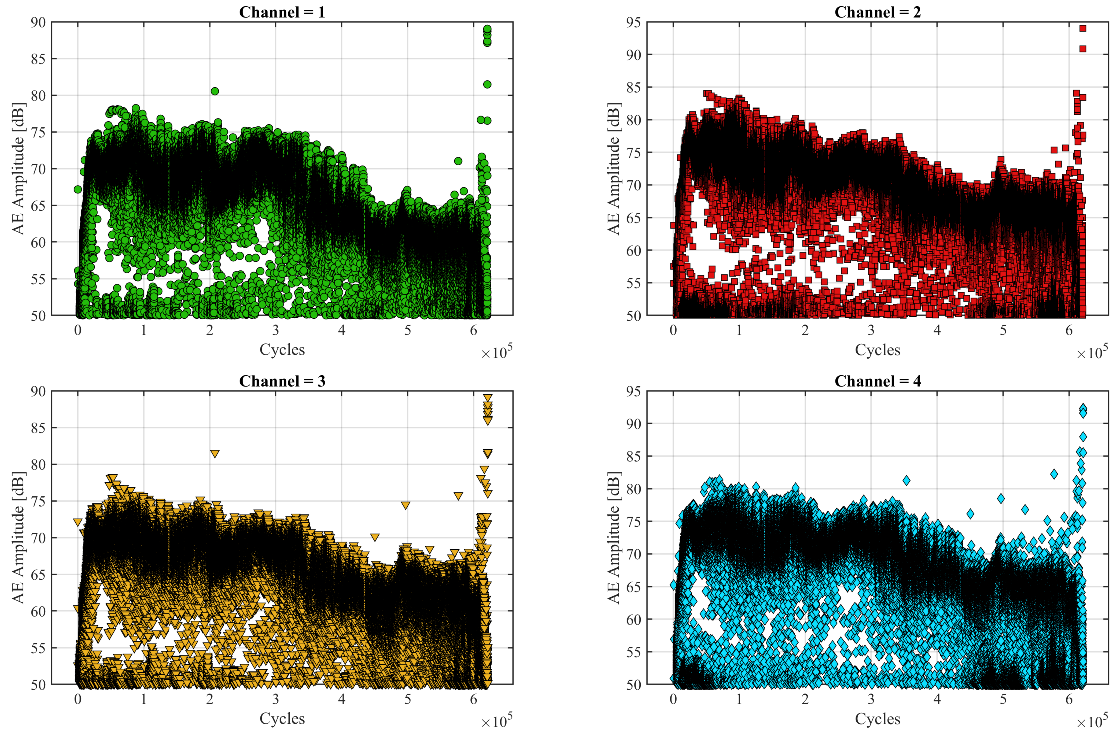

Energy

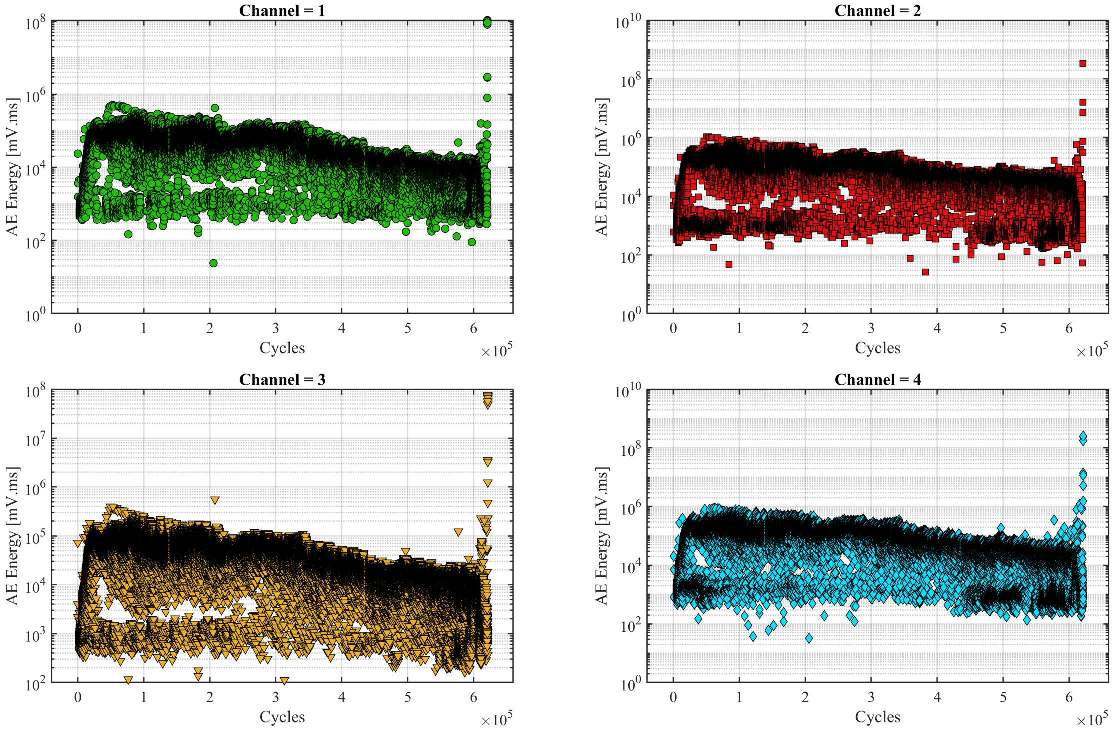

Duration

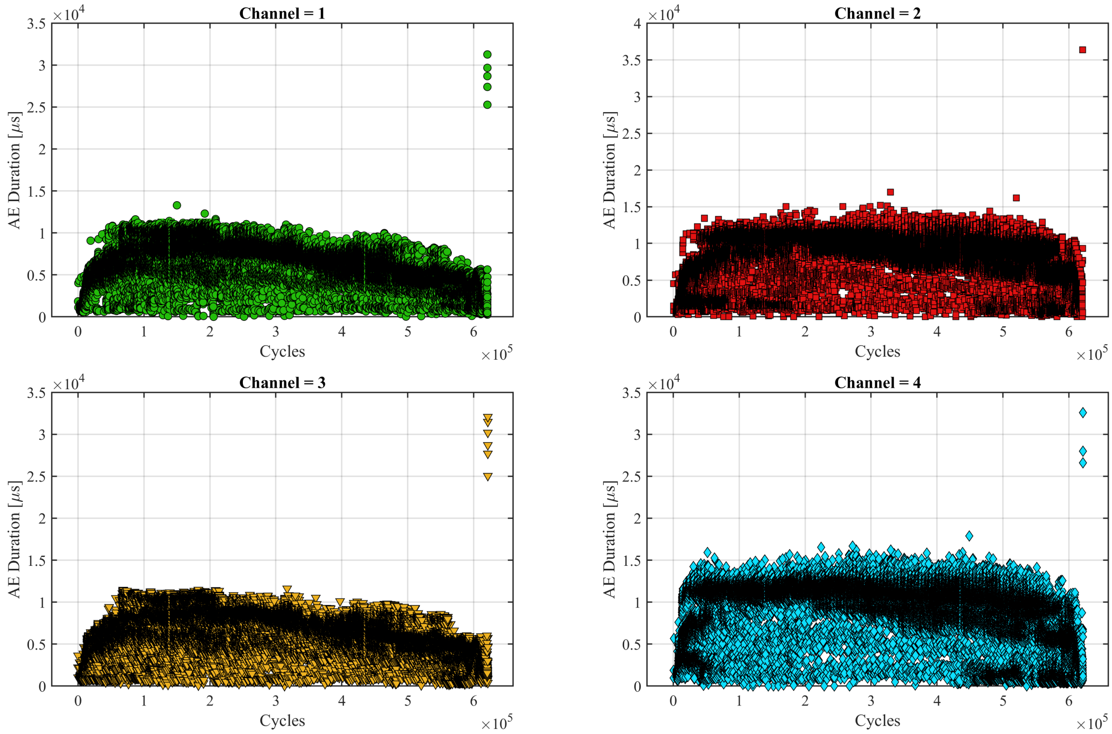

Rise Angle

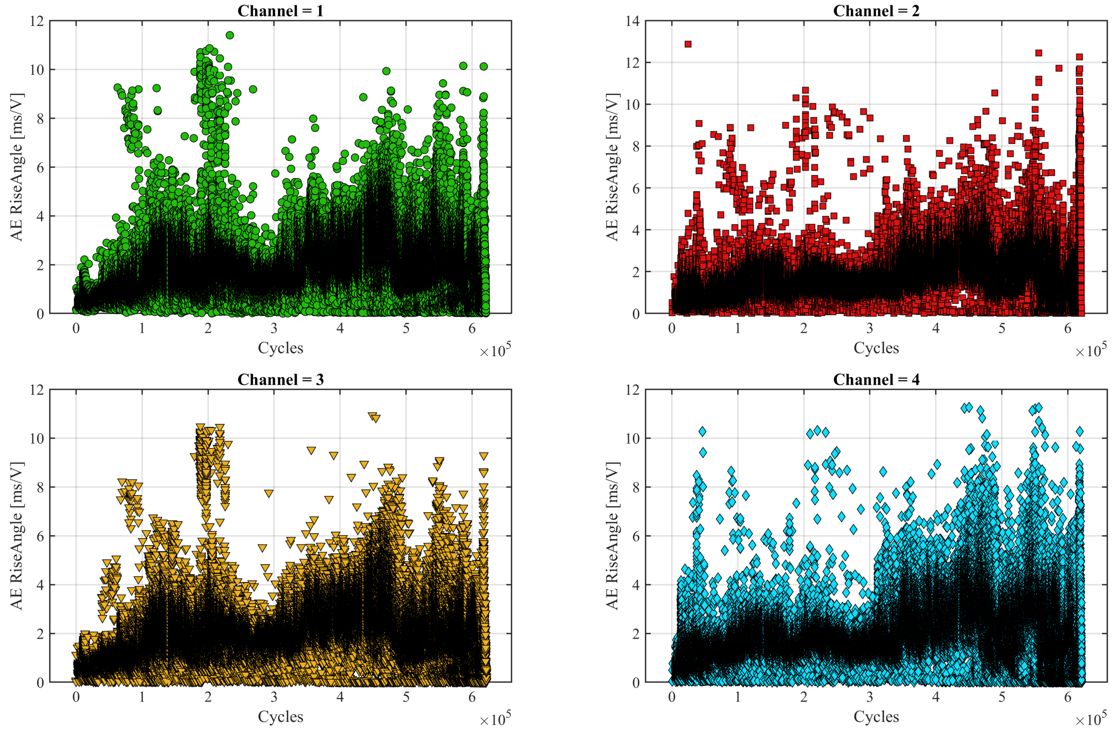

Average Frequency and Rise Angle

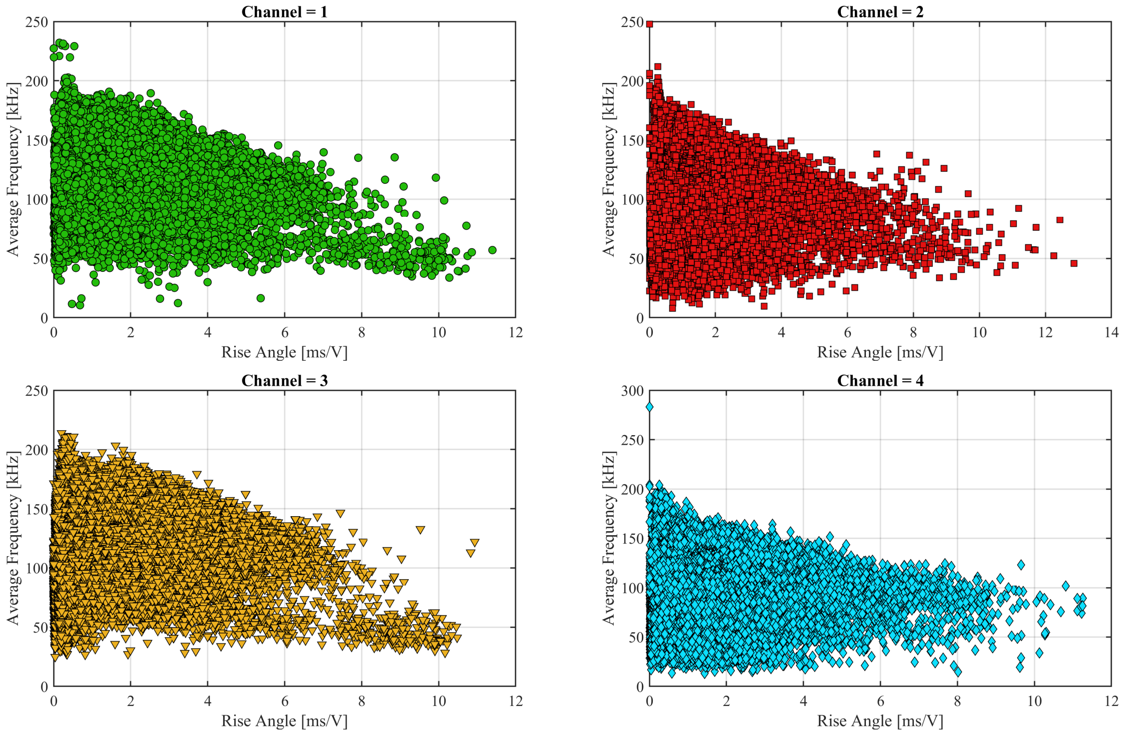

Entropy

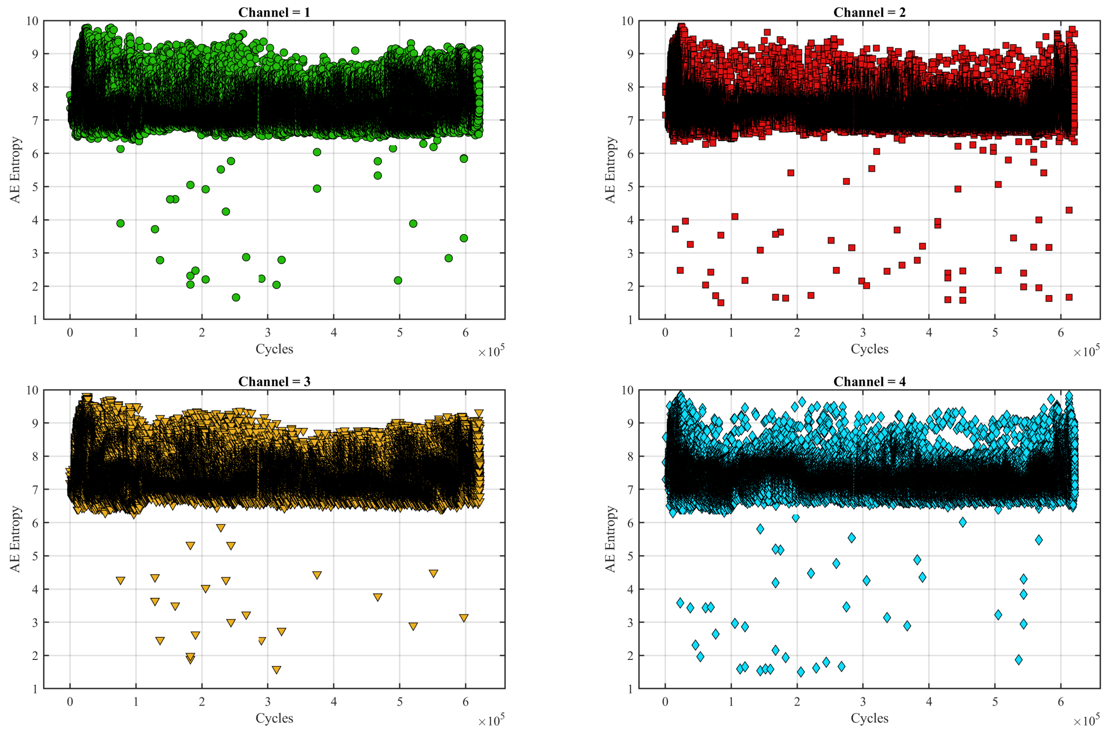

Root mean square (RMS)

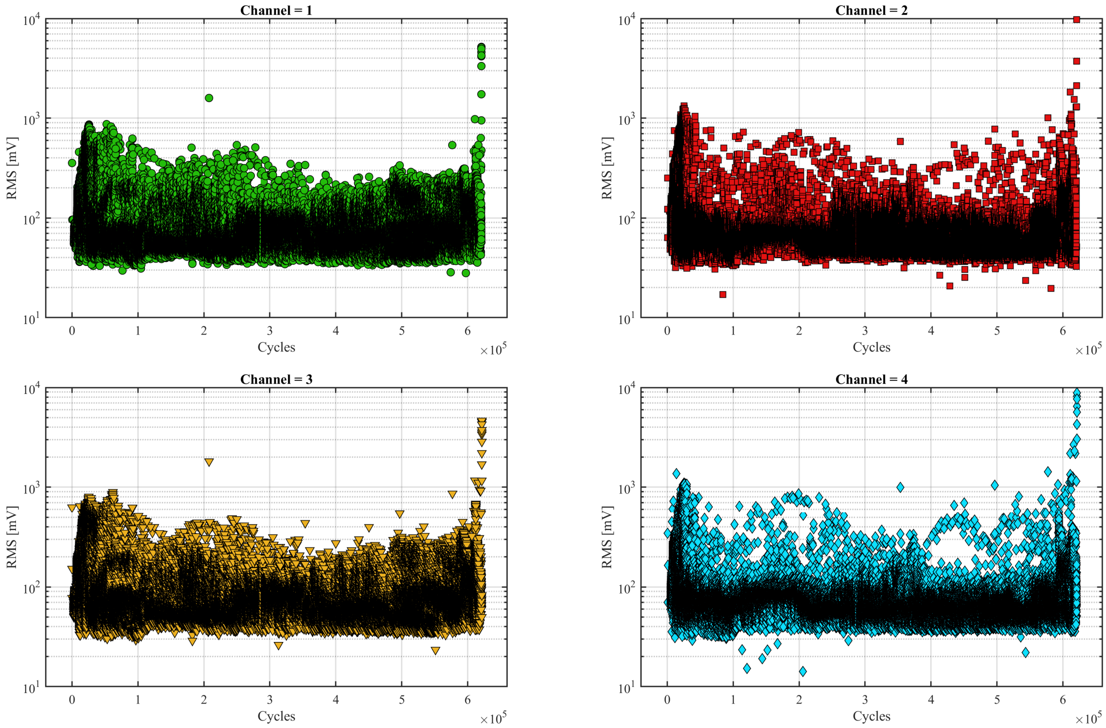

Crest Factor

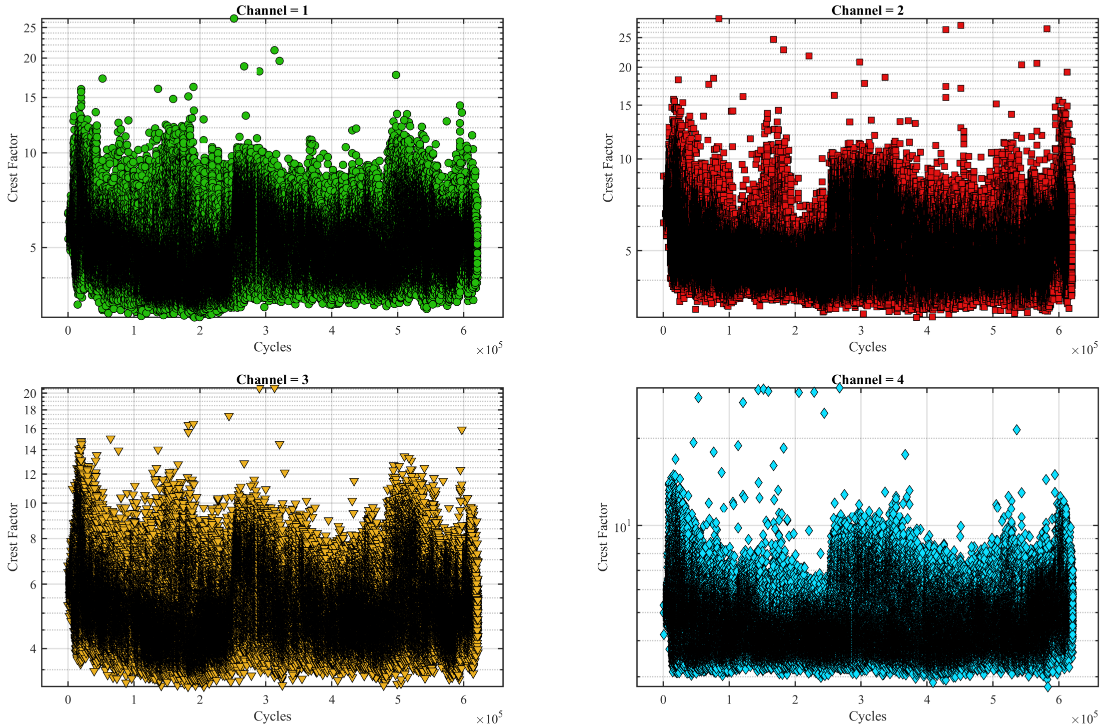

Kurtosis

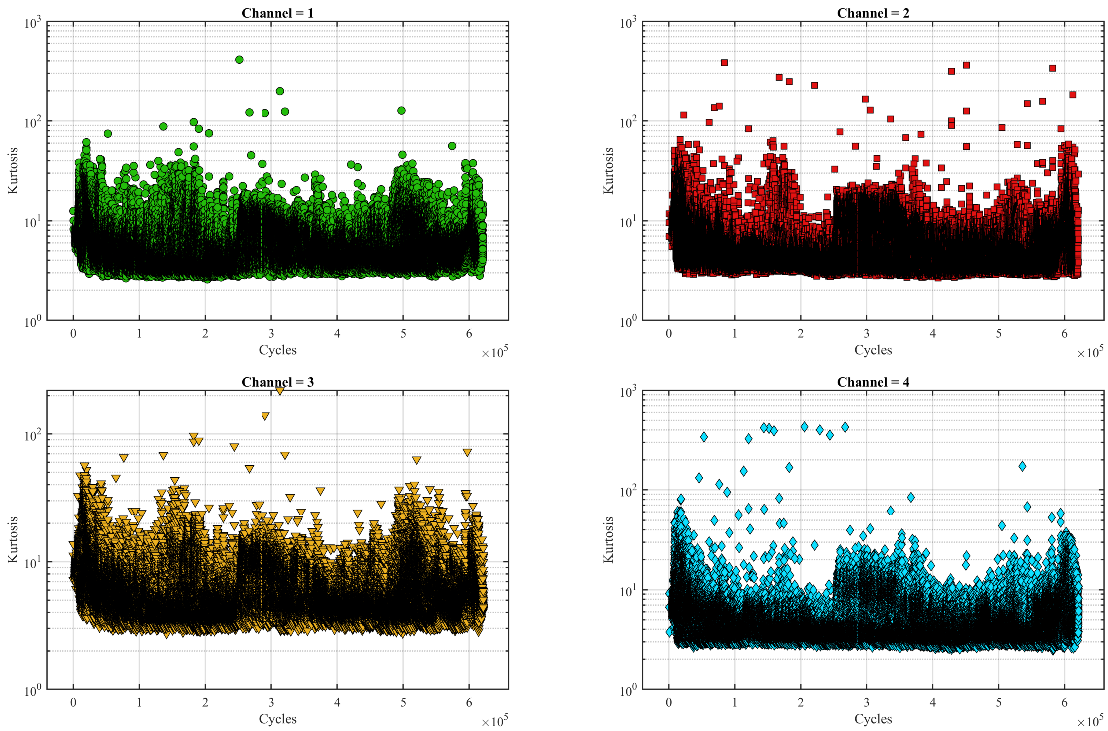

Centroid Frequency

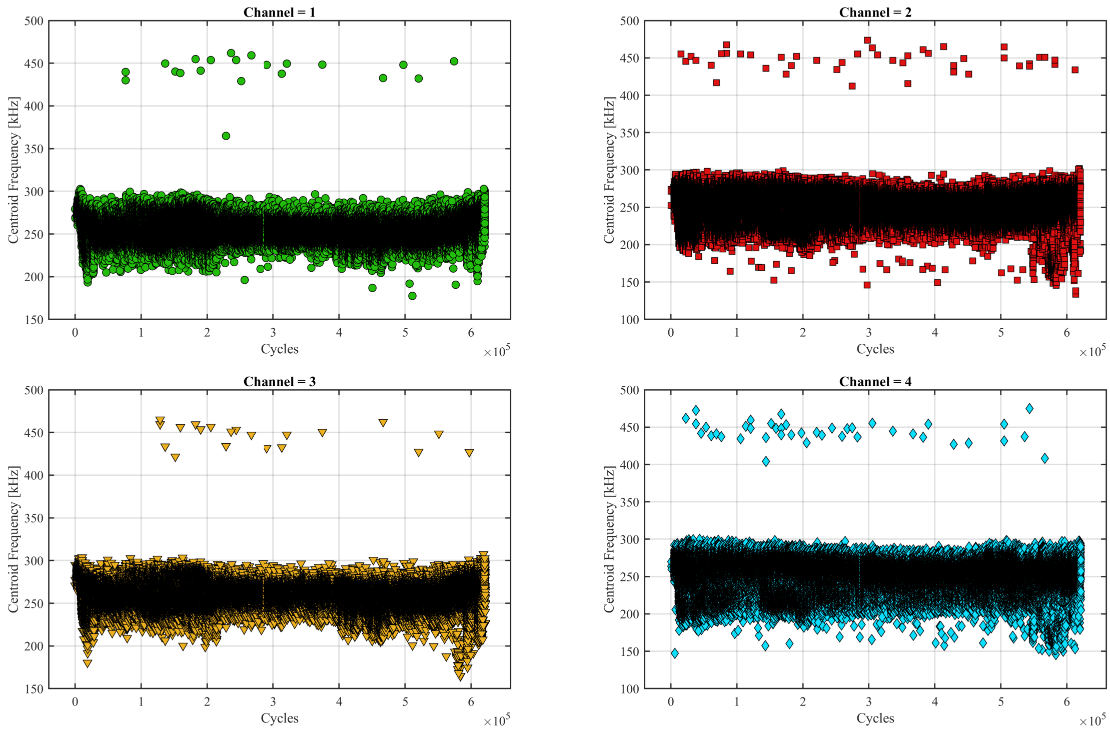

Peak Frequency

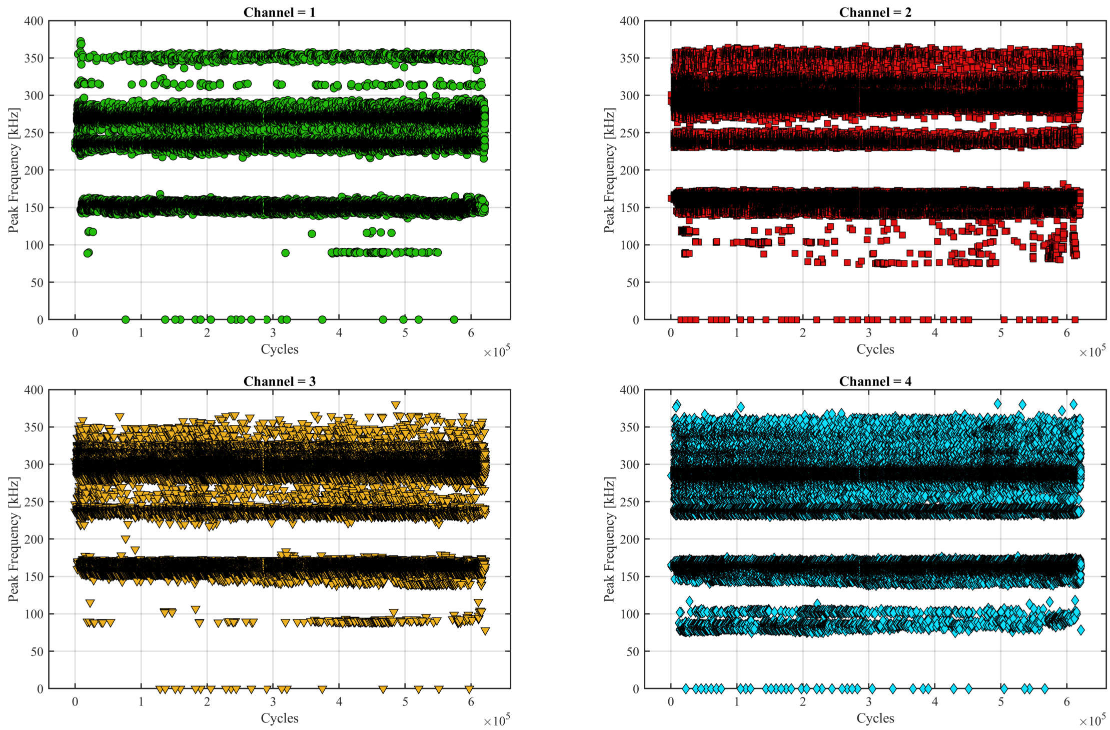

B

Quantitative analysis results

B.1. Growth Rate of AE Parameters

B.1.1. Count rate

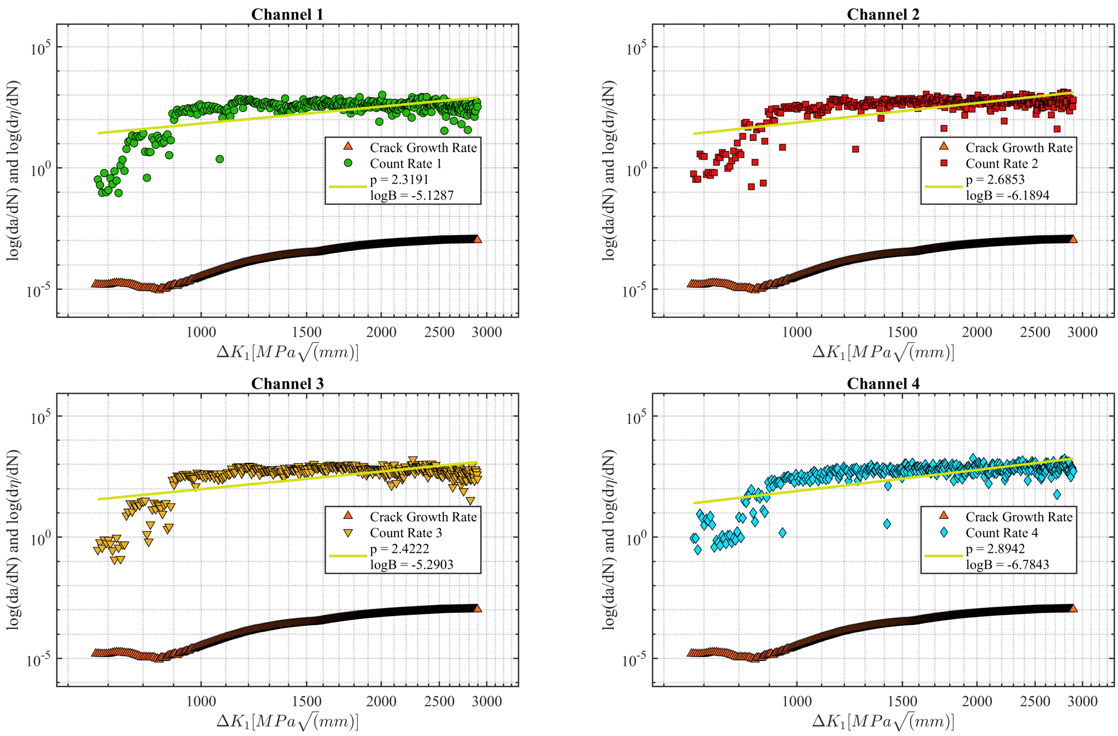

Figure B.1: Count rate with fatigue crack growth rate versus stress intensity factor range (ΔK)

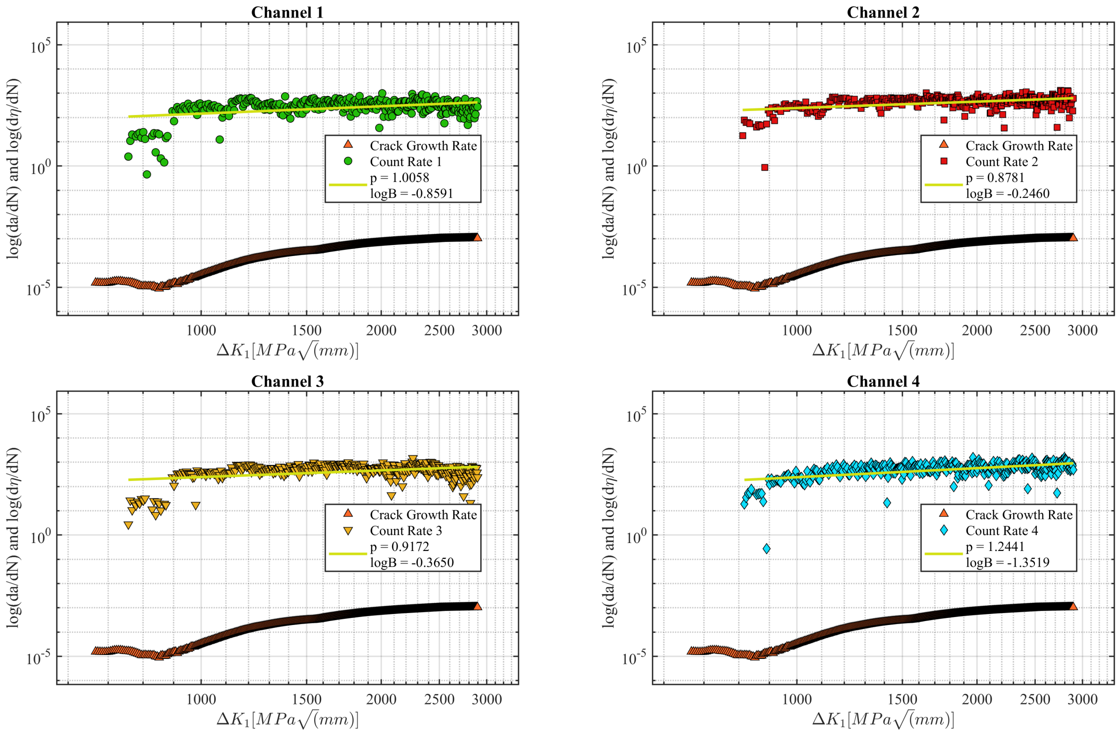

Figure B.2: Count rate with fatigue crack growth rate versus stress intensity factor range (ΔK) (Filtered)

B.1.2. Energy rate

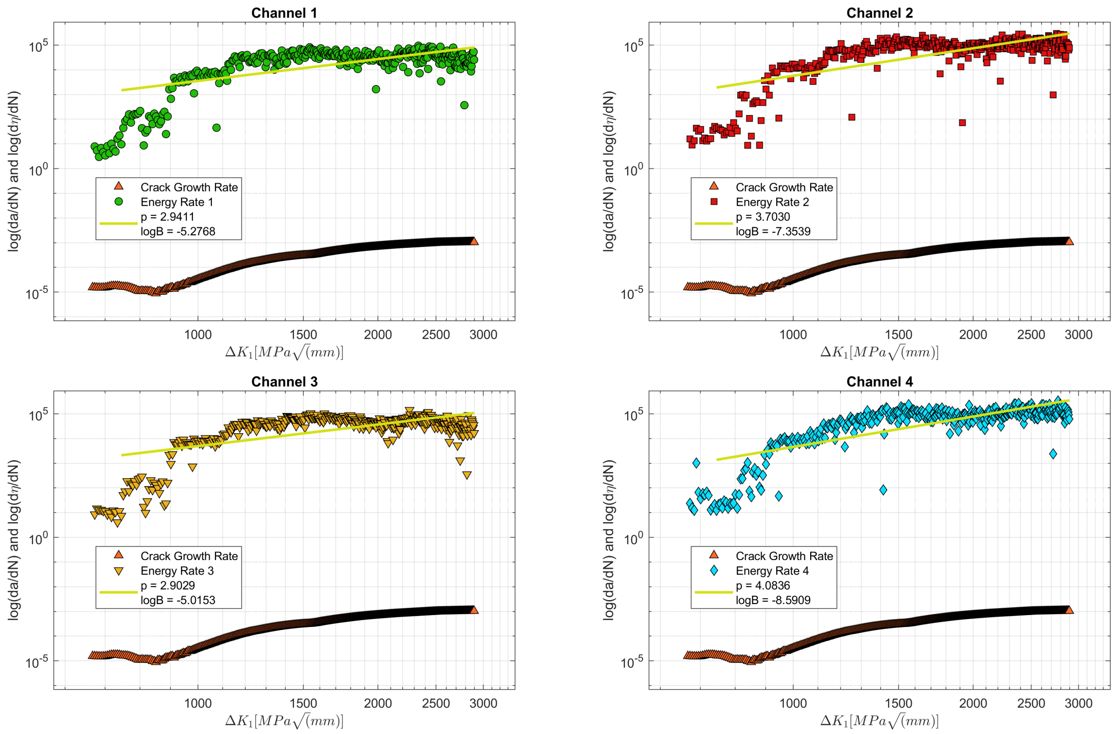

Figure B.3: Energy rate with fatigue crack growth rate versus stress intensity factor range (ΔK)

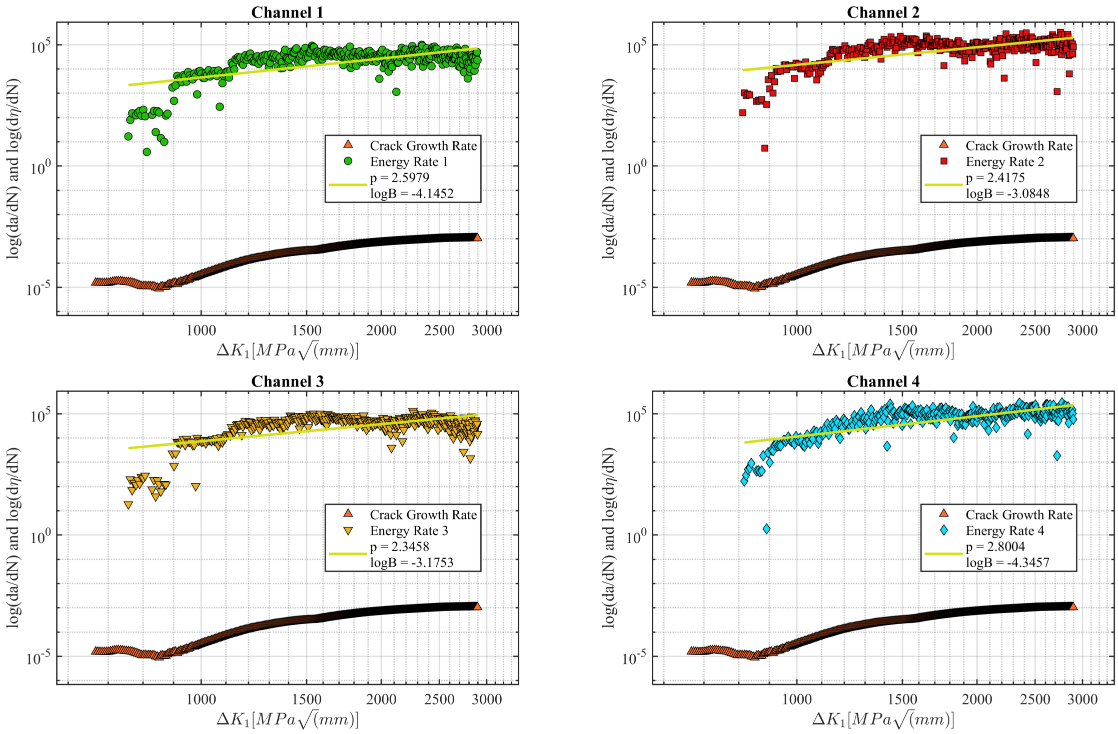

Figure B.4: Energy rate with fatigue crack growth rate versus stress intensity factor range (ΔK) (Filtered)

B.1.3. Entropy rate

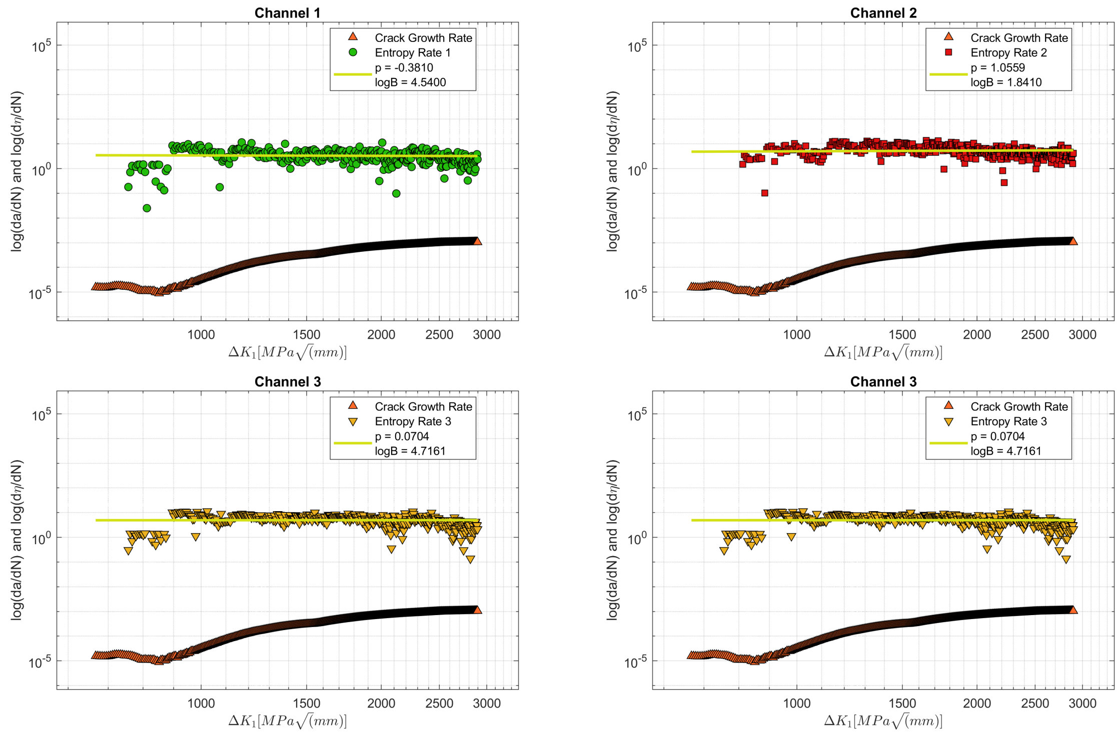

Figure B.5: Entropy rate with fatigue crack growth rate versus stress intensity factor range (ΔK)

B.1.4. Kurtosis rate

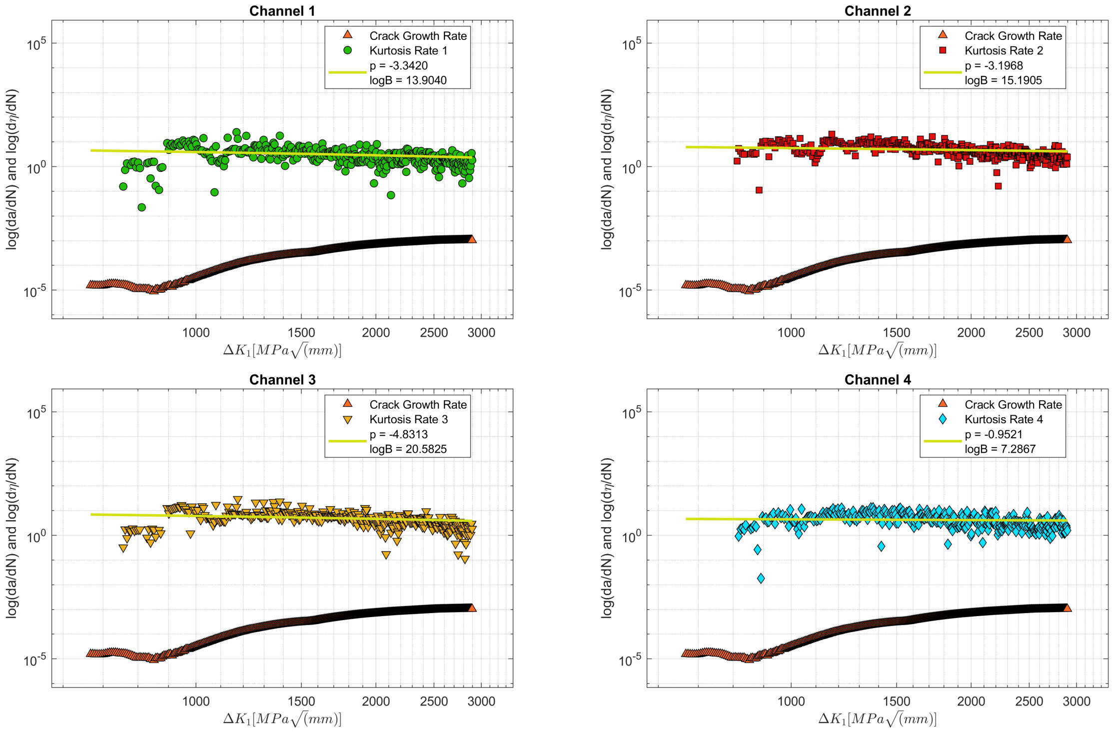

Figure B.6: Kurtosis rate with fatigue crack growth rate versus stress intensity factor range (ΔK)

B.2. Predicted Crack Growth Rate from AE Parameters

B.2.1. Count rate

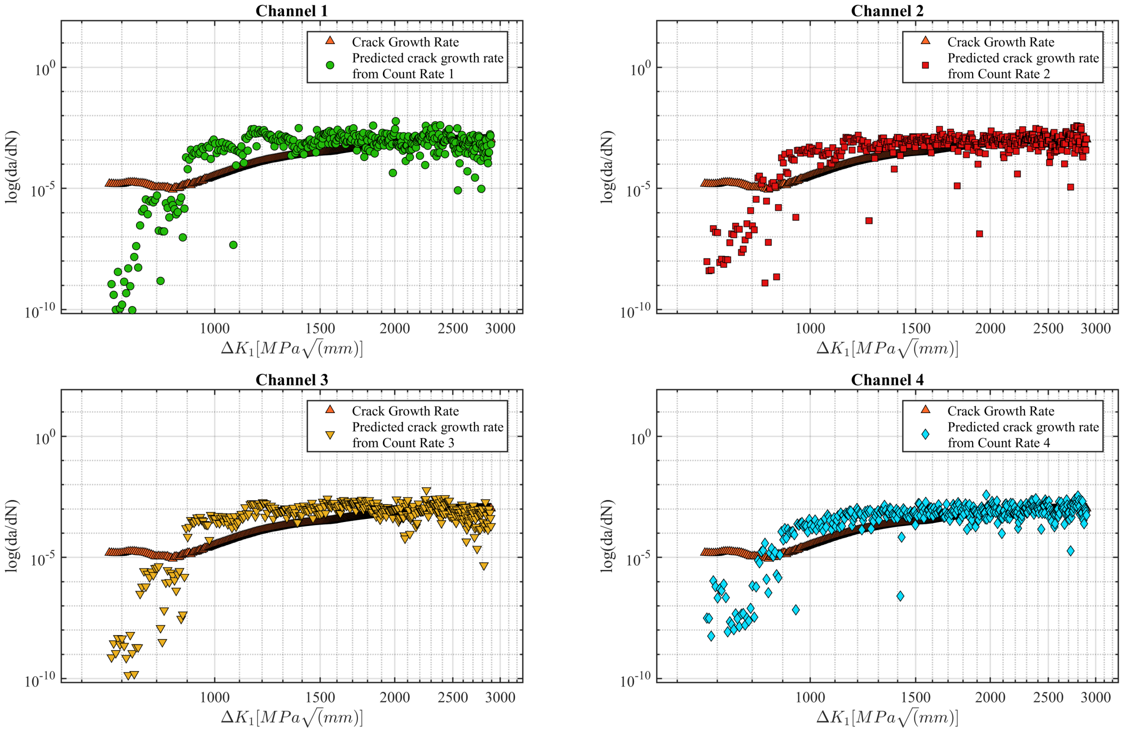

Figure B.7: Count rate with fatigue crack growth rate versus stress intensity factor range (ΔK)

B.2.2. Energy rate

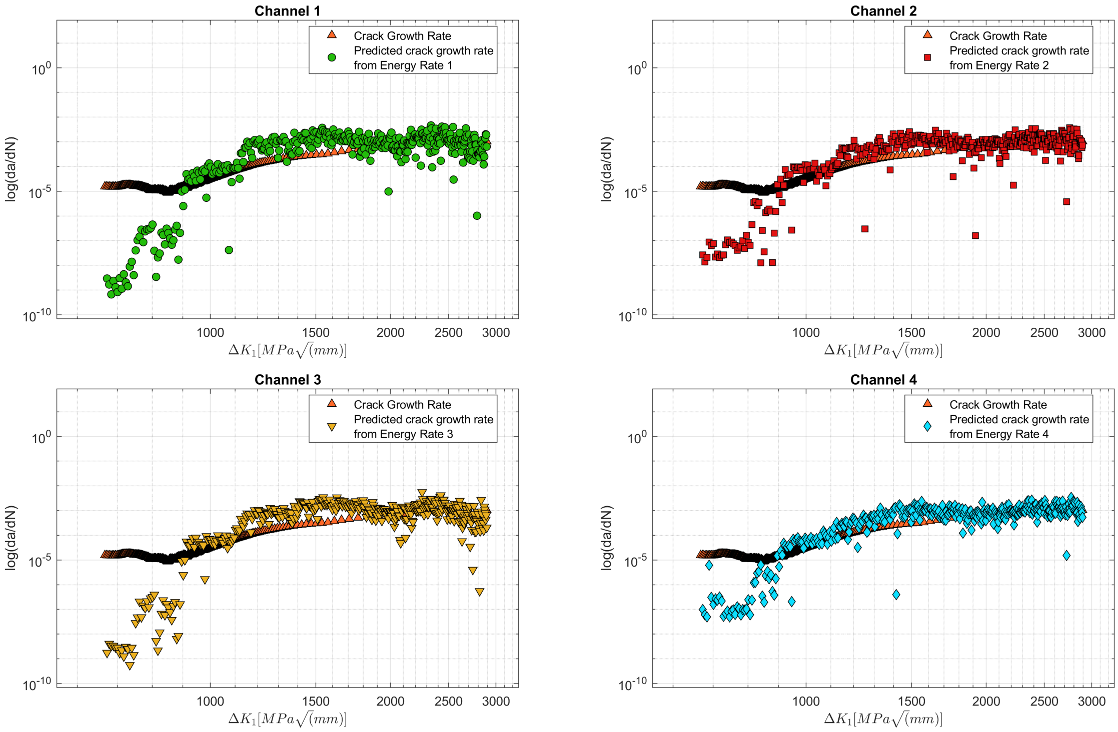

Figure B.8: Energy rate with fatigue crack growth rate versus stress intensity factor range (ΔK)

B.2.3. Entropy rate

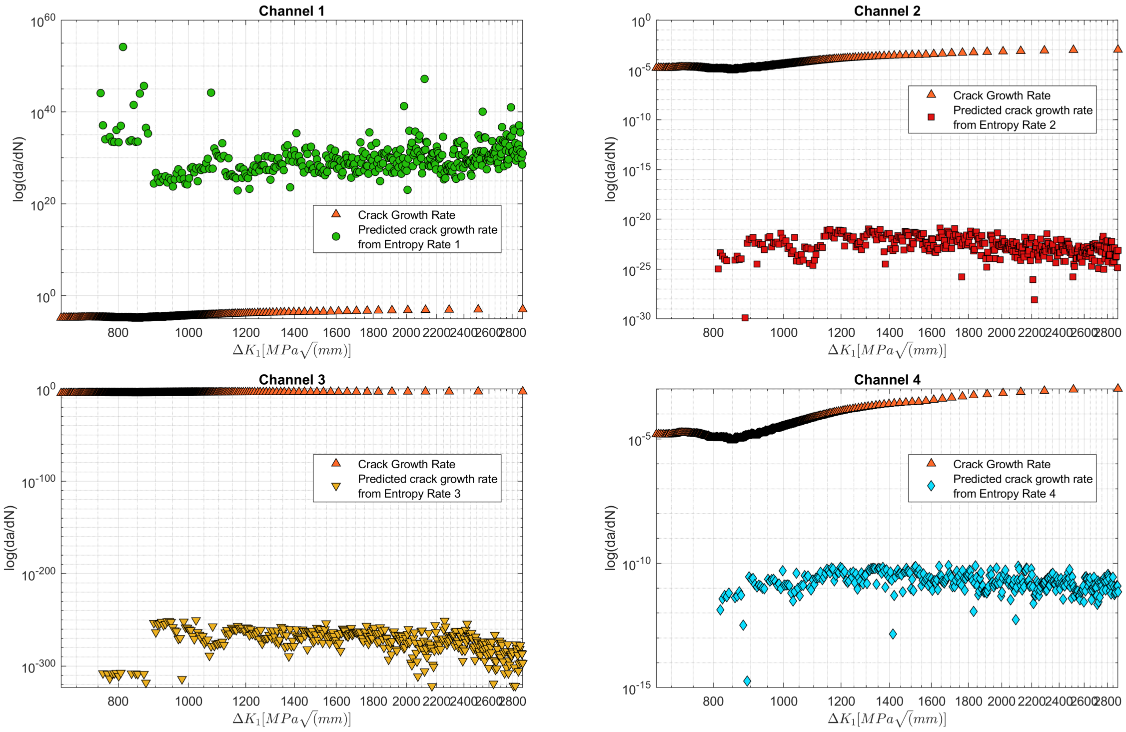

Figure B.9: Entropy rate with fatigue crack growth rate versus stress intensity factor range (ΔK)

B.2.4. Kurtosis rate

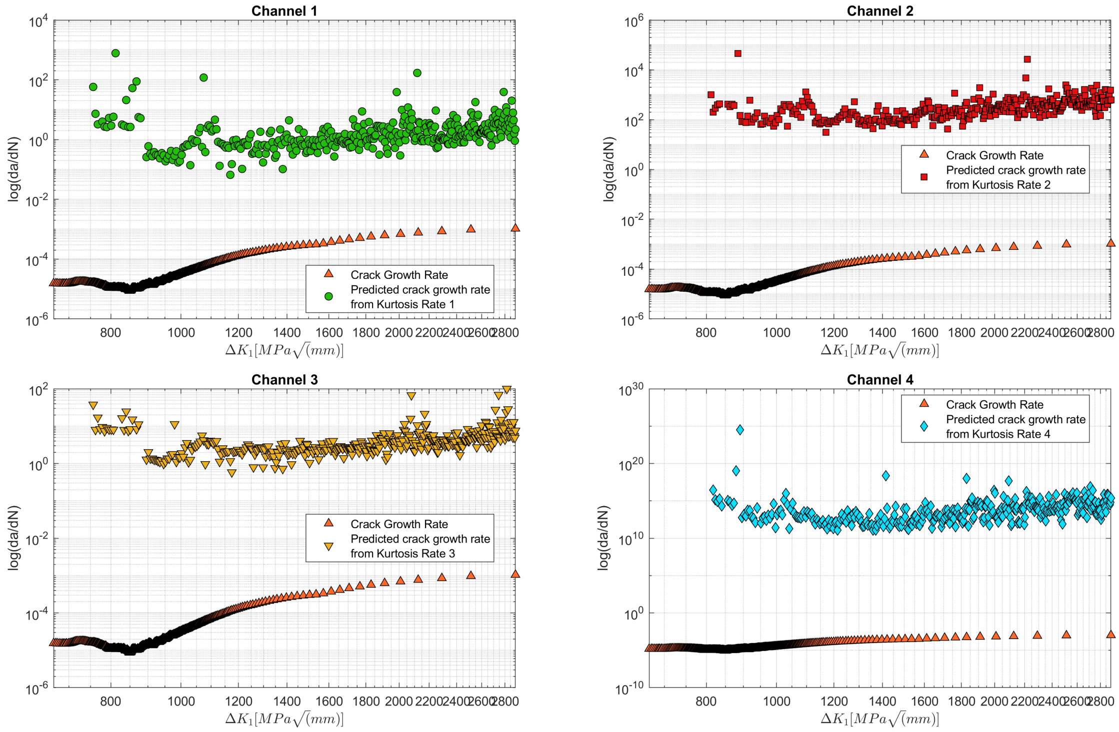

Figure B.10: Kurtosis rate with fatigue crack growth rate versus stress intensity factor range (ΔK)

C

Coefficient of Variance

Coefficient of Variance (CV) of AE data.

Table C.1: CV of AE parameters for all datasets of Specimen no. 1

Channel	Counts	Amplitude	Energy	Duration	RiseAngle	AvgFreq
1	8.38	0.63	12.53	6.49	18.69	2.39
2	9.14	0.43	5.48	11.69	23.67	1.64
3	4.41	0.58	6.73	5.55	16.42	3.38
4	10.43	0.27	3.68	5.44	15.04	2.58

Table C.2: CV of AE parameters for Specimen no. 2

Channel	Counts	Amplitude	Energy	Duration	RiseAngle	AvgFreq
1	1.48	1.44	14.67	1.27	1.04	3.67
2	1.60	1.61	10.06	1.41	1.16	3.42
3	1.53	1.39	12.26	1.27	1.01	4.03
4	1.61	1.58	11.81	1.42	1.15	3.40

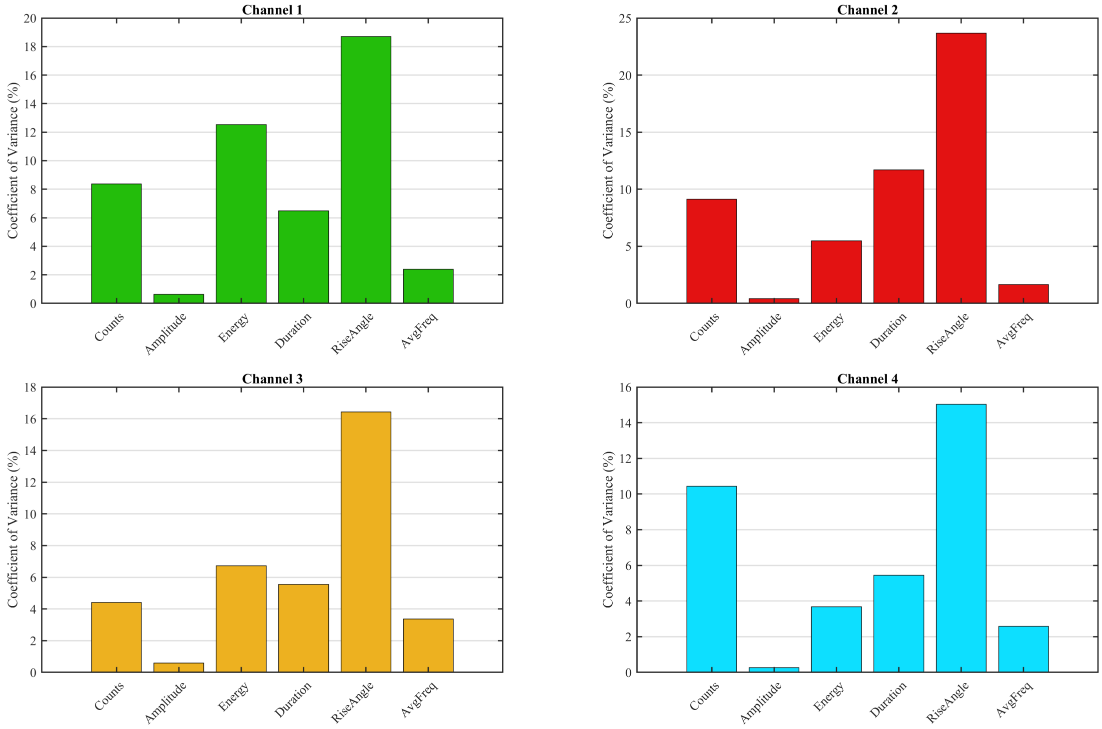

Figure C.1: Visualization of CV of AE Parameters for all Specimen No. 1 Datasets

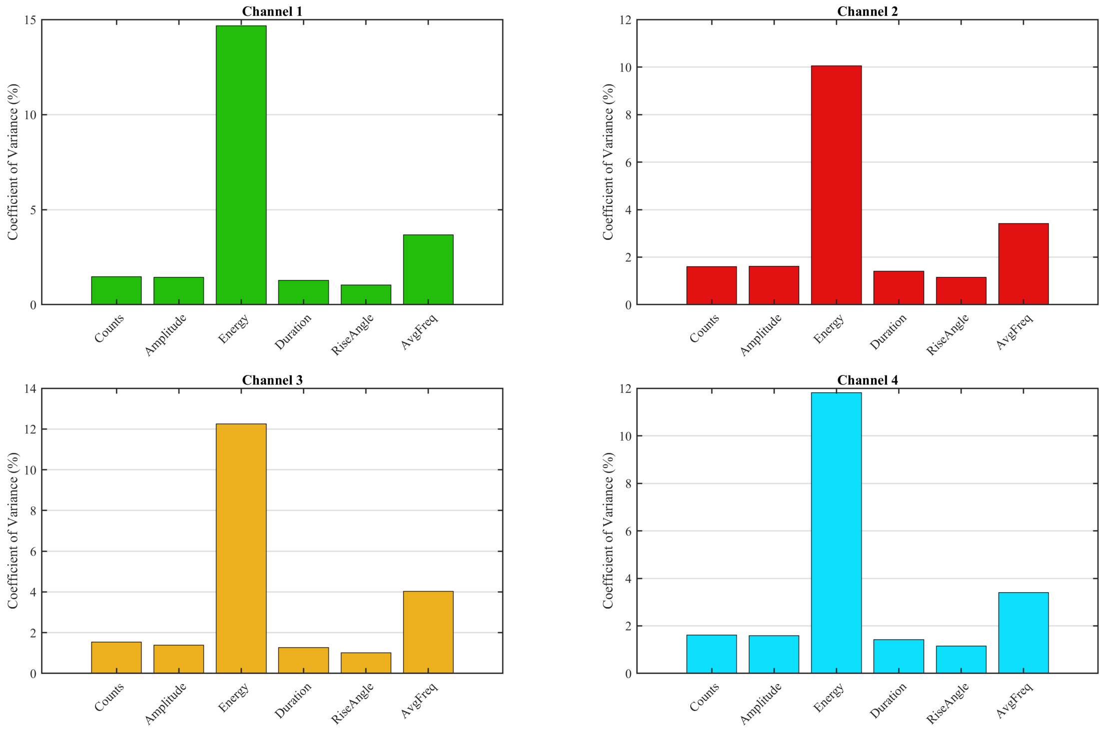

Figure C.2: Visualization of CV of AE Parameters for Specimen No. 2

Table C.3: CV of AE parameters of Amplitude filtered data for Specimen no. 2

Channel	Counts	Amplitude	Energy	Duration	RiseAngle	AvgFreq
1	0.35	0.54	8.43	0.34	0.55	0.13
2	0.39	0.57	5.50	0.35	0.55	0.20
3	0.36	0.48	6.85	0.35	0.55	0.15
4	0.45	0.60	6.57	0.40	0.56	0.21

Table C.4: CV of AE parameters of Amplitude filtered data for Specimen no. 2

Channel	RMS	CrestFactor	Kurtosis	Entropy	PeakFreq	CentroidFreq
1	0.71	0.22	0.53	0.06	0.22	0.05
2	0.93	0.23	0.63	0.05	0.27	0.06
3	0.86	0.22	0.51	0.07	0.26	0.05
4	0.68	0.22	0.67	0.05	0.28	0.07

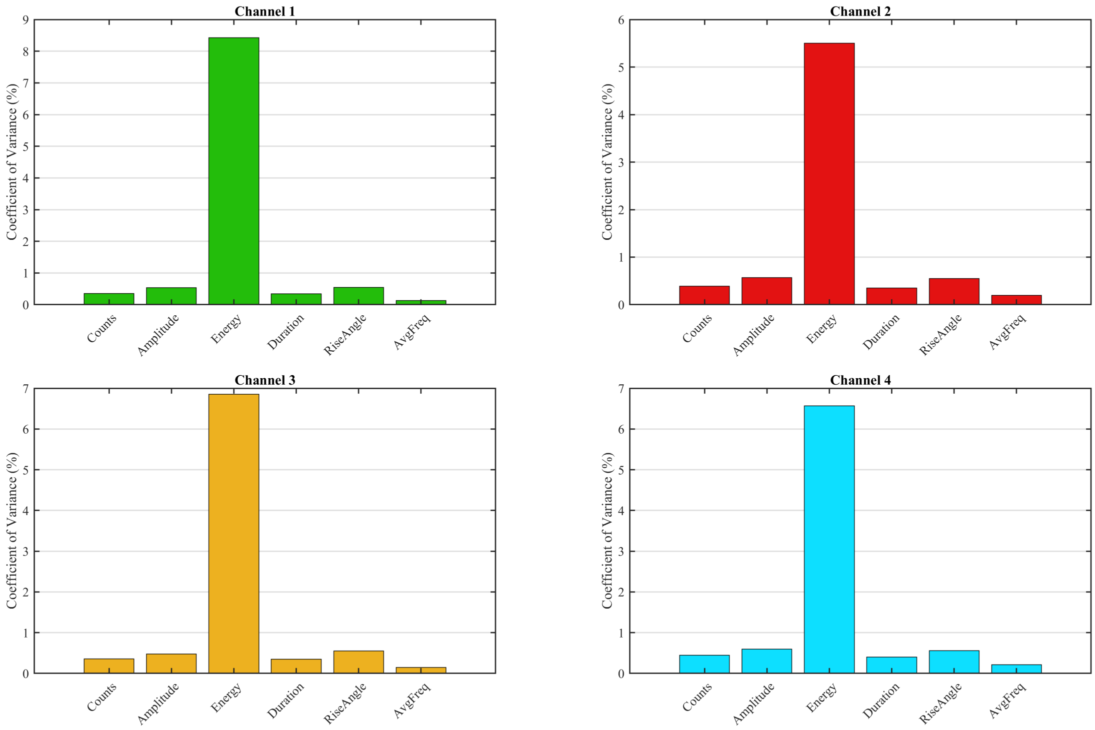

Figure C.3: Visualization of CV of AE Parameters of Amplitude filtered data for Specimen No. 2

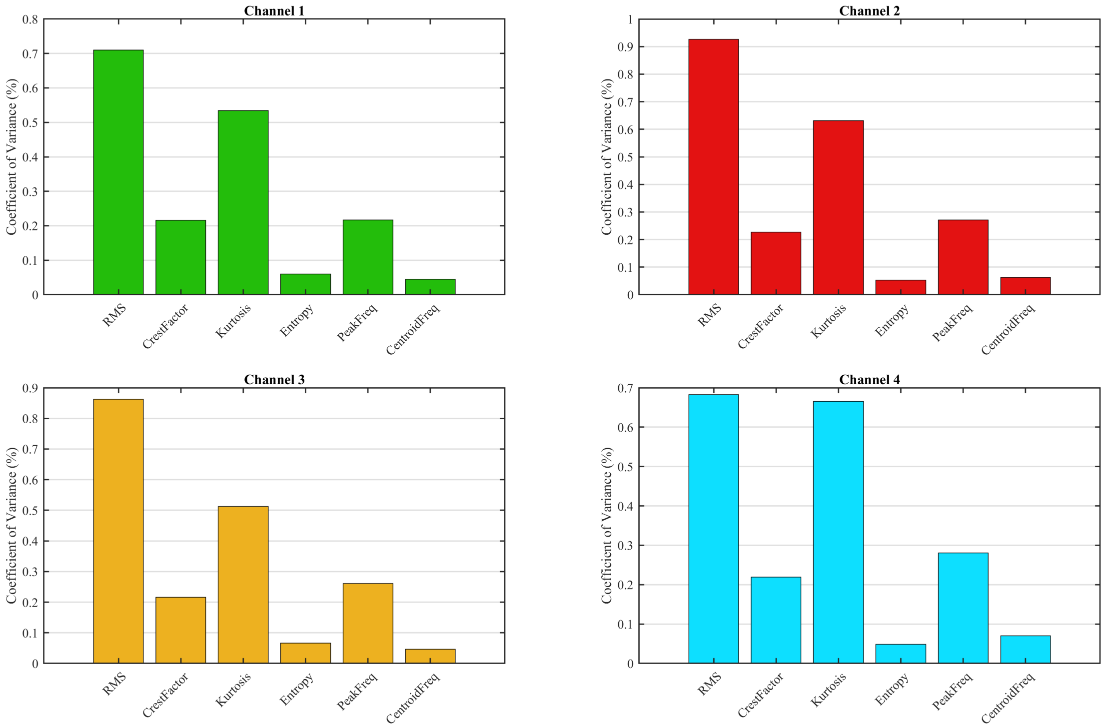

Figure C.4: Visualization of CV of AE Parameters of Amplitude filtered data for Specimen No. 2

Table C.5: CV of AE parameters for last 6 datasets of Specimen no. 1

Channel	Counts	Amplitude	Energy	Duration	RiseAngle	AvgFreq
1	0.86	0.92	4.11	0.73	1.20	3.83
2	1.36	0.69	2.13	0.85	1.04	4.31
3	0.75	0.69	2.81	0.62	0.58	4.00
4	1.45	0.74	4.54	0.93	0.95	4.29

Table C.6: CV of AE parameters for last 6 datasets of Specimen no. 1

Channel	RMS	CrestFactor	Kurtosis	Entropy	PeakFreq	CentroidFreq
1	0.64	0.11	0.26	0.08	0.62	0.09
2	0.55	0.14	0.33	0.09	0.19	0.06
3	0.50	0.13	0.24	0.06	0.51	0.10
4	0.68	0.13	0.26	0.10	0.15	0.06

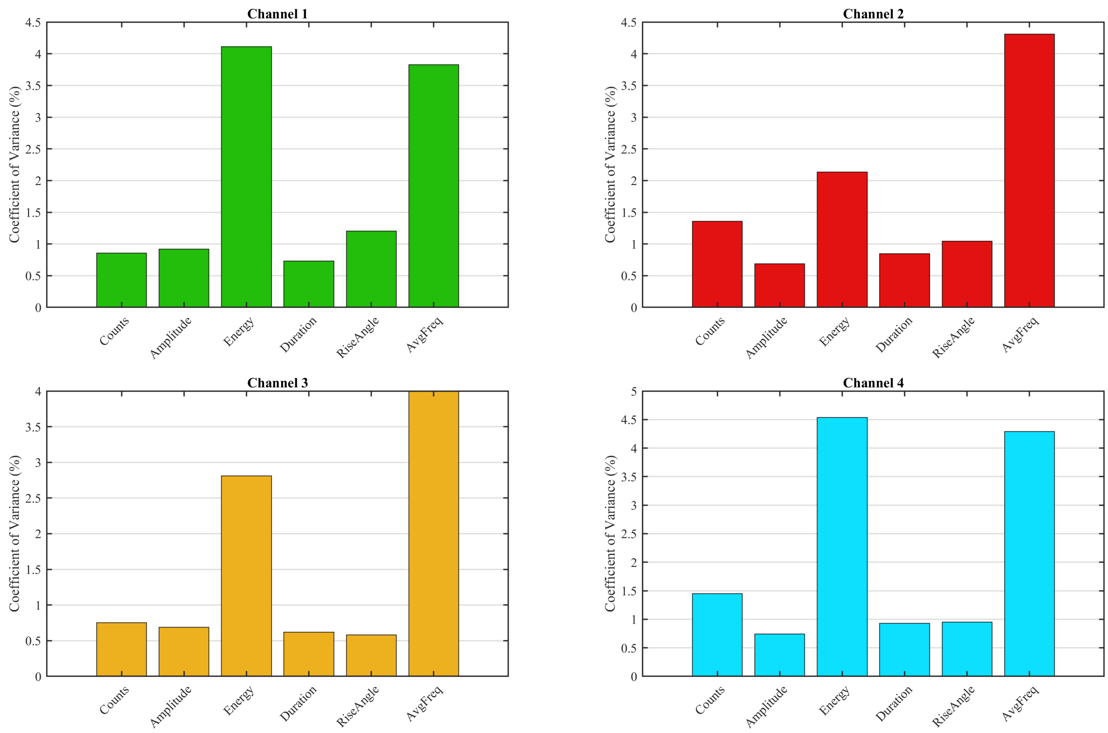

Figure C.5: Visualization of CV of AE Parameters for last 6 datasets of Specimen No. 1

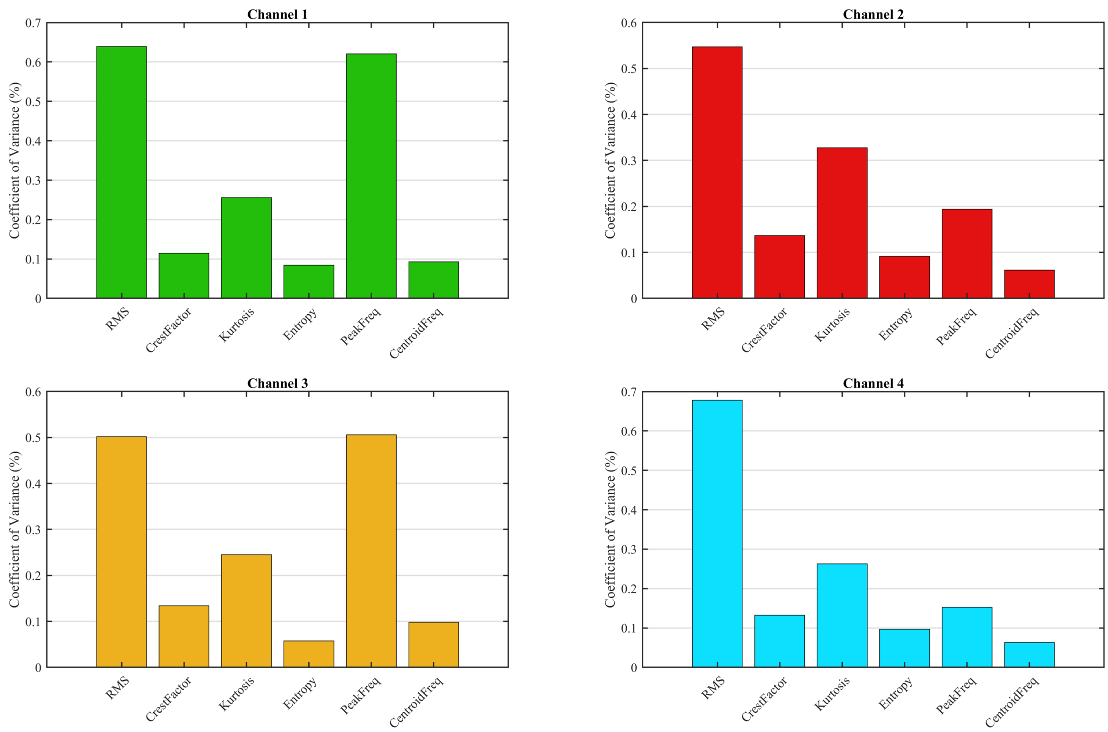

Figure C.6: Visualization of CV of AE Parameters for last 6 datasets of Specimen No. 1

D

AE signal waveforms

AE signals above 50 dB Amplitude

Figure D.1 and Figure D.2 have similar peak frequencies, whereas Figure D.3 exhibits higher frequency peaks.

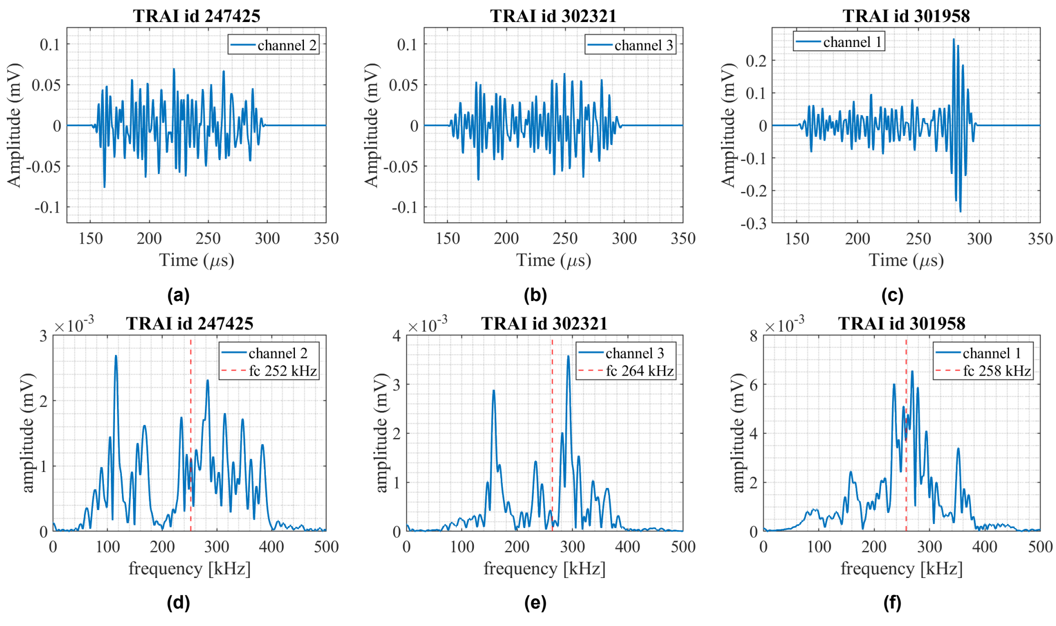

Figure D.1: AE signal waveforms - Early stage (around 28,000 cycles approx.)

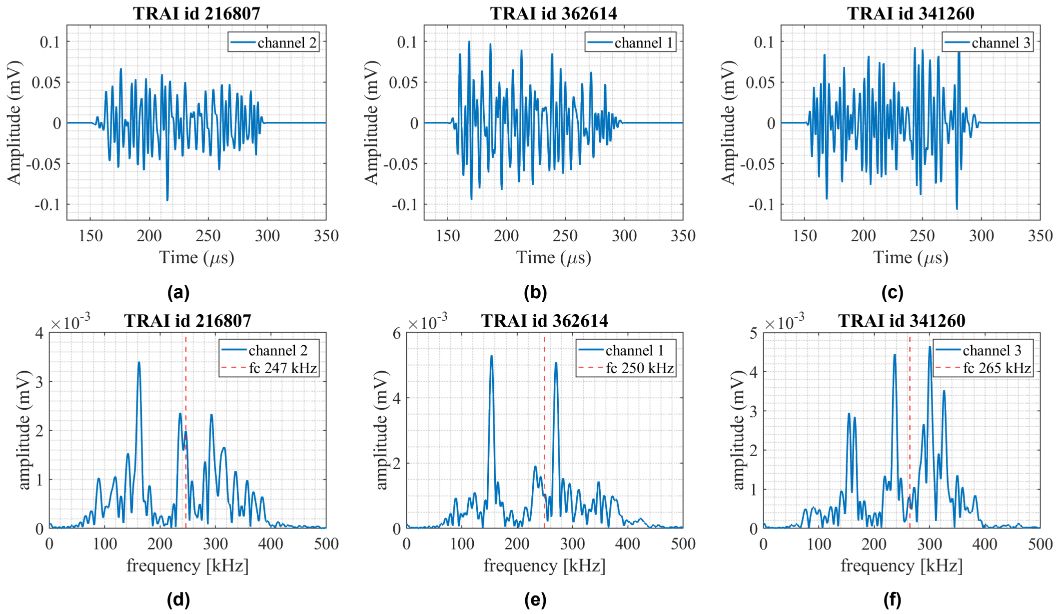

Figure D.2: AE signal waveforms - Middle stage (around 275,000 cycles approx.)

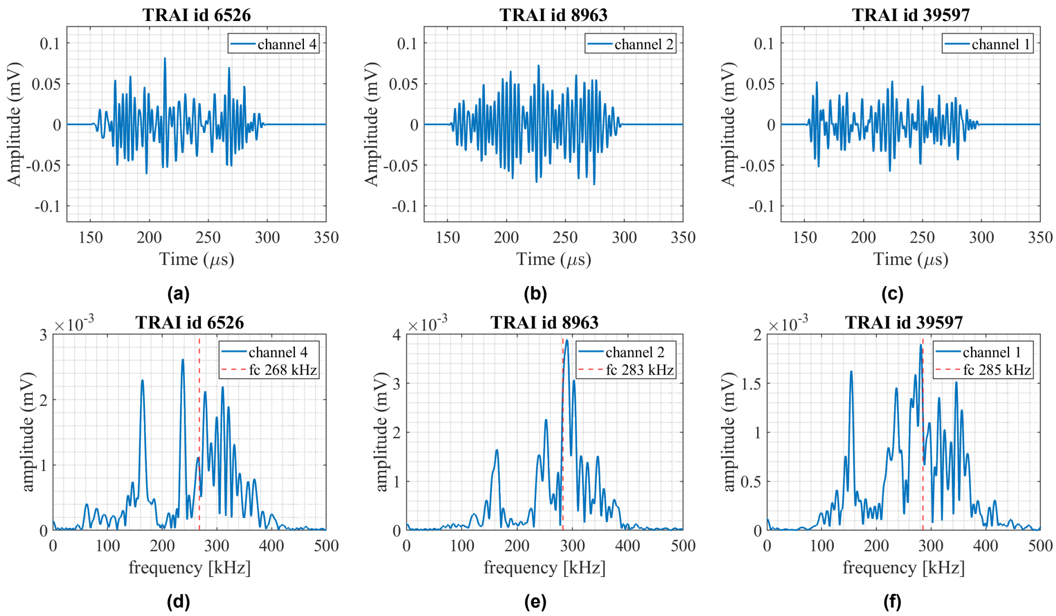

Figure D.3: AE signal waveforms - Final stage (around 620,000 cycles approx.)

AE signals below 50 dB Amplitude

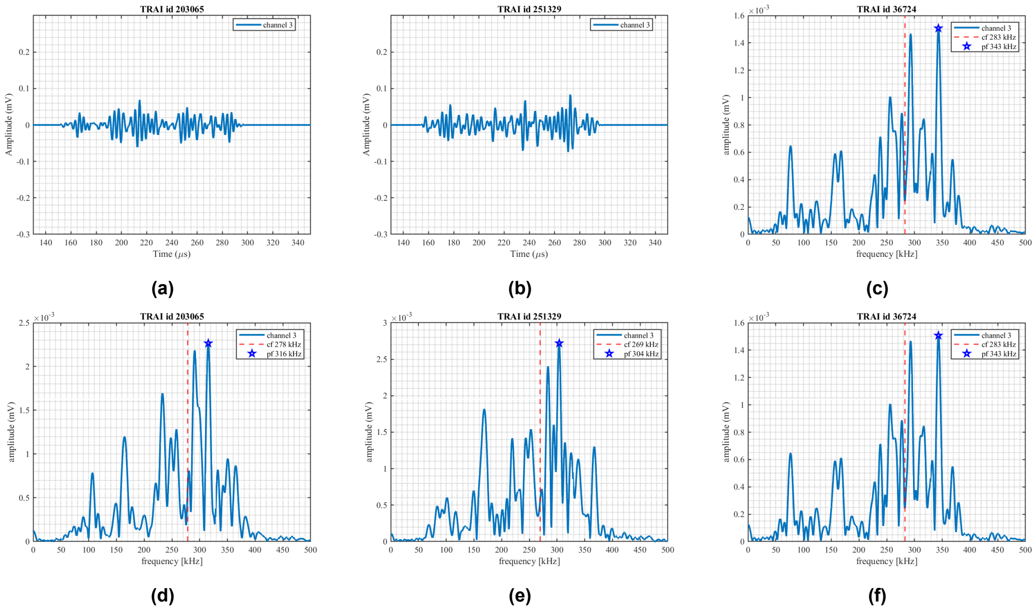

Figure D.4: AE signal waveforms - at Early (a,d), Middle (b,e) and Final stage (c,f)